6-1-2011

Simulation model of Pacinian corpuscle for haptic system design

Daniel Liu

Simulation Model of Pacinian Corpuscle for Haptic System Design

by

Daniel F. Liu

A Thesis Submitted in Partial Fulfillment of the Requirements for the Degree of Master of Science in Computer Engineering

Supervised by

Associate Professor Dr. Shanchieh Yang
Department of Computer Engineering
Kate Gleason College of Engineering
Rochester Institute of Technology
Rochester, New York

June 2011

Approved By:

Dr. Shanchieh Yang
Associate Professor
Primary Advisor

Dr. Daniel Phillips, Associate Professor
Committee Member, Department of Electrical Engineering

Dr. Marcin Lukowiak, Assistant Professor
Committee Member, Department of Computer Engineering

Thesis Release Permission Form

Rochester Institute of Technology

Kate Gleason College of Engineering

Title: Simulation Model of Pacinian Corpuscle for Haptic System Design

I, Daniel F. Liu, hereby grant permission to the Wallace Memorial Library to reproduce my thesis in whole or in part.

Daniel F. Liu

Date

Dedication

To my family and friends who have supported me throughout my life.

Acknowledgments

I would like to first acknowledge and thank my thesis advisor, Dr. Shanchieh Yang. His continued guidance and support is what made this work possible. I would also like to thank my committee members, Dr. Daniel Phillips for his feedback and insight on the topic and Dr. Marcin Lukowiak for his support and time.

I also would like to express my gratitude towards my fellow students and friends who I have worked alongside with at RIT. Together we created an environment that was both educational and fun, we provided invaluable support for each other, and our time together has been priceless.

Abstract

With the increasing need for tactile feedback in Human Computer Interfaces used in robotics, medical, and mobile devices, there has been an increasing interest in the design of tactile sensors, displays, and complete haptic systems to transfer tactile information to users. These systems have improved users ability to work with remote tools or virtual environments, from enhancing the accuracy of tools like robotic surgery to improving user experiences in virtual reality systems. Despite many advances, the potential of these technologies to provide augmented or realistic sensations of touch is limited in part by the lack of understanding the complex mechanisms involved in the human perception of touch.

To improve the understanding of tactile physiology, this work begins the design of a biophysically accurate simulation model of the receptor cell responsive to high frequency vibration, the Pacinian corpuscle. This receptor plays a key role in the fine control of tools and is a common target for vibrotactile haptic displays. The model incorporates computational and theoretical principles of the Pacinian corpuscles biophysics, which have been developed in past studies, to simulate its electrical response to mechanical, thermal and electrical stimuli. The accuracy and flaws of the model are demonstrated through comparisons with published physiological data. Experiments are also proposed to show how the simulation model can be used to quantitatively compare the results of different tactile displays and different external environments in order to improve the design of modern haptic systems.

Contents

List of Figures

List of Tables

Chapter 1

Introduction

Haptics, from the Greek word *haptesthai* - to contact or to touch, is the study of our somatosensory system and how we perceive the world through our sense of touch. While traditionally in the realm of perceptual and neuroscience, the study of haptics has now incorporated the new designs of haptic technologies to provide tactile feedback through human computer interfaces. Motivated by new advances in technology and the need for enhanced human computer interactions to improve user experience or device operation, haptic technologies are increasingly being designed into consumer electronics, robotic controls, and surgical devices. These feedback systems typically consist of tactile sensors or a virtual environment to operate in, haptic displays to produce physical stimulation, and a control system.

The goal of modern haptic technologies is to produce distinguishable, meaningful and natural tactile information to a user in order to improve the performance of a system. This is seen in the design of vibrotactile feedback in mobile phones screens to improve user experience[1], haptic rendering devices for computer-aided design to augment environment visualization [53], and haptic systems in surgical devices to improve the accuracy and outcome of robotic surgery[52], laparoscopy [54], and other minimally invasive operations. While current haptic systems are not capable of reproducing life-like stimuli in all cases, current research aims at improving hardware design, signal processing techniques, and improving our understanding of how touch is perceived and how we interface with

these devices.

1.1 Motivation

A significant portion of research in haptic systems has been focused on the design of different haptic system hardware to improve the resolution and accuracy of these sensors and displays and to target different modalities of touch. For tactile displays current technologies include using arrays of mechanical actuators [17][69], pneumatic balloons [14], electrode arrays [41], and peltier devices [32]. Modern tactile sensors include MEMs devices using PVDF [60], piezoelectric [3], and silicon devices [16] along with biological inspired devices mimicking properties of the human finger [51][70][13]. These systems and devices have limitations in measuring and reproducing life-like sensations of touch. Haptic systems currently cannot reproduce all modalities of touch, the interaction with the environment and the somatosensory system is different from natural touch, and there remains accuracy, resolution and time delays that limit functionality.

As seen with the design of biomimetic tactile sensors [51][70][13], there has been increasing interest in using our understanding of the human somatosensory system to inspire device design and to improve the quality of these system. This includes using biological theories and models of biological systems in the design of haptic systems. While researchers have always considered basic physiology, qualitative receptor responses, and psychophysical experiments to design and evaluate haptic devices [26][69][54], the use of complex biological theories and models is becoming more prevalent. This includes studying models of tissue biomechanics and how it affects tactile perception coupled with haptic devices [64], incorporating models of heat transfer in the signal processing of thermal haptic systems [44][38], and nerve fibre cable models to guide design of electrical stimulus patterns of electrotactile haptic systems [40][41]. There is also a growing interest in studying the tactile sensory capability of amputees and the design of neural prostheses that

provide sensory feedback [45] [50] [15] [43].

The overlap between the study of the somatosensory system and engineering of haptic systems is necessary to continue improving the performance of haptic systems. The complete system includes not only haptic technologies, but also the human system and our perception of tactile stimuli. For engineers to study this system as a whole, mathematical descriptions and simulation tools should be used as one method to understand the interaction between haptic devices and human tactile perception. Drawing from neuroscience and perceptual science research, existing models of mechanoreceptor responses [21][5][8][24], tissue and mechanical properties [46][64][33], models of somatosensory perception can be used to help design haptic systems.

1.2 Objective

The objective of this thesis is to develop a biophysical simulation model of the Pacinian corpuscle. This model will extend and utilize past research and models of the Pacinian corpuscle and related systems in order to design a comprehensive model of the behavior of the receptor that attempts to maintain a close relation with the biophysical theories of how the Pacinian corpuscle operates. The model will simulate changing mechanical and thermal stimuli across the surface of this receptor as inputs to generate the electrical action potentials of the Pacinian corpuscle. This requires the model to incorporate mechanical, mechanotransduction, electrophysiological, and heat transfer theories of the Pacinian corpuscle. The model will be characterized and the results will be compared against known published characteristics and behaviors of the receptor.

While there are numerous past and current efforts to model the Pacinian corpuscle, this work is an attempt to begin unifying and testing in simulation the different theories developed about the receptor. While there are clear limitations with relying on biophysical

models that have skeptical foundations or incompletely describe the system, it is still important to understand these theories and how they may or may not accurately model the receptor's behavior. There is also a clear limitation on relying on published experimental results and not being able to design physiological experiments to test the theories of the models of its hypothesized results, but that is beyond the scope of this research.

The purpose of this thesis work is to contribute to the long term goal of a biophysically accurate model of the Pacinian corpuscle (along with models of all cutaneous receptors in humans) that can be used to perform simulation experiments. With an accurate representation of the receptor's response to stimuli, the model can be coupled with models of different external environments or haptic displays in order to study the differences between natural environments and haptic displays and the differences between different types of haptic displays. This will offer a framework to quantitatively compare how the body encodes stimuli generated by these different environments and devices. This will enable the future development of improved haptic systems or signal processing techniques. With biophysically accurate models, computational models of the receptor encoding can also be developed to be used in time sensitive environments such as sensory substitution devices of neuroprosthetic limbs.

Chapter 2

Background Literature

There is a large body of research and theory that this study draws upon to create a simulated biophysical model of the Pacinian corpuscle. This chapter will cover the basic theories that draw from the fields of anatomy, physiology, biomechanics, electrophysiology, biophysics, and basic neuroscience. The purpose of this chapter is to provide a basic understanding and overview of the principles and theories used in the model to engineers who may be unfamiliar with these topics, along with providing the necessary details to implement the model. For a thorough understanding of each topic, refer to the cited references.

This chapter begins with an overview of related work (Section 2.1) followed by an introduction to the somatosensory system (Section 2.2) including details of the Pacinian corpuscle, the mechanoreceptor of interest, that need to be considered in its modeling. Section 2.3 gives an overview of the general electrophysiology theories of how neurons generate electrical signals, a key portion of the model. Section 2.4 explains the mathematics and modeling specific to the Pacinian corpuscle, which includes modeling its mechanical, transduction, electrical, and thermal properties. Finally Section 2.6 describes the simulation tools used since prepackaged scientific software was used as a reliable alternative to custom simulators.

2.1 Related Work

2.1.1 Functional Electrical Stimulation using SmartTouch Haptic Device

The SmartTouch system developed by Kajimoto, et. al. [40] [41] [39] from University of Tokyo is an example where electrophysiological modeling theory is used to determine optimal stimuli patterns for an electro-tactile haptic display. The haptic display they developed were varying arrays of surface electrodes with an effective diameter of up to 2-4 mm per electrode. These electrodes target the afferent nerve fibres of the Merkel, Meissner, Ruffini and Pacinian receptors, which they call the four primary colors of tactile sensation, although they only target three receptors (Merkel, Meissner, and Pacinian). They assume the afferent nerve fibres for each of the four receptors are located at different depths and orientations, specifically Pacinian and Merkel afferents are oriented horizontally to the skin while Meissner afferents are vertical, and the Pacinian is the deepest in subcutaneous tissue while Merkel afferents are shallow. Using arrays of electrodes they formulate an optimization problem to find optimal electrode stimulation patterns that will selectively stimulate only a single fibre.

Based on a simplified 2D orientation and location of the afferent nerve fibres, they model each afferent fibre type as a simple myelinated cable with an overall time constant and length constant and the nodes of ranvier are the targets to be stimulated. The time and length constants are derived from the membrane capacitance, membrane conductance, and axial (cytoplasmic) conductance of the myelinated fibre. The cable can then be represented by a 1D PDE which is equivalent to the standard 1D heat transfer problem. The electrodes are modeled as a series of simple monopoles that generate electric potential that propagates radially through a linearly resistive tissue. For a 1D arrays of electrodes, the potential generated by each electrode is simply superimposed, ignoring any dipole effects between electrodes. The conceptual setup and placement of their electrodes and nerve fibre compartments can be seen in Figure 2.1.

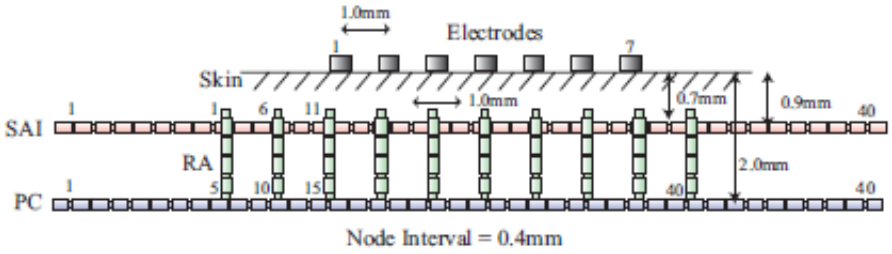

Figure 2.1: Electrode and nerve placement for Smart Touch simulation (adapted from [39]) in which the Merkel (SA1), Meissner (RA) and Pacinian (PC) afferents are modeled.

Then an optimization problem is setup to find the strengths (weight) of the current the electrodes in the array need to activate a fibre while suppressing the others. The stimulating electrodes can be a cathodic or anodic, and different patterns of electrode strength create an activating function for a specific nerve fibre which can be used in their haptic display to target a specific receptor or "tactile primary color". An example stimulation pattern and the resulting waveform generated on the fibre is seen in Figure 2.2.

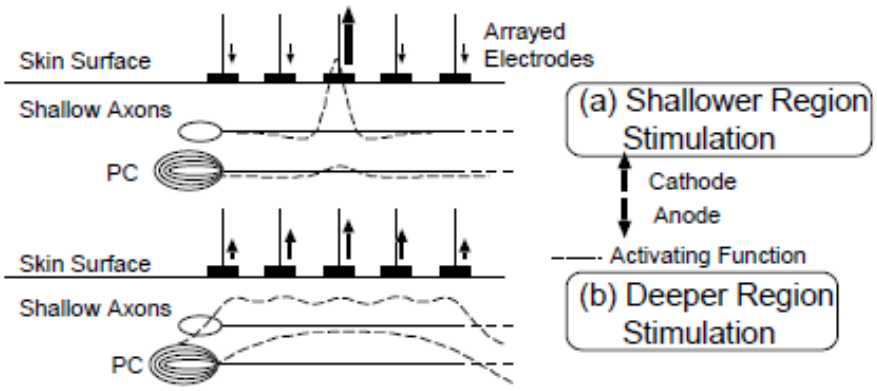

Figure 2.2: Activation pattern to stimulate a shallow (Merkel) afferent and deep (Pacinian) afferent. (Taken from [39]). The activation pattern are different weights/strength of cathodic or anodic currents across the different electrodes.

2.1.2 Grandori and Pedotti's Model of Pacinian Corpuscle

There have been other approaches to modeling the Pacinian corpuscle, including phenomenological models that do not directly consider biophysical properties of the corpuscle. Grandori and Pedotti's model [22] [21] is an example where they divide the mechanical to electrical transduction process of the Pacinian corpuscle in three functional mechanisms, outer lamellae filtering, mechano-to-neural transduction, and neural spike generation. Each of these mechanisms is modeled as a system of transfer functions or functions that describe some non-linear behavior.

The outer lamellae model consists of a 2nd order band pass filter that represents the mechanical processes of the lamellae. The mechano-to-neural transduction mechanism models three effects: a derivative effect, nonlinear asymmetric amplitude dependence, rapidly dying transient. The final spike generation mechanism creates an all or nothing spike train based on three properties: excitation of nerve is sensitive to first time derivative of receptor potential, firing threshold and refractory period have an exponential relationship to time, and noise makes the generation non-deterministic. An implementation of this model in MATLAB Simulink® is shown in Figure 2.3.

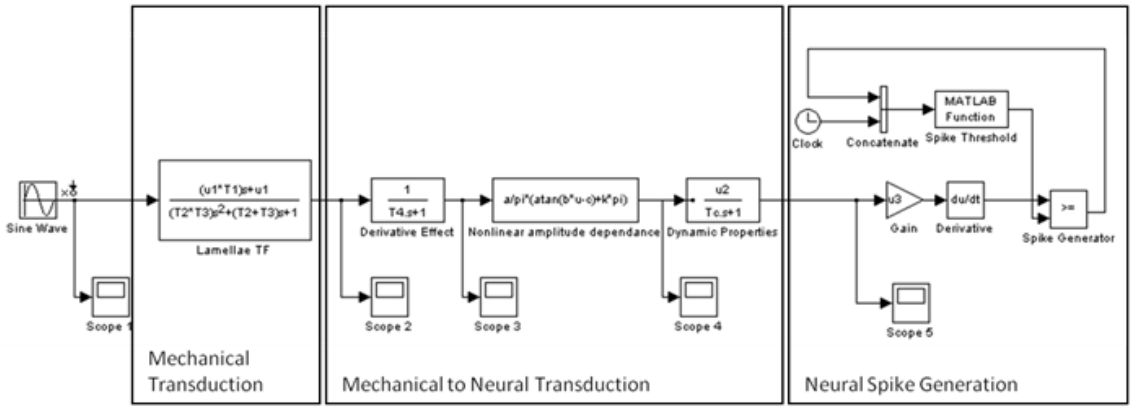

Figure 2.3: An implementation of Grandori and Pedotti's phenomenological model of the Pacinian corpuscle's transduction process. Reimplemented in MATLAB Simulink® from the work published in [22] [21].

2.2 Somatosensory Physiology

2.2.1 Overview

The somatosensory system is a diverse system that spans the entire surface and even parts of the interior of your body. It is primarily associated with your sense of "touch" (e.g., tactile, haptic, somatosensory), one of the five traditional senses. The somatosensory system can be broken down into a number of different modalities and is comprised of the sensory receptors receiving stimuli (see Table 2.1), the afferent neurons (in the peripheral nervous system and spinal cord) transmitting encoded stimuli, and the different centers in the brain (e.g., somatosensory cortex located in the postcentral gyrus).

The basic function of these receptors are for the receptor organs/body to receive external stimuli (whether it is mechanical, thermal, or chemical), to transduce this stimuli through a nonlinear transformation into an electrical current, which then gets propagated down the afferent sensory nerve ending (with properties shown in Table 2.2) as stereotypical electrical pulses (action potentials). The receptor organ is responsible for encoding information about a specific external stimuli into a series of action potentials (spike train) that get sent to the brain to be interpreted by higher level cognitive functions. The perception of these signals is a topic of neuroscience that will not be discussed in this work.

2.2.2 Pacinian Corpuscle

Haptic systems designed to interface with the human hand will be able to interface with all of these receptor types, but the primary concern of this study are the cutaneous mechanoreceptors 2.4, specifically the Pacinian corpuscle. Each mechanoreceptor has three key properties: receptive field area, frequency response range, and sensitivity. The mechanoreceptor of interest, the PC afferent, is a common target of haptic systems with vibrotactile displays. PC's have very unique response characteristics, they are extremely sensitive to vibrations (minimum sensitivity of 10 nanometers (nm) on the skin surface or 3 nm on the corpuscle surface at 200 Hz), they very strongly reject low frequency mechanical indentations (up to

Receptor Type	**Fibre group**	**Fibre name**	**Modality**
Cutaneous and subcutaneous mechanoreceptors			*Touch*
Messiner's corpuscle	Aα,β	RA	Stroking, fluttering
Merkel disk receptor	Aα,β	SAI	Pressure, texture
Pacinian corpuscle	Aα,β	PC	Vibration
Ruffini ending	Aα,β	SAII	Skin stretch
Hair-tylotrich, hair-guard	Aα,β	G1,G2	Stroking, fluttering
Hair-down	Aδ	D	Light stroking
Field	Aα,β	F	Skin stretch
Thermal receptor			*Temperature*
Cool receptors	Aδ	III	Skin cooling (25 °C)
Warm receptors	C	IV	Skin warming (41 °C)
Heat nociceptors	Aδ	III	Hot temperature($>$ 45 °C)
Cold nociceptors	C	IV	Cold temperature ($<$5 °C)
Nociceptor			*Pain*
Mechanical	Aδ	III	Sharp, pricking pain
Thermal-mechanical	Aδ	III	Burning pain
Thermal-mechanical	C	IV	Freezing pain
Polymodal	C	IV	Slow, burning pain
Muscle and skeletal mechanoreceptors			*Proprioception/Kinesthetic*
Muscle spindle primary	Aα	Ia	Muscle length and speed
Muscle spindle secondary	Aβ	II	Muscle stretch
Golgi tendon organ	Aα	Ib	Muscle contraction
Joint capsule mechanoreceptors	Aβ	II	Joint angle
Stretch-sensitive free endings	Aα	III	Excess stretch or force

Table 2.1: Table of somatosensory receptors, how they can be categorized, and their associated Modalities. Adapted from [42]

60 dB per decade) and they exhibit phase locking to stimuli in a similar fashion to the auditory system [37] [36]. Based on these properties and psychophysical experiments it has been demonstrated that the PC is key when using tools where distal vibrations generated by tool usage is sensed by the PC's sensitive response.

The morphology and structure of the Pacinian corpuscle is shown in Figure 2.5. The main body of the receptor is a capsule that is composed of layers of flattened cytoplasmic lamellae separated by fluid filled spaces that also contain collagen. There are two types of layers of lamellae, the outer layer with relatively larger spacings between layers and the

	Cutaneous nerve	Fibre diameter	Conduction velocity
Myelinated			
Large	Aα	12-20 μm	72-120 m/s
Medium	Aβ	6-12 μm	37-72 m/s
Small	Aδ	1-6 μm	4-36 m/s
Unmyelinated			
–	C	0.2-15 μm	0.4-2.0 m/s

Table 2.2: Basic classification of afferent sensory fibre groups in the peripheral nervous system. [42]

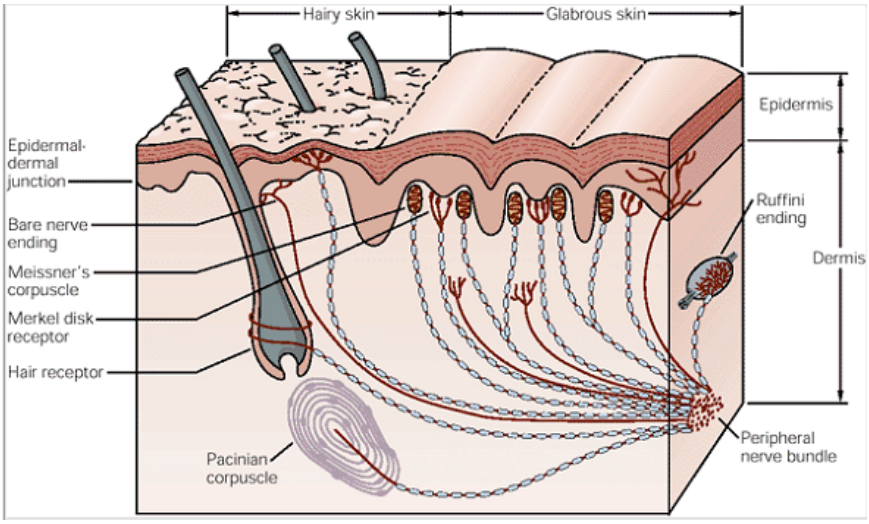

Figure 2.4: Illustration of cutaneous mechanoreceptors in humans. Taken from [42].

inner layer with distinctive hemilamellae tightly packed. [4] The outer core is determined to primarily act as a mechanical high pass filter, contributing to the sharp fall off of frequency response at low frequencies [46]. The inner core is considered to be modified Schwann cells, which may play a role in the electrophysiology of the PC's mechanotransduction [56].

This corpuscle surrounds an unmyelinated axon (e.g. unmyelinated terminus, neurite, dendrite). The unmyelinated terminus has small cytoplasmic extensions along its length that have similar appearances to dendritic spines. Dendritic spines are typically electrically active membranes that are sites that receive synaptic activity, so it has been hypothesized

Receptor	Receptive field	Frequency Range	Best Frequency	Sensitivity Threshold
Messiner's corpuscle (RA)	1-100 mm^2	1-300 Hz	50 Hz	2 μm
Merkel disk receptor (SAI)	2-100 mm^2	0-100 Hz	5 Hz	30 μm
Pacinian corpuscle (PC)	10-1000 mm^2	5-1000 Hz	250 Hz	0.01 μm
Ruffini ending (SAII)	10-500 mm^2	0-8 Hz	0.5 Hz	40 μm

Table 2.3: Table of mechanoreceptors and relevant sensory properties (receptive field, frequency response, sensitivity). Adapted from [69].

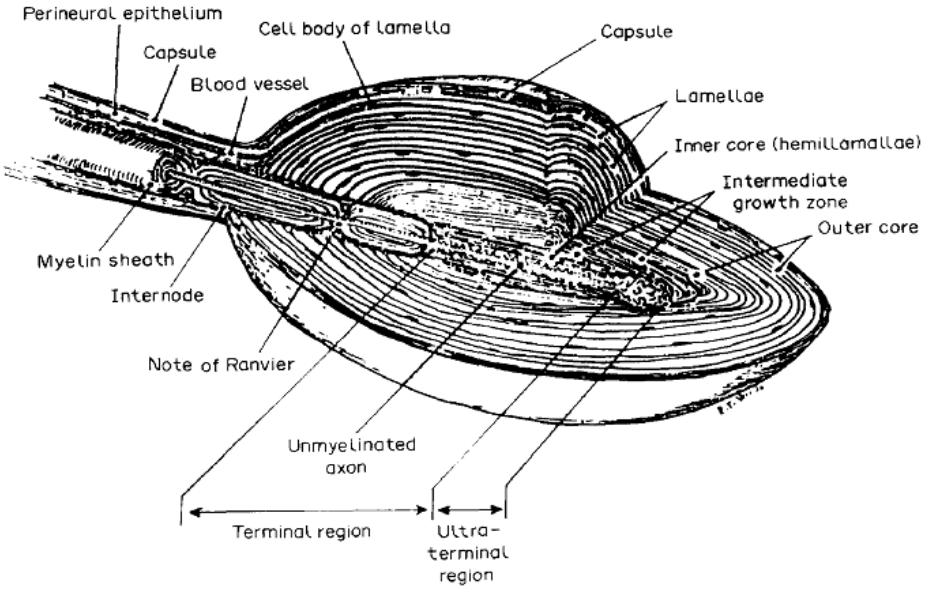

Figure 2.5: Illustration of the Pacinian corpuscle [4].

that the extensions of the PC are the site of mechanical transduction [58] [4]. The hypothesis that this is an active membrane has been shown with the discovering of sodium channels in this portion of the membrane [55][56] and of possible glial-neuronal synaptic connections [57]. It has been further hypothesized that various mammalian mechanosensitive receptors ranging from mechanosensitive Na^+, transient receptor potential, or degenerin/epithelial sodium family of channels respond to mechanical forces to generate the PC's electrical response.

The proximal side of the unmyelinated neurite, before the neurite leaves the capsule, changes into a myelinated neurite. In almost all samples one node of Ranvier lies inside

the capsule [61]. After the neurite leaves the capsule it remains a myelinated neurite that can be categorized as a Aα or Aβ nerve fibre (See Table 2.2).

The direct study of the unmyelinated neurite has been historically limited due to the difficulty in decapsulating the neuron [48]. There are still no known direct patch clamp studies of the neurite to understand its electrophysiology, which limits our understanding of the behavior of this receptor. Despite that, a large number of electrophysiological recordings have been performed on its afferent nerve ending in order to characterize the overall response to mechanical stimuli. Sato was one of the first to characterize the frequency response (response to sinusoidal vibrations) of the PC along with its response to temperature variations [63]. Bolanowski and his colleagues continued collecting more detailed frequency and temperature response recordings [11] [9]. Electron microscopy studies were performed to discover the structure of the unmyelinated neurite [10] and currently studies continue to try to understand how they encode stimuli, what are the functions of PCs along with other mechanoreceptors, and how they are used in perception [43] [65] [7].

2.3 Electrophysiology

In order to understand the biophysical mechanisms of the sensory nerve fibres, the general theory of how nerve fibres generate and propagate action potentials needs to be understood. The primary functional unit of a nerve fibre is its cell membrane. The membrane and proteins embedded in it are responsible for generating the potential changes necessary to propagate an action potential. Figure 2.6 shows a diagram of a neuron's cell membrane. Like all cell membranes it is composed of a phospholipid bilayer that separates the extracellular and intracellular (cyotoplasmic) space. The phospholipid molecules consists of a hydrophillic head (polar) and two hydrophobic tail (non-polar). In water (e.g., the membrane *in vivo* or in solution) the molecules arrange themselves in a bilayer with the hydrophillic heads facing outwards and the hydrophobic tails facing inwards, driven by the hydrophobic effect. Water and water soluble molecules cannot directly pass through this

bilayer. The non-polar tails, which are approximately 30Å, act as a dielectric (insulator) which gives the membrane a high resistance (1000 to 10000 Ωcm^2) and also capacitance (approximately $1\mu F/cm^2$) [59].

Surrounding the nerve membrane is an aqueous solution with varying concentrations of ion species such as Na^+, K^+, Ca^{2+}, Cl^- and organic anions A^-. Different concentrations of these ion species in the intracellular and extracellular spaces create a potential difference across the membrane. This membrane potential is how the neuron transfers information, its primary signaling mechanism. In order for the neuron to change the membrane potential, different proteins called ion channels are distributed throughout the surface the membrane. These ion channels will open under specific conditions to allow different ions to flow across the membrane. There are a large population of these channels opening and closing based on a stochastic process, but the overall statistical behavior of these channels are well formed and predictable. The opening and closing of these populations of ion channels is what creates the stereotypical action potential signal that all neurons generate, which will be discussed later.

There are many types of ion channels that can be classified by their gating mechanism (what external signal causes these channels to open or close) and by their ion specificity (which ion species will the channel transfer). Possible gating signals include voltage, ligands (chemical binding), photons, protons (pH sensitive channels) and mechanical force while ion specificity can include Na^+, K^+, Ca^{2+}, Cl^-, or combination of ions. For basic electrophysiology we are concerned primarily with voltage-gated Na^+ and voltage-gated K^+ channels. When mechanotransduction is considered in later sections, the theories on mechanosensitive ion channels will be introduced (Section 2.4.3).

With these voltage-gated ion channels, they remain closed when the membrane is at its resting potential (the flow and concentration of ionic species in the intracellular and extracellular space is in equilibrium). The resting potential is typically negative relative to the extracellular space for most nerve membranes. When the membrane voltage rises above a threshold, the channels begin to rapidly open to generate an action potential. First

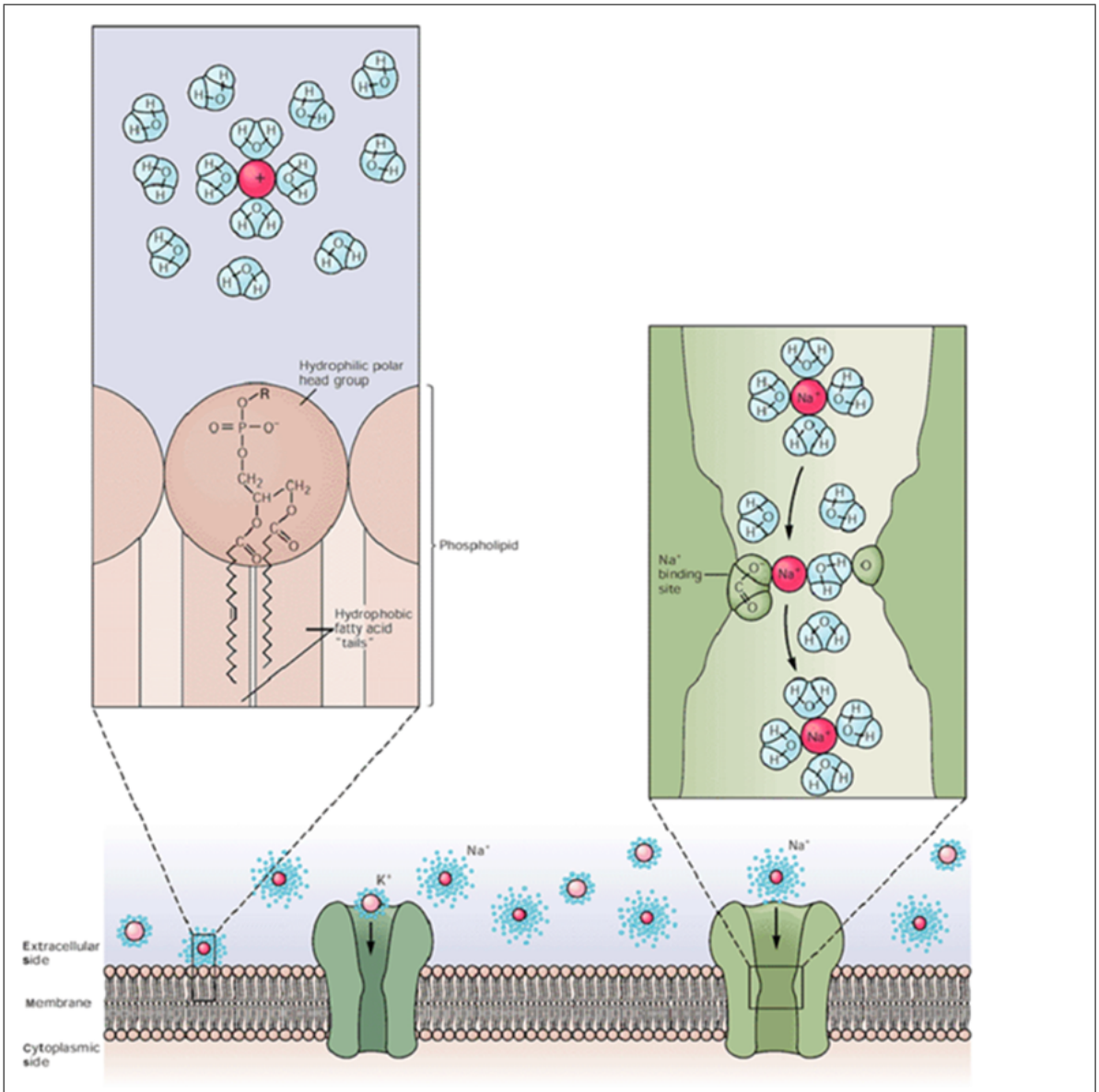

Figure 2.6: A diagram of a neuron's membrane adapted from the text "Principles in Neural Science" [42].

The lipid bilayer (left enlargment) formed with its hydrophobic tails joined and hydrophillic heads exposed, is surrounded by water with ions in solution. Due to the effective size of the ion in water, it is improbable the ions will flow across the membrane.

The membrane is also includes ion channels (right enlargement and bottom) that under certain conditions will allow specific species of ions to cross the membrane.

the voltage-gated Na^+ channel opens, allows an influx of sodium ions, and this influx of positive charges causes the membrane potential to rise. This increase in potential causes a cascade for more nearby sodium channels to open. Once the sodium channels have opened, they begin to deactivate and close. At the same time once the potential reaches a certain upper threshold voltage-gated K^+ channels open, allowing an efflux of K^+ ions to leave the nerve fibre, causing a drop in potential until it drops below the initial resting potential. Now the fibre is in a refractory (or hyperpolarization) state where no new action potential can be generated until the fibre recovers. This refractory period is caused by the inactivation process of the Na^+ channel and the hyperpolarization voltage caused by the K^+ channel. The period caused by the inactivation of Na^+ is actually called the absolute refractory period because no new action potential can be generated while the period caused by hyperpolarization is a relative refractory period where a stronger stimuli can still generate an action potential.

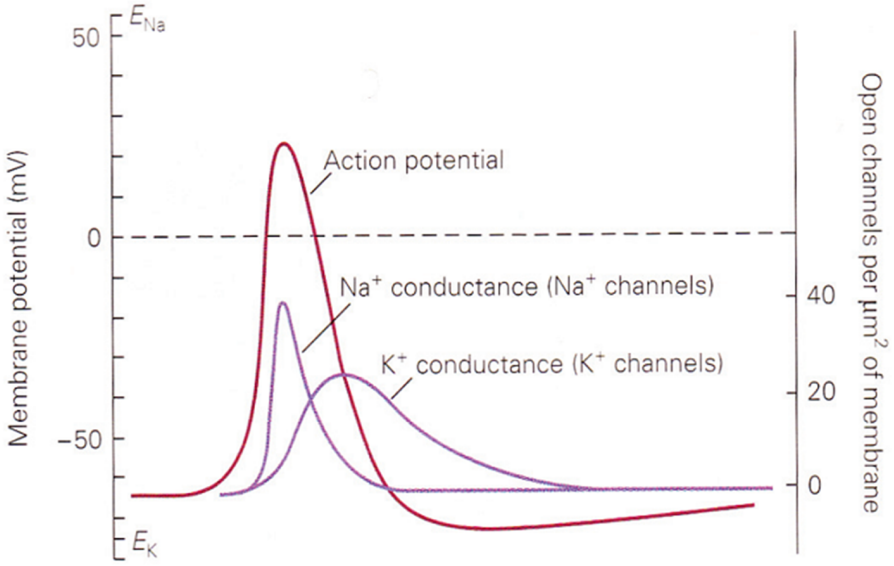

Figure 2.7: Stereotypical action potential signal with Na^+ and K^+ conductance [42].

The refractory period is a key process that controls the rate at which spikes are generated and also allows the action potential to propagate down a nerve fibre. If an action potential is moving down one direction of the fibre, the rate at which is moves is much quicker than the

rate the refractory period recovers, which means a single action potential that has traveled some distance will only continue to generate new action potentials ahead of it, not behind it. The way action potentials travel through the nerve fibre is discussed in Section 2.4.5.

2.4 Pacinian Corpuscle Models

2.4.1 Loweneski and Skalak Mechanical

Loweneski and Skalak developed a model of the mechanical transmission properties of the Pacinian corpuscle [46]. Their model was based on three mechanical properties of the corpuscle and the interaction of its layers:

- *(Lamella Compliance)* The lamella layers are thin elastic impermeable tissue that act as barriers between fluids and retains shape by elastic force
- *(Lamella Connection Compliance)* Interconnection matrix between lamellae act as weak elastic connections between lamellae but do not restrict flow to inter-lamellar fluid
- *(Viscous Resistance)* Inter-lamellar fluid between each lamellae provides viscous resistance

The geometry of the Pacinian corpuscle is first reduced to a simple cylindrical model where mechanical compression and pressure is generated symmetrically across the length of the inner core and nerve ending, shown in Figure 2.8.

The model then makes a number of assumptions including the core of the corpuscle is a rigid plate, fluid inertia is negligible because Reynold's number of the flow is small and mass of lamellae is ignored. The three mechanical properties along with the lamellae form the equivalent computation mechanical and electrical models seen if Figure 2.9. The elasticity due to the thin elastic membrane (lamella compliance) is modeled as a simple spring between each lamella and a fixed plane. The elasticity due to the lamella weak elastic

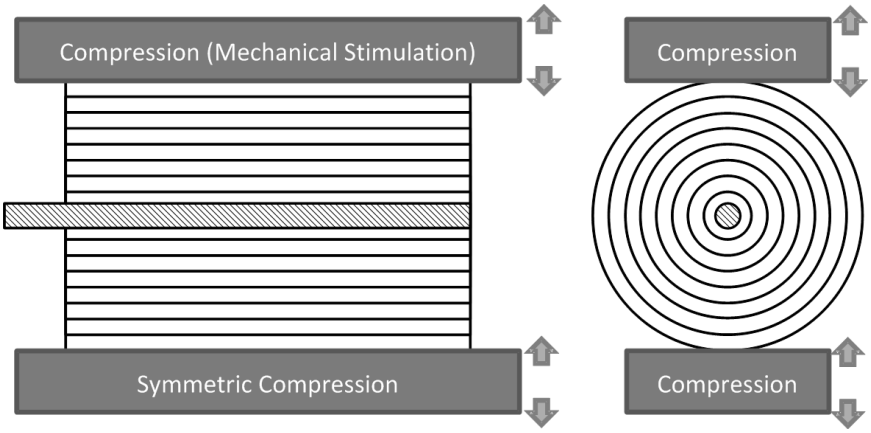

Figure 2.8: Reduction of Pacian corpuscle geometry by Loewenstein and Skalak.

interconnections (lamella connection compliances) is also modeled as a simple spring that is between each layer. Viscous resistance of pressure caused by the inter-lamellar fluid is modeled as dashpot. Each of these discrete mechanical components has an equivalent electrical component listed in Table 2.4 that is used to create the electrical model.

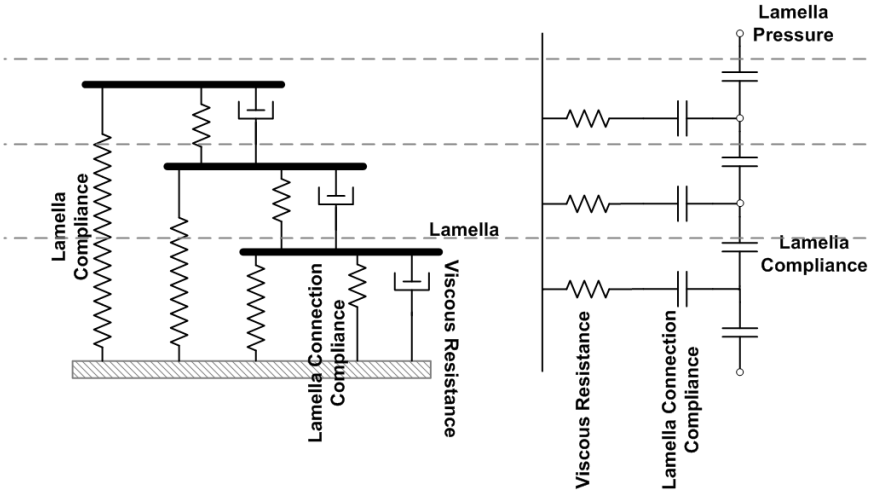

Figure 2.9: Computation mechanical and electrical model of Pacinian corpuscle mechanical transmission proposed by Loewenstein and Skalak.

Loewenstein and Skalak created a numerical example of the corpuscle [46] based on their analysis of transmission and published experimental mechanical data from Hubbard [35]. Their example consisted of 30 layers with all parameters listed in Table 2.5.

Mechanical Quantity		Electrical Quantity	
Pressure	F/cm^2	Voltage	$volts$
Displacement	cm	Charge	$coulombs$
Velocity	cm/sec	Current	$amperes$
Mass	g	Inductance	$henries$
Viscous resistance (Friction)	$F \cdot sec/cm^2$	Resistance	Ω
Compliance	cm^3/F	Capacitance	$farads$

Table 2.4: Equivalent mechanical and electrical quantities between pressure and voltage.

Lamella no.	Lamella compliance $(cm^3/F, farad)$	Lamella connection compliance	Viscous resistance $(F/cm^3, \Omega)$
1	1.69×10^{-3}	1.32×10^{-7}	4.88×10^{5}
2	1.44×10^{-3}	1.59×10^{-7}	3.24×10^{5}
3	1.23×10^{-3}	1.89×10^{-7}	2.27×10^{5}
4	1.05×10^{-3}	2.22×10^{-7}	1.66×10^{5}
5	8.96×10^{-4}	2.57×10^{-7}	1.25×10^{5}
6	7.65×10^{-4}	2.95×10^{-7}	9.72×10^{4}
7	6.54×10^{-4}	3.36×10^{-7}	7.70×10^{4}
8	5.58×10^{-4}	3.80×10^{-7}	6.21×10^{4}
9	4.77×10^{-4}	4.28×10^{-7}	5.09×10^{4}
10	4.08×10^{-4}	4.80×10^{-7}	4.22×10^{4}
11	3.49×10^{-4}	5.37×10^{-7}	3.54×10^{4}
12	2.99×10^{-4}	5.98×10^{-7}	3.00×10^{4}
13	2.56×10^{-4}	6.64×10^{-7}	2.56×10^{4}
14	2.19×10^{-4}	7.36×10^{-7}	2.20×10^{4}
15	1.88×10^{-4}	8.14×10^{-7}	1.91×10^{4}
16	1.62×10^{-4}	8.98×10^{-7}	1.66×10^{4}
17	1.39×10^{-4}	9.89×10^{-7}	1.45×10^{4}
18	1.20×10^{-4}	1.09×10^{-6}	1.27×10^{4}
19	1.03×10^{-4}	1.19×10^{-6}	1.12×10^{4}
20	8.94×10^{-5}	1.31×10^{-6}	9.87×10^{3}
21	7.53×10^{-5}	1.77×10^{-6}	4.79×10^{3}
22	6.37×10^{-5}	1.97×10^{-6}	4.18×10^{3}
23	5.41×10^{-5}	2.18×10^{-6}	3.64×10^{3}
24	4.62×10^{-5}	2.42×10^{-6}	3.18×10^{3}
25	3.98×10^{-5}	2.68×10^{-6}	2.77×10^{3}
26	3.44×10^{-5}	2.97×10^{-6}	2.41×10^{3}
27	3.01×10^{-5}	3.29×10^{-6}	2.09×10^{3}
28	2.65×10^{-5}	3.64×10^{-6}	1.81×10^{3}
29	2.36×10^{-5}	4.02×10^{-6}	1.56×10^{3}
30	2.13×10^{-5}	4.45×10^{-6}	1.34×10^{3}

Table 2.5: Equivalent mechanical and electrical quantities between pressure and voltage.

2.4.2 Hodgkin Huxley Dynamics

The Hodgkin Huxley model is the classical model of neuron potential dynamics, developed by Alan Hodgkin and Andrew Huxley in 1952. For their work they received the Nobel Prize in Physiology or Medicine, and their model is still the standard today to accurately describe neurons and other excitable cells.

The model begins with a circuit representation of the the nerve membrane where the current caused by each ion is modeled as a non-linear variable conductance in series with a battery seen in Figure2.10. The variable conductance represents the variable number of channels that are open allowing ions to flow through generating current, and the battery is the resting potential (Nernst potential) that represents the equilibrium balance of ions. An assumption is made that each ion species travels across the membrane independently from the other ions, which means the ion pathways operate in parallel. This means the contributing current for each ion is in parallel of all other contribution ions currents. There are three ionic currents, the Na^+ channel, K^+ channel, and a leakage channel that models the natural permeability of the membrane.

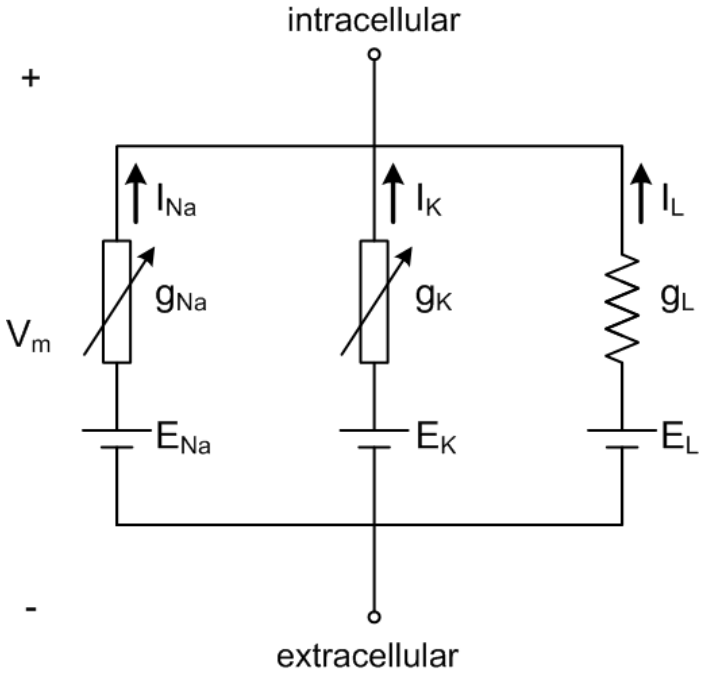

Figure 2.10: Basic circuit representation of Hodgkin Huxley's model.

These parallel ionic currents follow Kirchhoff's current law where the total current of the membrane is the sum of each ionic current. Note the factor μ is not part of Hodgkin Huxley but an addition by Bell and Holmes in order to scale the conductance (and in effect

the ionic current) by a factor to support an overall higher response frequency.

$$I_m = \mu \cdot (I_{Na} + I_K + I_L) \tag{2.1}$$

Each ionic current is simply the conductance times the voltage difference.

$$I_{Na} = \eta g_{Na}(t, v_m) \cdot [V_m - E_{Na}] \tag{2.2}$$

$$I_K = \eta g_K(t, v_m) \cdot [V_m - E_K] \tag{2.3}$$

$$I_L = \eta g_L \cdot [V_m - E_L] \tag{2.4}$$

Note the coefficient η is a temperature dependent coefficient discussed in Section 2.4.4 that was not part of Hodgkin Huxley's original model. The conductance of the voltage-gated Na^+ and K^+ channel change depending on time and the voltage based on the stochastic behavior of the population of each channel. The leakage of ion is a simple constant leakage conductance.

The conductance of the Na^+ and K^+ channels are relative to the probability that a large population of channels is open. Therefore the conductance when a given number of channels N_i exists with a probability of p_i being open where a single open channel has a conductance of γ_i is as follows

$$g_{Na} = N_{Na} p_{Na} \gamma_{Na} \tag{2.5}$$

$$g_K = N_K p_K \gamma_K \tag{2.6}$$

The maximum conductance is the conductance when all N_i channels are open

$$\bar{g}_{Na} = N_{Na} \gamma_{Na} \tag{2.7}$$

$$\bar{g}_K = N_K \gamma_K \tag{2.8}$$

When N_i is large, the law of large number says we can assume the result will be close

to the expected value so we assume

$$g_{Na} = \bar{g}_{Na} p_{Na} \tag{2.9}$$

$$g_K = \bar{g}_K p_K \tag{2.10}$$

Each channel is separated into independent subunits that each have a probability of being open. For Na^+ there are three activating subunits and one inactivating subunit, which we will call m-gate and h-gate respectively. For K^+ there are four activating subunits called n-gates. In order for a whole Na^+ or K^+ channel to be open, all four subunits must be open. Therefore the probability that a ion channel is open is

$$p_{Na} = m^3 h \tag{2.11}$$

$$p_K = n^4 \tag{2.12}$$

where the variables m, h, and n are the probability that the corresponding gate is open.

Each of these subunit gates are changing independently and the behavior of each gate is assumed to be a first order kinetic process with an opening (α) and a closing (β) rate.

$$\frac{dm}{dt} = Q_{10}[\alpha_m(1-m) - \beta_m m] \tag{2.13}$$

$$\frac{dh}{dt} = Q_{10}[\alpha_h(1-h) - \beta_h h] \tag{2.14}$$

$$\frac{dn}{dt} = Q_{10}[\alpha_n(1-n) - \beta_n n] \tag{2.15}$$

Note Q_{10} is a temperature dependent coefficient discussed in Section 2.4.4. Each of the rates depend on time and the membrane voltage and the exact equations of the rates were

fitted by Hodgkin and Huxley in their original experiments [34].

$$\alpha_m(v_m,t) = \frac{0.1(25-v_m)}{exp\left[0.1(25-v_m)\right]-1} \qquad \beta_m(v_m,t) = 4\cdot exp\left(-\frac{v_m}{18}\right) \tag{2.16}$$

$$\alpha_h(v_m,t) = 0.07\cdot exp\left(-\frac{v_m}{20}\right) \qquad \beta_h(v_m,t) = \left[exp\left(\frac{30-v_m}{10}\right)\right]^{-1} \tag{2.17}$$

$$\alpha_n(V_m,t) = \frac{0.01(10-v_m)}{exp\left(\frac{10-v_m}{10}\right)-1} \qquad \beta_n(v_m,t) = 0.125exp\left(\frac{-v_m}{80}\right) \tag{2.18}$$

It is also useful to note an equivalent form of the Hodgkin Huxley subunit probability equations that describes the first order kinetics in terms of its steady state response (m_∞, h_∞, n_∞) and time constant (τ_m, τ_h, τ_n).

$$\frac{dm}{dt} = (m_\infty - m)/\tau_m \tag{2.19}$$

$$\frac{dh}{dt} = (h_\infty - h)/\tau_h \tag{2.20}$$

$$\frac{dn}{dt} = (n_\infty - n)/\tau_n \tag{2.21}$$

$$m_\infty = \alpha_m/(\alpha_m+\beta m) \qquad \tau_m = 1/(\alpha_m+\beta_m) \tag{2.22}$$

$$h_\infty = \alpha_h/(\alpha_h+\beta h) \qquad \tau_h = 1/(\alpha_h+\beta_h) \tag{2.23}$$

$$n_\infty = \alpha_n/(\alpha_n+\beta n) \qquad \tau_n = 1/(\alpha_n+\beta_n) \tag{2.24}$$

In Bell and Holmes' model of the electrophysiology of the Pacinian corpuscle [5] they made a few modifications when implementing Hodgkin Huxley's dynamics. First the Na^+ ion channel is replaced by a mechanosensitive channel (see Section 2.4.3). They scale the ionic currents (Equation 2.2 - 2.4) by a factor of μ (chosen as $\mu = 8$) in order to support a frequency response of up to 1000 Hz. Different maximum conductances for Na^+ (Equation 2.7) and K^+ (Equation 2.8), along with the leakage current (Equation 2.4) were also chosen.

2.4.3 Mechanosensitive Channel

The one of the potential means of conversion from mechanical pressure to neural potentials is hypothesized to be caused through the nerve membrane by mechanosensitive ion channel. These types of channels were first reported by Sachs and Guharay in 1984 [25]. These mechanosensitive ion channels have been primarily been studied in bacteria, simple single cell eukaryotes (e.g., protists), and insect animal models. While the exact source for mechanotranduction has not been determined in Pacinian corpuscles, there is evidence that mechanosensitive voltage-gated Na+ selective ion channels are responsible [68][56]. Other possible sources of mechanotransduction include channels currently not known to exist in Pacinian corpuscles such as degenerin/epithelial Na channels (DEG/ENaC) and transient receptor potential channels (TRP). While it is not known if these other channels exist in the Pacinian corpuscle, the dynamics of these channels can suggest ways the Pacinian corpuscle transduction occurs. Another possible source of mechanotransduction is the existence of a glutamate signaling pathway causing synaptic behavior between the Pacinian corpscule's neural and glial (lamellae) membranes [57].

There has been a significant amount of recent research on discovering different mechanosensitive ion channels or transduction pathways such as the TRP and DEG/ENaC family of proteins. While these proteins have not been found directly in the capsule of the Pacinian corpuscle, there is circumstantial evidence that these proteins could be the source of mechanical transduction since they have been observed in other mechanoreceptors and in the afferent nerve fibres Aα and Aβ [68] that are the afferent nerve fibres of Pacinian corpuscles. In recent reviews of research on the molecular bases of mechanosensory transduction [67] [49] [20] it is seen there is a significant amount of discovery of these molecular systems along with conceptual models of their operations. A good reference on the state of the art of molecular mechanotransduction studies ranging from bacterial MS channels to mammalian TRP, DEG/ENaC and theoretical models of mechanotranduction are the volumes "Mechanosensitive Ion Channels, Part A" and "Mechanosensitive Ion Channels, Part B" in the series *Current Topics in Membranes* [27] [28].

The model of mechanosensitive channel that are of concern for this study is the older traditional model Bell and Holmes used in their Pacinian corpuscle theory [5] [6], which is related to the models of mechanosensitive channels derived by Sachs, Guharay and Lecar [25] [62]. There are basic principles that are shared by all the models. All models assume that the opening and closing dynamics of the channel depend on the free energy of the channel caused by an applied force. The gating mechanism has two possible states, open (o) or shut (s) and it is assumed that the gate is represented by a nonlinear one-dimensional spring with a potential energy function $\phi(x)$ shown in Figure 2.11. The basic principle is each state o, s behaves as an oscillator around its equilibrium point and a certain amount of energy is needed in order to transition between the o and s states, signified by the point x_b on the potential field example in Figure 2.11.

Bell and Holmes deviate from Sachs and Lecar's model in the way they describe the mechanics of the potential energy function. Bell and Holmes also extend this gating mechanism into a full channel model similar to Hodgkin Huxley's voltage-gated Na+ channel. They assume the mechanosensitive channel has four gating mechanisms (three activating m-gates and one inactivation h-gate). The activating m-gate mechanism has a dependence on the free energy caused by applied force while the inactivating h-gate is based on Hodgkin Huxley's h-gate.

The formal derivation of this model by Bell and Holmes [5] [6] is provided as follows to show what physical principles the model is based on since there has been a lack of experimental and physical evidence on the dynamics of these channels in the Pacinian corpuscle. It is important to keep in mind what assumptions and approximations are made in their derivation.

In a one dimensional (x) system given a potential energy function $\phi(x)$ and a constant force F, the Lagrangian for the gate (as in classical mechanics) is of the form

$$L = T - V = \frac{m}{2}\left(\frac{dx}{dt}\right)^2 + Fx - \phi(x)$$

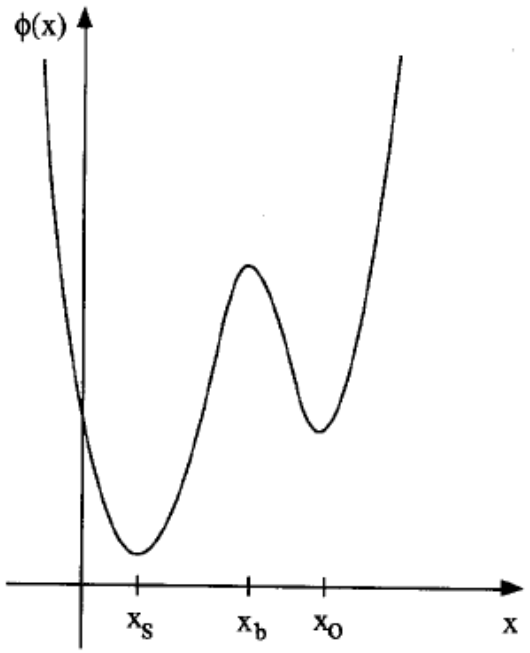

Figure 2.11: Example form of the potential energy function of the mechanosensitive channel's gating mechanism modeled as a non-linear spring. The x-axis is the distance of deformation caused by a force, x_s is the point of equilibrium energy when the state is shut, x_o is the point of equilibrium energy when the state is open, and x_b is the potential barrier that needs to be overcome to transition between states.

where T is the kinetic energy and V is the potential energy. $\frac{m}{2}(\frac{dx}{dt})^2 - Fx$ is the total kinetic energy in the system, which includes the work from the constant F force. From Hamilton's principle, the system's motion is described by

$$m\frac{d^2x}{dt^2} + \phi'(x) = F$$

By approximating the system as quasi-static, the force required set the potential energy of the system at a specific position is the derivative of the potential

$$\phi'(x) = F \tag{2.25}$$

The available energy of the system is then

$$E(x) = \phi(x) - Fx \tag{2.26}$$

Now considering x as a function of the force, x can be expanded as a function of the equilibrium point in addition to the force using a Taylor series expansion. x_j for $j = s, b$ are the equilibrium points and if we assume the force is very small $F << 1$, the expansion can be approximated by taking only the first two orders of the expansion. The coefficients of the expansion are labeled as constants $c_{j,1}$ instead of the formal Taylor series coefficients.

$$x \sim x_j + c_{j,1}F + cj, 2F^2 + \cdots \tag{2.27}$$

Then substituting Equation 2.25 with the x expansion in Equation 2.27 you get an approximation of the balance between force and energy. The equation is also expanded using a Taylor series expansion up to only the second order of the expansion (because of the assumption F is very small).

$$\phi'(x_j + c_{j,i}F + \cdots) = F \tag{2.28}$$

$$\phi'(x_j) + c_{j,1}\phi''(x_j)F + \cdots = F \tag{2.29}$$

It is obvious that $\phi'(x_j) = 0$ because x_j is the equilibrium point and by definition the first derivative is zero and also because Equation 2.28 shows it is zero. From Equation 2.28 it is also determined that $c_{j,1} = 1/\phi''(x_j)$. All other terms of the expansion ($F^2, F^3, \cdots$) have coefficients of zero so they are not shown. Substituting in 2.27 into 2.26 you get the following approximation of the energy of a state.

$$E_j \sim \phi(x_j) - x_j F - \frac{1}{\phi''(x)}F^2 \tag{2.30}$$

Now the free energy of the gate can be determined by Helmholtz free energy which is

defined as

$$A \equiv U - T^* S \tag{2.31}$$

where A is the free energy, U is the internal energy of the system, T^* is the absolute temperature, and S is the entropy. To find the amount of free energy necessary to transition from shut to open states, the change in free energy from the shut (s) to the boundary (b) state is found.

$$\Delta A_{s\to o} = \Delta E_{ns} - T^* \Delta E_{strain} \tag{2.32}$$

where E_{ns} is the energy that is not related to the small force experienced by the gate and E_{strain} is the energy from the force. Bell and Holmes use $\Delta E_{ns} = -\Delta p V_{ch}$ where Δp is the change in the dipole moment and V_{ch} is the potential across the channel (the membrane potential). ΔE_{strain} is just the difference between the available energy given a force

$$\begin{aligned} \Delta E_{strain} &= E(x_b) - E(x_s) \\ &\sim \phi(x_b) - \phi(x_s) - (x_b - x_s)F - \left(\frac{1}{\phi''(x_b)} - \frac{1}{\phi''(x_s)}\right) F^2 \end{aligned} \tag{2.33}$$

Therefore the final Helmholtz free energy for this gate is

$$\begin{aligned} \Delta A_{s\to o} \sim &-\Delta p V_{ch} + \\ &T^* \left[\phi(x_b) - \phi(x_s) - (x_b - x_s)F - \left(\frac{1}{\phi''(x_b)} - \frac{1}{\phi''(x_s)}\right) F^2\right] \end{aligned} \tag{2.34}$$

It is also assumed that the coefficient $\frac{1}{\phi''(x_b)} - \frac{1}{\phi''(x_s)}$ is much smaller than $\phi(x_b) - \phi(x_s$ so the F^2 term can be eliminated. Based on the assumed form of the potential function in Figure 2.11, it is known $\phi''(x_s) > 0 > \phi''(x_b)$, but nothing else is formally known about relative magnitude of $\phi(x)$ or $\phi''(x)$. It is also possible if the force is small enough ($F << 1$) then the significance of F^2 will be much less than the F term so F^2 can be neglected.

The free energy of the gate now affects the rate of the gate opening and closing. Using

Eyring's absolute reaction rate theory, the rate at which the channel open is found. The free energy varying over time is not considered because of the quasistatic assumption made earlier.

$$\alpha_{s\to o} = \alpha_0 T^* exp(-\frac{\Delta A}{\kappa T^*}) \tag{2.35}$$

Where α_0 is a scale constant that is related to the ratio of Boltzmann's constant and Planck's constant in the original Eyring equation formulation, κ is Boltzman's constant, and T is the absolute temperature. Substituting Equation 2.34 with Eyring's equation 2.35 and grouping coefficients into single variables, the following is obtained

$$\alpha_m = \alpha_{s\to o} = a_0 T^* exp(a_1 F + a_2 V_{ch} + a_3) \tag{2.36}$$

$$\alpha_m = a_0 T^* exp(a_1 F + a_2 V_{ch}) \tag{2.37}$$

This is now the opening rate of the m-gating mechanism of the mechanosensitive channel.

Sachs and Lecar has a similar derivation as Bell and Holmes for their model [62]. The key difference lies in their initial description of the energy function in Figure 2.11. They assume the same basic shape, but they model the open and shut state as independent Hookean springs with associated spring constants for both states (K_o, K_s). The equilibrium points of each state are separate and they define a sharp boundary in between which is the potential energy needed to cross from the shut to open state. The obtain the following model of energy

$$\Delta E_{strain} = E_o^0 - E_s^0 - (x_o - x_s)F - (\frac{1}{K_o} - \frac{1}{K_o})F^2 \tag{2.38}$$

The basic form of the model is the same as Bell and Holmes derivation in Equation 2.33 except for the second order effects. If it is determined that the second order effects are significant, it will be possible to compare the differences between these two models.

The assumption is then made that the overall mechanosensitive channel behaves like the typical Hodgkin Huxley voltage gated Na+ channel. The channel is defined to have

three activating gating mechanisms (m-gates) and an inactivating gating mechanism (h-gate). Both gates follow Hodgkin Huxley's definition where they change based on first order kinetics.

$$\frac{dm}{dt} = Q_{10}\left[\alpha_m(1-m) - \beta_m m\right] \tag{2.39}$$

$$\frac{dh}{dt} = 0.2 \cdot Q_{10}\left[\alpha_h(1-h) - \beta_h h\right] \tag{2.40}$$

Note that the coefficient Q_{10} is defined as the temperature dependent equation $3^{(T-6.3)/10}$ discussed in Section 2.4.4. A difference is in Equations 2.40 the h-gate rate $\frac{dh}{dt}$ is scaled by 0.2. This effectively increases the time constant of this first order rate equation by 5, slowing down the h-gate response. This change likely increases the refractory period of the action potential relative to the maximum firing rate of the fibre. The effect of the change is more easily visualized when the gate dynamics are in its alternative form.

$$\frac{dh}{dt} = Q_{10}\frac{(h_\infty - h)}{5 \cdot \tau_h} \tag{2.41}$$

$\beta_m, \alpha_h, \beta_h$ are all taken directly from Hodgkin and Huxley's original model and depend only on the membrane voltage (V_m). α_m depends on both membrane voltage and the basic form of the equation is taken from Equation 2.36. Bell and Holmes make an arbitrary fit of the coefficients for α_m and the final rates for their force and voltage-gated Na+ channel are

$$\alpha_m(v_m, F) = 0.000792027(T + 273.15)exp(F + 0.01v_m) \tag{2.42}$$

$$\beta_m(v_m) = \frac{1}{0.25exp(\frac{v_m}{18})} \tag{2.43}$$

$$\alpha_h(v_m) = \frac{0.01(10 - v_m)}{exp(\frac{10-v_m}{10}) - 1} \tag{2.44}$$

$$\beta_h(v_m) = \frac{0.125}{exp(\frac{v_m}{80})} \tag{2.45}$$

From this the overall conductance of this channel is now defined as

$$g_{Na} = \bar{g}_{Na} m^3 h (V_m - E_{Na}) \tag{2.46}$$

2.4.4 Neuron Thermal Properties

There are three aspects of Hodgkin Huxley dynamics that can change given different temperatures: the subunit rate (dm/dt, dh/dt, dn/dt), the resting potential (E_{Na}, E_K, E_L), and the maximum conductance ($\bar{g}_{Na}$, $\bar{g}_K$, g_L). The mechanosensitive channel model also has a temperature dependent term (see Section 2.4.3).

The subunit rate equations are scaled by a factor called Q_{10}, which was defined for neurons by Hodgkin Huxley [34]. This describes the rate of change as a result of a change in 10 $^\circ C$, which in this case is 3. The change in temperature is relative to 6.3 $^\circ C$, the temperature at which Hodgkin Huxley derived their neuron model for the squid axon. The temperature is measured in Celsius.

$$Q_{10} = 3^{\frac{T-6.3}{10}} \tag{2.47}$$

The resting potentials E_{Na} and E_K are considered Nernst potentials, which arise as a result of the forces that act upon the diffusion force of the different concentration of an ion species across a membrane and the electric field force that acts upon the charged ions. At the equilibrium point of this balance of forces the potential difference is called the Nernst potential, defined as

$$E_{ion} = -\frac{RT^*}{nF} ln \frac{[ion]_{in}}{[ion]_{out}} \tag{2.48}$$

where R is the gas constant, F is Faraday's constant, T^* is the absolute temperature in kelvins, and n is the valence (number of free electrons in the outer shell). As seen in the equation, the resting potential is proportional to the temperature. Since the resting potentials were measured by Hodgkin and Huxley in the squid axon in at 6.3 $^\circ C$, the potential

can be scaled to the appropriate temperature. In this case T is still in Celsius.

$$E_{ion} = \frac{T + 273.15}{279.45} \tilde{E}_{ion} \tag{2.49}$$

Note although the leakage resting potential E_L does not model a specific ion species (it lumps all species into a single potential) it is assumed that the same proportional dependence on temperature still applies.

Another temperature dependence is the maximum conductances $\bar{g}_{Na}$, $\bar{g}_K$, g_L have a dependence on a linear factor of temperature. This was shown by FitzHugh and other researchers [18][19]. They determined that the maximum conductances depends on the factor η as follows:

$$\eta = A[1 + B(T + 6.3)] \tag{2.50}$$

$$I_{ion} = \eta g_{ion}(t, v_m) \cdot [V_m - E_{ion}] \tag{2.51}$$

It is unclear what the exact values of parameters A and B should be since from the experimental data of FitzHugh and others [18], the maximum conductance varies from different experiments. For this study we adopt the values FitzHugh chose for their experimental studies in [19].

$$\eta = 1.1389[1 + 0.05853(T + 6.3)] \tag{2.52}$$

$$\tag{2.53}$$

The final dynamic that depends on temperature is the mechanosensitive channel model derived by Bell and Holmes [6]. See Section 2.4.3 for more details.

$$\alpha_m(v_m, F) = 0.000792027(T + 273.15)exp(F + 0.01v_m) \tag{2.54}$$

2.4.5 Cable Theory

While the Hodgkin Huxley describes the behavior of the neuron membrane at a small point (see Section 2.4.2), the cable theory describes how a local change in potential along the neuron cable will propagate through the remainder of the cable. This is how an action potential will move down the nerve fibre of the Pacinian Corpuscle (or any nerve fibre in the body) to transfer information to the rest of the somatosensory system.

Assuming the neurite is an ideal capacitive-resistive cylindrical cable, the model simplifies the cable into a one dimensional system. With a diameter d, capacitance over area of membrane C_m ($\mu F/cm^2$), and cytoplasmic resistance R_a ($\Omega \cdot cm^3$) the effective resistances and capacitance can be calculated.

$$c_m = C_m \pi d \tag{2.55}$$

$$r_a = \frac{R_a}{\pi (d/2)^2} \tag{2.56}$$

From now the one dimensional c_m and r_a will be used. The current changing over the length of the cable x can be represented as a differential equation where the change in longitudinal (x direction) current at any infinitesimal small point along the cable, the current moving along the x-axis at that point is equal to the membrane current being injected into the cable across that distance. This also means the velocity of the current in the x direction is the total current being injected into the cable.

$$\Delta i_x = i_m \Delta x \tag{2.57}$$

$$\frac{\delta i_x}{\delta x} = i_m \tag{2.58}$$

Only observing the effect of the cable's longitudinal (x direction) resistance, over a infinitesimal distance of x, the change in V_m follows Ohm's Law

$$\Delta V_m = i_x r_a \Delta x \tag{2.59}$$

This means

$$\frac{1}{r_a}\frac{\delta V_m}{\delta x} = i_x \tag{2.60}$$

Thus when only observing the effects of the longitudinal resistance the membrane voltage change can now be described as

$$\frac{1}{r_a}\frac{\delta V_m^2}{\delta^2 x} = i_m \tag{2.61}$$

What is left to consider are all of the current sources contributing to the membrane current. One of these current sources come from the capacitance of the cable.

$$i_c = c_m\frac{\delta V_m}{\delta t} \tag{2.62}$$

Additional current sources to the membrane current can come from ion channels, leakage currents, or currents coming from branches of the neurite (or other neurites connecting to the current cable). For ion channels and leakage currents, these are represented by the Hodgkin Huxley currents in Section 2.4.2. The final general form of the cable equation is

$$\frac{1}{r_a}\frac{\delta V_m^2}{\delta^2 x} = c_m\frac{\delta V_m}{\delta t} + i_s \tag{2.63}$$

where i_s is current form additional sources (e.g., Hodgkin Huxley, branches).

Two key parameters describe the properties of the cable, the cable's time constant (Equation 2.64) and length constant (Equation 2.65).

$$\tau = r_m c_m \tag{2.64}$$

$$\lambda = \sqrt{\frac{r_m}{rl}} \tag{2.65}$$

The time constant describes how fast the cable's membrane potential can change in response to current changes. The length constant describes how far current or voltage will

spread along the length of the cable.

In order to simulate the continuum description of the cable (Equation 2.63), the model is uniformly discretized across x into Δx compartments or sections, and each of these sections in series has an equivalent linear circuit representation seen in Figure 2.12.

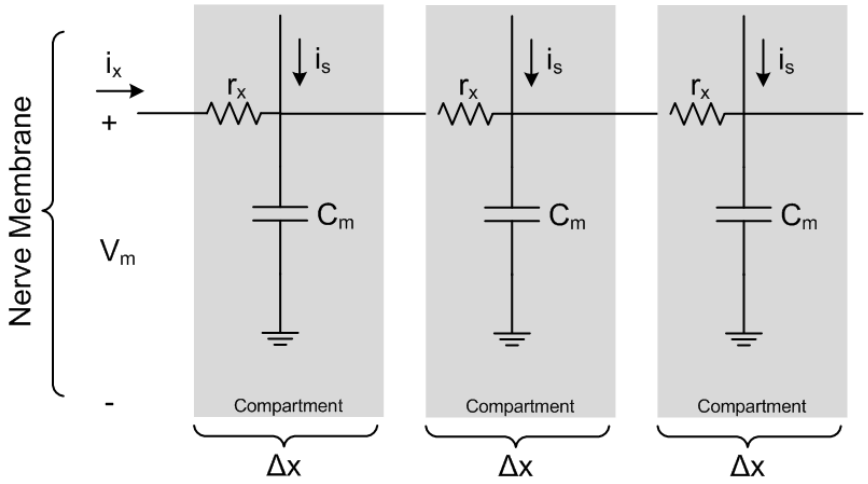

Figure 2.12: Discretized circuit representation of the cable theory equations.

2.4.6 Excitable Spines Cable Theory

There is an extension to the cable theory derived by Baer and Rinzel that models creates a continuum model of a neuron that has excitable spines [2]. For some neurites there exists small protrusions of the cell membrane (primarily structures called dendritic spines) that can be a source of action potential generation. They typically serve as the receptor area of synapses and have ion channels that can be described by the Hodgkin Huxley model. Baer and Rinzel's continuum model of the cable assumes the main cable is passive (capacitive cable c_m with leakage resistance r_l) and lumps the contributing currents from spines as a current source (I_{ss}) and resistance (r_{ss}). The distribution of spine densities over the length of the cable x is modeled through the density function $\bar{n}(x)$ and the spines injecting current (I_{ss}) into the main cable are modeled as a capacitance with current sources from

ion channels, main cable, and external sources.

$$\frac{1}{r_a}\frac{\delta V_m^2}{\delta^2 x} = c_m\frac{\delta V_m}{\delta t} + \frac{1}{r_l}V_m + \bar{n}(x)r_\infty\frac{V_{sh}-V_d}{r_{ss}} \tag{2.66}$$

$$c_{sh}\frac{\delta V_{sh}}{\delta t} = -(I_{ion} + \frac{V_{sh}-V_d}{r_{ss}} - I_s(x,t)) \tag{2.67}$$

where r_∞ is the resistance if the cable was semi-infinite ($R_m/\pi\lambda d$), and sh stands for the spine head. This model assumes that there is no coupling between spine heads (Equation 2.67) and they are only related to each other through the main cable.

An alternative to Baer and Rinzel's continuum model to model excitable spines is to model each spine explicitly as a branch of the main cable. Each spine will be a separate cable that is connected through the cable's cytoplasm to the main cable body. The geometry and parameters of each neuron will need to be defined. This creates an approximation of excitable spines that is closer to the physical properties of the spine, instead modeling the spines as a continuum that is connected to cable through a lumped resistance. The modeling of each individual spine is what is used in this study's PC model.

2.4.7 Myelinated Nerve

The afferent nerve of the Pacinian corpuscle is a Aα or Aβ cutaneous nerve [42]. These cutaneous nerve are some of the largest in the body (Aα are 12-20μm in diameter, Aβ are 6-12 μm) and support the largest conduction velocities (Aα are 72-120 m/s, Aβ are 36-72 m/s). The Aα and Aβ nerves are also myelinated, which means the fibre is surrounded by layers of insulating myelin (layers of Schwann cells) with gaps called nodes of ranvier in between sections of myelinated nerve (see Figure 2.13). The myelin portions of the nerve fibre act as an insulated cable with a reduced leakage resistance and overall capacitance, typically 100 times less for both resistance and capacitance when compared to the unmyelinated nerve fibre [59]. The behavior of the myelinated segments is similar to a passive cable with no ion channels generating active currents. The nodes of Ranvier behavior is approximately described by the original Hodgkin Huxley model where ion channels will

generate action potentials.

The functional purpose of the myelinated fibre is to act as a long distance transmission line. With the myelinated section's small leakage resistance and membrane capacitance, the conduction velocity of the fibre is greatly increased. The nodes of Ranvier with ion channels act as repeaters that maintain the strength of the action potential signal as it propagates down the axon. The large diameter of the Pacinian corpuscle's Aα and Aβ myelinated fibres also increases the conductance velocity allowing the fibre to transmit across the peripheral nerve system at a fast rate.

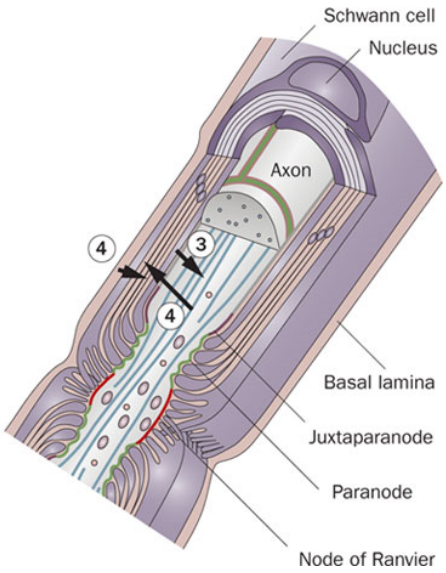

Figure 2.13: Parts of a myelinated nerve fibre. [66]

2.4.8 Summary of Bell and Holmes Model

The following is a brief summary of the key equations used by Bell and Holmes [5] that describe the membrane dynamics of the Pacinian corpuscle. Only the parameters and models implemented by Bell and Holmes are included in this summary, some of the theory in the section above are not related.

Spine Cable Theory Without Longitudinal Variation

This equation is derived from Section 2.4.5 with a membrane resistance added, but ignoring all variations along the x-axis. This assumption was made by Bell and Holmes [5]. Note $\tilde{n} = \bar{n}r_\infty$ and also does not vary with respect to x. Also since no geometry is considered all of the resistances and capacitances are in terms of area (Ωcm^2 and S/cm^2). Only the linking resistance between the spine (sh) and cable (m) is in terms of Ω which is derived based on the values in Table 2.6 ($r_{ss} = 4R_a l_{sh}/(\pi d_{sh}^2)$).

$$C_m \frac{\delta V_m}{\delta t} = -\frac{1}{R_m} V_m + \tilde{n} \frac{V_{sh} - V_m}{r_{ss}} \tag{2.68}$$

Membrane Currents (Hodgkin Huxley [34] and Bell Holmes [5])

$$C_m \frac{dV_{sh}}{dt} = \frac{V_m - V_{sh}}{r_{ss}} + \mu \cdot \left[\bar{g}_{Na} m^3 h \cdot [V_m - E_{Na}] + \bar{g}_K n^4 \cdot [V_m - E_K] + g_L \cdot [V_m - E_L]\right] \tag{2.69}$$

Channel dynamics

$$\frac{dm}{dt} = \frac{m_\infty - m}{\tau_m} \tag{2.70}$$

$$\frac{dh}{dt} = \frac{h_\infty - h}{5 \cdot \tau_h} \tag{2.71}$$

$$\frac{dn}{dt} = \frac{n_\infty - n}{\tau_n} \tag{2.72}$$

$$m_\infty = \alpha_m/(\alpha_m + \beta m) \qquad \tau_m = 1/(\alpha_m + \beta_m) \tag{2.73}$$

$$h_\infty = \alpha_h/(\alpha_h + \beta h) \qquad \tau_h = 1/(\alpha_h + \beta_h) \tag{2.74}$$

$$n_\infty = \alpha_n/(\alpha_n + \beta n) \qquad \tau_n = 1/(\alpha_n + \beta_n) \tag{2.75}$$

$$\alpha_m(v_m, F) = 0.000792027(T + 273.15)exp(F + 0.01v_m) \tag{2.76}$$

$$\beta_m(v_m, t) = 4 \cdot exp\left(-\frac{v_m}{18}\right) \tag{2.77}$$

$$\alpha_h(v_m, t) = 0.07 \cdot exp\left(-\frac{v_m}{20}\right) \qquad \beta_h(v_m, t) = \left[exp\left(\frac{30 - v_m}{10}\right)\right]^{-1} \tag{2.78}$$

$$\alpha_n(V_m, t) = \frac{0.01(10 - v_m)}{exp\left(\frac{10-v_m}{10}\right) - 1} \qquad \beta_n(v_m, t) = 0.125exp\left(\frac{-v_m}{80}\right) \tag{2.79}$$

Parameter	**Hodgkin Huxley Value**	**Bell Holmes Value**
$\bar{g}_{Na}$	0.12 S/cm^2	0.18 S/cm^2
$\bar{g}_k$	0.036 S/cm^2	0.018 S/cm^2
g_L	0.0003 S/cm^2	0.00005 S/cm^2
E_{Na}	115 mV	115 mV
E_K	-12 mV	-12 mV
E_L	-10.613 mV	-3.8038 mV
C_m	1.0 $\mu F/cm^2$	1.0 $\mu F/cm^2$
R_m	- -	2500 Ωm^2
r_a	- -	70 Ω/cm
l_{sh}	- -	0.5 μm
d_{sh}	- -	0.1 μm
d_m	- -	5 μm
r_{ss}	- -	$44.6 \times 10^7 \Omega$
$\tilde{n}$	- -	*arbitrary*
μ	- -	8
T	6.3 $^\circ C$	37 $^\circ C$

Table 2.6: Table of parameters used in membrane current equations by Bell and Holmes. Values marked as '- -' were not part of the specified model and values marked as *arbitrary* do not require a specific value and any arbitrary value can be used.

2.5 Experimental Data

The primary sources of experimental data are taken from the studies performed by Bolanowski and colleagues [11] [9] where the neural frequency response of the receptor to mechanical stimuli frequency, amplitude and temperature. The mechanical deformation stimuli in the experiments are primarily sinusoidal stimuli that was actuated on the surface of the

Pacinian corpuscle's lamellae capsule. Figure 2.14 shows as an example the response of a single Pacinian corpuscle measured in one of Bolanowski's studies.

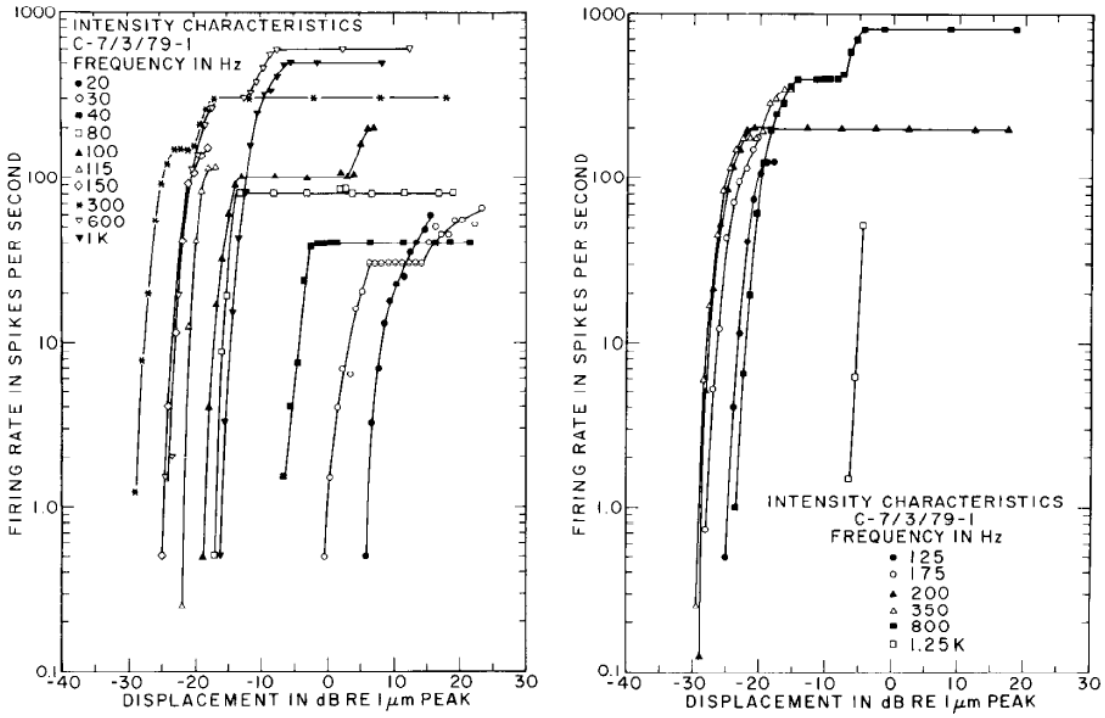

Figure 2.14: Characteristic of a single Pacinian corpuscle related neural firing rate to stimuli amplitude (in terms of dB relative to 1 μm peak to peak) and stimuli frequency. Taken from Bolanowki, et. al. 1984 [9].

2.6 Simulation Environment

2.6.1 NEURON

The NEURON simulator, developed by Hines and Carnevale at Yale beginning in 1984, is a simulation environment for biological models of individual or networks of neurons [29] [12]. The stated purposes of the simulation tool is to "provide numerically sound, computationally efficient tools for conveniently constructing, exercising, and managing models, so that special expertise in numerical methods or programming is not required for

its productive use." [12]. Over 700 scientifically published models have been reported using NEURON, which motivated the use of this simulation environment for this study. NEURON is capable of simulating complex branching morphologies and channel dynamics all with intuitive methods to adjust model and simulation parameters. All these factors play a key role in this study. Of course NEURON has many other functionalities such as modeling ionic diffusion, secondary messengers, and others, but these will not be used in this model of the PC.

NEURON was originally designed with the Hoc programming language as its main interface to design models in. NEURON now allows models to be developed in Python using in conjunction with or completely replacing the Hoc interpreter. [30] This interfaces to other scientific tools available in Python (e.g., NumPy, FiPy). To define membrane dynamics, a separate language, NMODL [31], is used. NMODL is used to define all of the membrane dynamics of an area patch of membrane, such as Hodgkin Huxley dynamics or modified Bell and Holmes dynamics. For Hodgkin Huxley membrane dynamics, the ionic currents for Na^+, K^+ and leakage current are defined, which includes their conductance equations and subunit (m, h, n) first order kinetics. Since the dynamics are defined over an area of the membrane, to apply a membrane to a cylindrical cable the membrane model is simply assigned to the cable. The NEURON simulator performs the discretization of the cable, the calculation of each segment's area, and applies the simulated membrane dynamic current results to each segment.

Numerical Differential Equation Solver

The standard solver of membrane dynamics in NEURON is a variation of the Crank-Nicholson (central difference) solver [12]. It is implemented as part of NEURON's NMODL system as the `cnexp` solver. It is shown to be stable and accurate when the first order state variables (gating subunit variables m, h, n) are linear, which is true in the case of Hodgkin Huxley dynamics and Bell and Holmes modifications.

The Crank-Nicholson numerical solver is stable and more accurate than traditional numerical solvers, namely the forward Euler and backward Euler numerical integration methods [12]. There is also a relatively minimal increase in computational complexity when compared with forward and backward Euler methods. The general form of the Crank-Nicholson method given a differential equation $V(t)$ is

$$V(t + \Delta t) = 2V(t + \frac{\Delta t}{2}) - V(t) \tag{2.80}$$

The local error of this method is proportional to the square of the step size (Δt) and is considered numerically stable [12]. Oscillations of numerical results do occur when a large amplitude change is experienced with a time constant significantly smaller than the time step Δt, but at a steady state the oscillating results decrease with amplitude approaching the analytical solution. These oscillations are of larger concern when simulating neural responses to sinusoidal stimuli changes, where time step Δt must be less than half of the wavelength of the stimuli to satisfy Nyquist-Shannon sampling theory.

In addition to local error contributed by the extrapolation error of each time step, there is also global error where local errors propagate over time causing the trajectory of the results to deviate from the analytical solution of the system. There is no standard or easy method to analyze this source of error as it depends on the dynamics of the full system being solved. Decreasing the simulation time step (Δt) can decrease the global error but limited floating point precision can also contribute to the error. Certain systems with chaotic properties and stiff dynamics equations can have global errors that rapidly increase.

Spatial Cable Solver

Neural systems in the NEURON simulator are defined as explicit geometric cables. The spatial dimension of the cable current is solved through standard discretization of the cable equations through segmentation (Section 2.4.5). To ensure accuracy of the discrete form, the number of segments per cable (the length of each segment) is important. the NEURON simulator has a general guideline for choosing the number of segments of a given cable

called the d_lambda rule [12] that can be calculated using the following function written in Python.

```
from neuron import h
def d_lambda_nseg(cable, L, d_lambda, freq):
    cable.push()          # Makes cable the primary reference point
    return h.int((L/(d_lambda*h.lambda_f(freq))+0.9)/2)*2+1
```

Code Implementation Examples

The PC model implemented is a single neuron with different types of cables and membrane dynamics all interconnected through cytoplasmic connections. To illustrate how the NEURON simulator is used to setup part of the PC model, an example is given.

To create a new cable, a call to `neuron.h.Section()` is used. The returned object is a Section object that has parameters that can be assigned. The following code can be used to setup a cable's parameters as a spine with a NMODL membrane called `pc_mem` with a length of 1 μm and diameter of 1 μm.

```
from neuron import h
head = h.Section()       # Create new neuron Section for spine head
head.nseg = 9            # Discretize head into 9 segments
head.L = 1               # Set head length
head.diam = 1            # Set head diameter
head.Ra = 70             # Set cytoplasmic/axial resistance (Ohms cm)
head.insert('pc_mem')    # Insert pc_mem membrane into head
```

The following code can be used to setup a passive fibre (a cable whose membrane includes only a leakage/membrane resistance).

```
fibre = h.Section()       # Create new neuron Section for passive fibre
fibre.nseg = 421          # Discretize fibre into 421 segments
fibre.L = 600             # Set fibre length
fibre.diam = 5            # Set fibre diameter
fibre.Ra = 70             # Set cytoplasmic/axial resistance (Ohms cm)
fibre.insert('pc_pas')    # Insert passive membrane into fibre
```

Whenever a membrane model is added to a Section, certain public variables of membrane are now available to be set throughout the cable. In the case of the `pc_pas` model, there is a conductance parameters available `g`. This can be set individually for each discrete segment of the cable. The following code can be used to set `g` on all of the segments.

```
for seg in fibre:         # Loop through all segments of the fibre
   seg.pc_pas.g = 0.0004 # Set conductance of the passive membrane
```

Segments of different sections can be connected/linked together through their cytoplasm. To connect the spine head to the main cable the function *`section1`*`.connect(`*`section2, section2 seg position, section1 seg position`*`)` can be used as follows.

```
head.connect(fibre,1,0)
```

When NEURON discretizes a cable, it divides the cable in `nseg` segments and assigns each segment to a position ranging from 0 to 1. This means that the position reference of a section is normalized to the maximum length of the whole cable section. For this study it is assumed for all cables the 1 position is distal while the 0 position is proximal.

Chapter 3

Methodology

3.1 Introduction

The model implemented in this study is primarily extended from the theories and models used by Bell and Holmes in their "Model of the Dynamics of Receptor Potential in a Mechanoreceptor" [5]. Bell and Holmes developed one of the only electrophysiology models of the Pacinian receptor and this was chosen because it is a representation of the biophysical and electrical processes of the Pacinian's sensory transduction. A model of this level of detail allows the simulation of physical properties of the receptor (e.g., nerve morphology, membrane conductance, membrane capacitance) and models of the molecular basis of mechanotransduction that contribute to the generation of receptor potentials. This model captures the dynamics and physical details of the receptor to study the sources of mechanotransduction that phenomenological models (i.e., black box models) currently cannot represent. This model also enables the study of three means of activation for the Pacinian corpuscle, through mechanical forces, external electrode stimulation and thermal changes.

The model is composed of four different components: mechanical, channel dynamics, unmyelinated terminus cable, and myelinated afferent fibre. The model of mechanical properties is taken directly from Loewenstein and Skalak's computational model, a simplified representation of fluid flow and elastic forces due to the morphology of the Pacinian corpuscle as a mechanical/electrical model [46]. The channel dynamics and unmyelinated

nerve ending models are taken from Bell and Holmes' Pacinian corpuscle model [5]. The model of the myelinated afferent fibre is based on an approximated model of myelin as a passive cable and nodes of ranvier as Hodgkin Huxley dynamics.

Model Implemented	**Modifications**	**References**
Mechanical		
Loewenstein and Skalak PC Mechanical Transmission Model	No modifications	[47], Section 2.4.1
Bell and Holmes Channel Dynamics		
Bell and Holmes Mechanosensitive Ion Channel	No modification	[5], [6], Section 2.4.3
Bell and Holmes Implementation of Hodgkin Huxley Dynamics and Currents	Added FitzHugh maximum conductance temperature dependence ([18], Section 2.4.4), added resting potential temperature dependence ([59], Section 2.4.4)	[5], Section 2.4.2, 2.4.8
PC Unmyelinated Terminus		
Bell and Holmes reduced implementation of Baer and Rinzel Continuum Spine Model	Removed Bell and Holmes' assumption that there is no longitudinal response, changed continuum model to full spine cable model with explicit geometries (Section 2.4.5)	[5], Section 2.4.8
Myelinated Afferent Fibre		
Simple Myelinated Fibre	Custom implementation of alternating capacitive (myelin) and active (node of ranvier) fibre (Section 2.4.7)	[59]

Table 3.1: Summary of component models implemented, what modifications were made, and related references.

3.2 Mechanical

The chosen mechanical model is developed by Loewenstein and Skalak's [46] because of its simplistic representation that approximates the behavior and frequency response of the physical structure. While only a mechanical/electrical interpretation of the underlying mechanics and biophysics, this simplification reduces the computational complexity of the model. It reduces a model that could consist of a 3D finite element model where fluid movement is modeled by the Navier-Stokes equation and lamellar interconnections is modeled by elastic shell model theory. Instead the model reduces the system into a scalar linear time invariant system.

The assumptions made by Loewenstein and Skalak's model reduces the possible mechanical stimuli into a 1D transient signal. This reduction prevents the simulation of spatial variations in the mechanical stimuli, but is shown by Loewenstein and Skalak [46] to have a reasonable qualitative agreement with experiments by Hubbard for static displacement and dynamic displacement [35]. See background literature Section 2.4.1 for details on how this model is derived from physical properties. The frequency response of the model is shown in Figure 3.1. While this model means spatial variations in mechanical stimuli over the geometry of the corpuscle cannot be simulated, for the experiments conducted in this study this is a sufficient approximation. At a macro-scale with most mechanical haptic stimulators, it is assumed that spatial control of the stimuli will be uniform at the scale of the Pacinian corpuscle's approximate length of 600 μm.

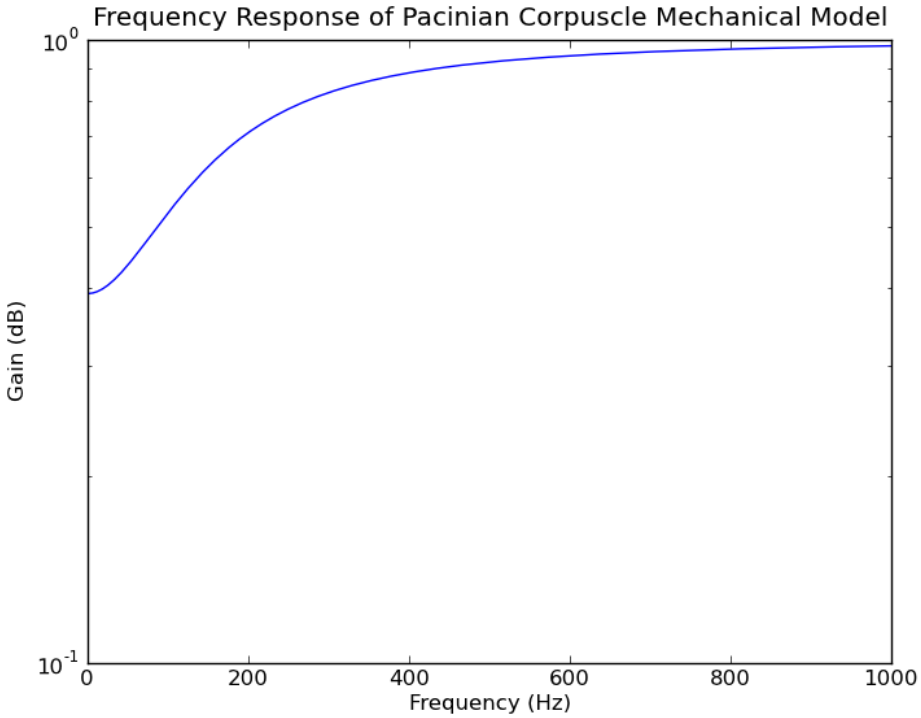

Figure 3.1: Frequency response of Loewenstein and Skalak's mechanical model.

It is assumed this model is a sufficient representation of the mechanical properties of the

Pacinian corpuscle and variations or alternative models is beyond the scope of this study. There is an observed discrepancy in the frequency response of this model where the PC has been shown to reject low frequencies at a rate of up to 60 db per decade [37].

3.3 Electrophysiology

The model of the Pacinian Corpuscle's electrophysiology encompasses Bell and Holmes' model [5] along with a model of the myelinated afferent nerve fibre and the thermal properties of channel dynamics. This is the only model found that theorizes a full biophysical model of the Pacinian neurite that includes ion channel dynamics, a hypothesized pathway of mechanical to neural transduction, and neural cable properties. By using a model with this level of physical detail, the goal is to capture nonlinear dynamics that otherwise would be extremely difficult to model given more computational or phenomenological modeling techniques.

Bell and Holmes' model describes the mechanosensitive channel hypothesized to be a strain activated Na+ channel, the remaining nerve membrane dynamics related to Hodgkin Huxley's channel dynamics, and the dendritic excitable spines cable model derived by Baer and Rinzel [2]. The implementation of these theories for this study in the NEURON simulation environment is summarized as follows. A diagram of the different electrophysiological components (excluding temperature) is shown in Figure 3.2 with the equivalent circuit representation of the model shown in Figure 3.3.

3.3.1 Nerve Fibre Cable

In Bell and Holmes model [5], the Pacinian corpuscle's nerve fibre cable is represented by Baer and Rinzel's continuum model of excitable spine dendrites. The model was reduced by assuming a completely uniform geometry and distribution of spines and channels along the neurite and by assuming no longitudinal response. The myelinated afferent nerve and its nodes of Ranvier are also not considered in the Pacinian corpuscle's action potential

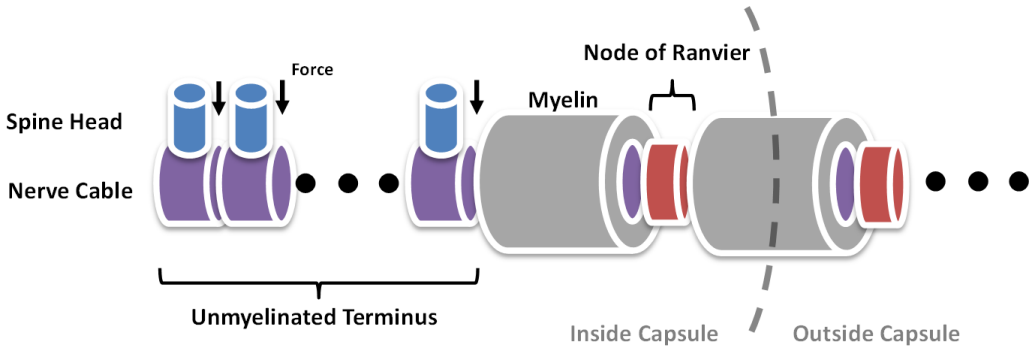

Figure 3.2: Diagram of the electrophysiological components implemented in this study. Parts not to scale.

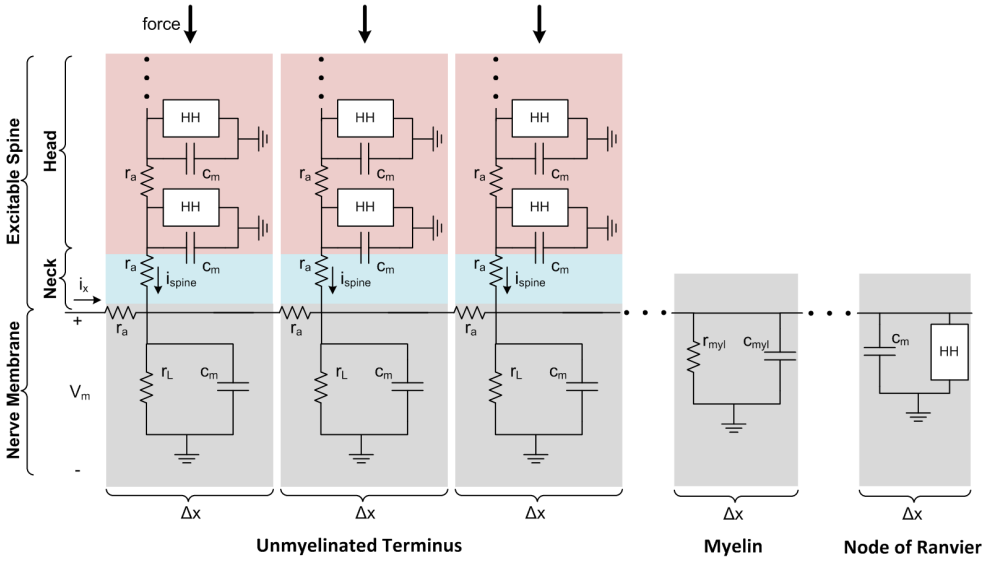

Figure 3.3: An equivalent circuit representation of the electrophysiological components implemented in this study. Refer to Figure 3.2 for system diagram.

generation. This means the one dimensional cable is not considered and only the local response of a small area of the PC and its spines are modeled. The parameters of the cable chosen by Bell and Holmes reflect a typical approximation of the dimensions and characteristics of the neurite. Figure 3.4 shows a diagram and circuit representation of Bell and Holmes' model.

For the model used in this study, the longitudinal response is considered and the cable equation is modeled (see Section 2.4.5 for explanation of cable theory). As an alternative to

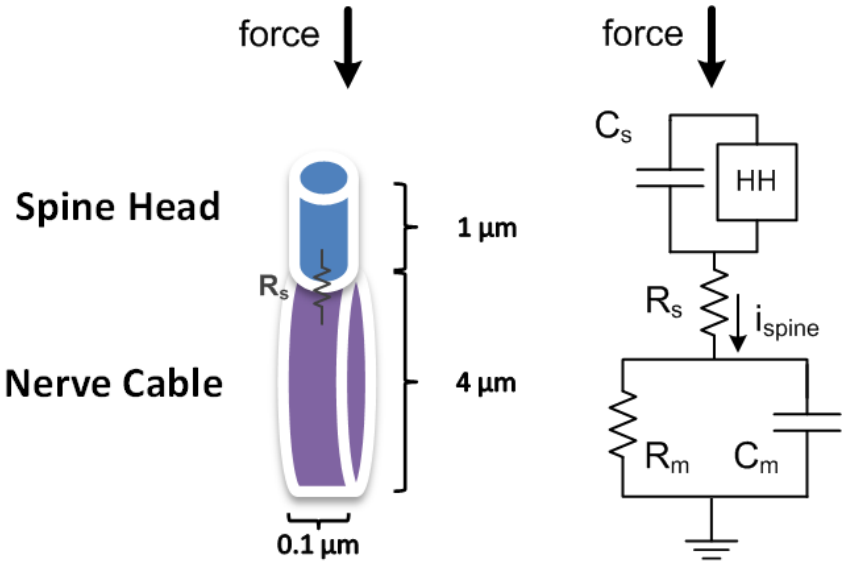

Figure 3.4: Diagram and circuit of Bell and Holmes' model of the Pacinian corpuscle.

the continuum model, the geometry and distribution of the spines are explicitly modeled. This means each spine is considered its own cable, and is connected to the main PC's neurite. The spines are still coupled only through the neurite, there is no coupling between spines through the extracellular space. These design choices allows the model to more completely consider the effects caused by the geometry and longitudinal response of the neurite and afferent nerve fibre that Bell and Holmes did not consider in order to simplify their model. By explicitly modeling the geometry of the neurite and fibres, there is a direct relationship between the anatomy of the receptor and the simulation. This allows geometry parameters to be easily varied to understand what role the morphology of the neurite plays.

With the model implemented in the NEURON simulator, the discretization process is as defined by the simulator. The geometry of the unmyelinated neurite and spines were chosen based on the electron microscopy scan of the neurite [9] and the myelinated afferent nerve geometry was chosen based on anatomical studies [61]. See Table 3.2 for the reasonable ranges of geometry parameters.

The myelinated afferent fibre is included in this study, which was not considered in past models. A simple approximate model of the myelinated fibre is used where a series of

Geometry Feature	Range of Values
Unmyelinated Neurite	
Neurite Diameter	2-5 μm
Neurite Length	600 μm
Number of Spines	1684
Spine Base Diameter	0.14 - 4.63 μm (median 0.59 μm, σ^2 1.10)
Spine Widest Diameter	0.14 - 2.99 μm (median 0.89 μm, σ^2 0.27)
Spine Height	6.76 - 0.14 μm (median 1.26 μm, σ^2 1.56)
Myelinated Afferent Nerve	
Myelinated Nerve Diameter	4.1-6.9 μm (mean 5.8 μm, σ 0.8)
Myelin Section Length	144-496 μm (mean 285 μm, σ 85)
Node of Ranvier Length	1-2 μm

Table 3.2: Table of reasonable geometry values of the Pacinian corpuscle.

alternating myelin segments (250 μm length, 5 μm diameter) and node of Ranvier segments (2 μm length, 5 μm diameter) were connected to the proximal side of the PC unmyelinated neurite. Approximately four pairs of these segments (4 myelin segments with 3 nodes of Ranvier) are implemented in the simulation for a fibre with a total length of 1006 μm. The end of the last segment is a closed boundary. The myelin segment is modeled as a simple passive cable with a 50 fold decreased membrane conductance and capacitance from the passive properties of the unmyelinated terminus. The node of Ranvier are modeled as an active membrane with standard Hodgkin Huxley Na^+, K^+ and leakage channel models. Figure 3.3 shows the schematic of the myelin fibre model and Table 3.3 shows the model parameter values.

Myelin passive conductance	0.000008 S/cm^2
Myelin passive capacitance	0.02 Fcm^2
Myelin length	250 μm
Myelin diameter	5 μm
Node of Ranvier dynamics	Hodgkin Huxley [34]
Node of Ranvier capacitance	1 Fcm^2
Node of Ranvier length	$2\mu m$
Node of Ranvier diameter	$5\mu m$

Table 3.3: Parameters used in Myelin model.

The PC found *in vivo* can have highly variable geometries, as seen in Table 3.2. To better understand how the geometry affects the action potential generation, the parameters are systematically varied. The geometry of each major component (spines, unmyelinated

terminus, myelinated fibre) are modeled as uniform in order to restrict the model complexity.

3.3.2 Nerve Membrane Dynamics

The nerve membrane dynamics of the spine are implemented as the Bell and Holmes dynamics. Although Bell and Holmes theories of PC transduction were developed in the early 1990s, there have been no other known attempts to create a biophysically accurate models of this receptor. This is due partly because the exact mechanisms of mechanical to electrical transduction has not been known, and it has only been recently where new advances in molecular biology and neuroscience are revealing more details about the Pacinian corpuscle, tactile perception, and the somatosensory system in general. To begin understanding the behavior and biophysics of this receptor better, we will use this study to begin with Bell and Holmes model.

Bell and Holmes membrane dynamics uses traditional Hodgkin Huxley currents and channel dynamics except for replacing the Na^+ channel with their derivation of the mechanosensitive Na^+ channel discussed in Section 2.4.3 and 3.3.3. In their model temperature effects were considered only for Hodgkin Huxley's Q_{10} factor (Section 2.4.4) and the temperature parameter of the mechanosensitive channel (Section 2.4.3). In this study all temperature parameters discussed in Section 2.4.4 are included in the model.

3.3.3 Mechanosensitive Channel

The mechanosensitive channel derived by Bell and Holmes [5][6] (see Section 2.4.3 for explanation of theory) is the key model to convert mechanical stimuli (mechanical force or strain) into a potential change that will generate the Pacinian corpuscle's action potential. The channel is a Hodgkin Huxley Na^+ channel with the opening rate of activating subunit (α_m) is replaced by the force activated Bell and Holmes mechanosensitive opening rate.

All remaining dynamics and equations remain the standard Hodgkin Huxley equations.

$$g_{Na} = \bar{g}_{Na} m^3 h (V_m - E_{Na}) \tag{3.1}$$

$$\alpha_m(V_m, F) = 0.000792027(T + 273.15) exp(F + 0.01 V_m) \tag{3.2}$$

$$\beta_m(V_m) = \frac{1}{0.25 exp(\frac{V_m}{18})} \tag{3.3}$$

$$\alpha_h(V_m) = \frac{0.01(10 - v_m)}{exp(\frac{10 - V_m}{10}) - 1} \tag{3.4}$$

$$\beta_h(V_m) = \frac{0.125}{exp(\frac{V_m}{80})} \tag{3.5}$$

There are three major concerns about this model. Currently there is only circumstantial evidence that a force/voltage-gated Na^+ channel replaces the standard voltage-gated Na^+ channel. It also has not been possible to directly measure the currents and voltages along the unmyelinated neurite of the Pacinian corpuscle, which means the model of the theoretical force/voltage-gated Na^+ channel cannot be tested. The final concern is the parameters that Bell and Holmes' fitted to the α_m model were designed through their simulation and analysis, and the methodology for the fit is not published. This means there is a high amount of uncertainty of whether or not this model or the fitted parameters are appropriate to represent the transduction process. There is also a concern of if in α_m the force is a linear or quadratic term, although Bell and Holmes show that force should primarily be linear [6].

The general form of a_m when F is linear is shown in Equation 3.6.

$$\alpha_m = a_0(T + 273.15) exp(F + a_2 V_m) \tag{3.6}$$

With only two parameters it is possible to perform a parametric sweep across both parameters to understand the sensitivity and effects of the parameter values.

3.4 Simulation Environment

The simulation was implemented as a Python script. The tools used in the simulation of this model are NumPy and NEURON Simulator along with python visualization tools. The NumPy library applies the LTI system for the mechanical model (Section 2.4.1) to an input signal. NumPy applies the filter defined in Section 2.4.1 to a transient signal. The NEURON Simulator is responsible for solving all electrophysiological currents and dynamics, represented as the circuit model in Figure 3.3. The simulation tools are coupled through a Python script. The NEURON simulator is setup to solve their systems over the time dimension using a fixed step that is synchronized.

For the NEURON simulator, the geometry of the neuron needs to be discretized in the same way as the cable equation needs to be discretized into segments. Table 3.4 shows the parameter used to setup the NEURON simulation environment.

Component	**Diameter**	**Length**	**Number of Segments**	**Segment Length**
Neurite Spine	0.1 - 2 μm	0.5 - 2 μm	5 - 9	0.1 - 0.22 μm
Unmyelinated Neurite	1 - 5 μm	600 μm	421	1.43 μm
Myelin Section	5 μm	250 μm	5	50 μm
Node of Ranvier	5 μm	2 μm	3	0.67 μm

Table 3.4: Discretization parameters used for NEURON simulation

Due to the difficulties in estimating and quantifying errors, simulation time steps must be chosen through experimentation by simulating the specific model. While an extremely small time step will minimize the error to a point, it significantly increases simulation time. In these simulations we are primarily looking for qualitative results of the system's frequency response and we place less emphasis on absolute numerical accuracy. Therefore we use a simulation time step that shows stable results in simulating the Pacinian corpuscle model at 1000 Hz, 37 $^{\circ}C$, with a predetermined baseline set of parameters. The simulation time step chosen is 0.025 ms which represents a simulation frequency of 40 kHz.

3.5 Simulation Experiments

Maintaining the assumption that the spines are uniformly distributed and are of uniform shape, the mechanical force of stimuli is uniformly applied to all spines, the Hodgkin Huxley m subunit closing rate (β_m), h subunit and n subunit are fixed, the parameters of interest in the PC model are shown in Table 3.5. These are parameters that can be considered uncertain as to their exact values. This is not an exhaustive list, there are other parameters that could vary or could be inaccurate in this model, but this is a reduced list to understand the significance of these parameters. The ideal situation is to parametrize all values whose primary source are not statistically significant measurements from PCs and to parametrize (and constrain) values that have been measured that have significant variances. In general this is beyond the scope of this work where the goal is to test if this model is qualitatively representative of the PCs response.

PC component	**Number of free parameters**	**Listing**
Spine membrane dynamics	10	(2) a_0, a_2 from α_m equation (1) h subunit τ_h scale factor (3) maximum conductance $\bar{g}_{Na}$, $\bar{g}_K$, g_L (3) resting potential E_{Na}, E_K, E_L (1) C_m
Spine geometry and count	3	(1) length (1) diameter (1) number of spines
Unmyelinated neurite membrane	2	(1) C_m (1) R_m
Unmyelinated neurite geometry	2	(1) length (1) diameter
Myelinated fibre membrane	2	(1) myelin conductance (1) myelin capacitance
Myelinated fibre geometry	4	(1) myelin length (1) myelin diameter (1) node of ranvier length (1) node of ranvier diameter
Thermal parameters	2	(2) FitzHugh A, B from η parameter
Total	25	- -

Table 3.5: List of parameters that are considered as uncertain in this study of the model. This is not an exhaustive list of parameters that can be varied in the model but represents a reduced set of parameters examined in experimental simulations.

The spine membrane parameters are chosen due to the biophysically uncertain values chosen by Bell and Holmes and the uncertainty that the mechanosensitive channel model is representative of the true underlying transduction process of the PC. All geometry parameters are chosen due to the natural variability and diversity of Pacinian corpuscle morphology. The passive membrane parameters of the neurite and myelinated fibre are chosen because these parameters can affect the conduction velocity and response frequency (time constants) of the passive and regenerative portion of the PC cable. This study will run a series of simulations that are representative, but not a thorough sweep, of the parameter space given in Table 3.5.

3.6 Simulation for Haptic Systems

While simulations can be conducted to verify the accuracy of the model and to understand the underlying mechanisms of PC transduction, it is also possible to conduct experiments that can be used to understand the interactions between haptic systems and humans. The scenario presented in this example compares the difference between two different theoretical haptic environments/displays, electrotactile and mechanical.

To understand how an electrotactile display, which consists of an array of skin surface electrodes along the pad of the finger, could generate stimuli equivalent to a specific mechanical stimuli, the difference in the response of the receptor to electrical and mechanical stimuli can be measured and compared. To study this difference, an extracellular electrode is included in the NEURON simulator. The location of the electrode can be specified in a 3D coordinate system, along with the coordinates of all PC segments. It is assumed the extracellular space is linear and purely resistive, which means there are no capacitive or inductive properties. The time course of the stimulating current can then be specified to simulate any arbitrary electrode waveform and to observe the response of the PC. A conceptual diagram of the electrode stimulation experiment is shown in Figure 3.5 where the current being injected at each and every segment of the neurite and fibre depends on the

distance from the electrode, the resistivity of the tissue medium and the strength of the electrode current.

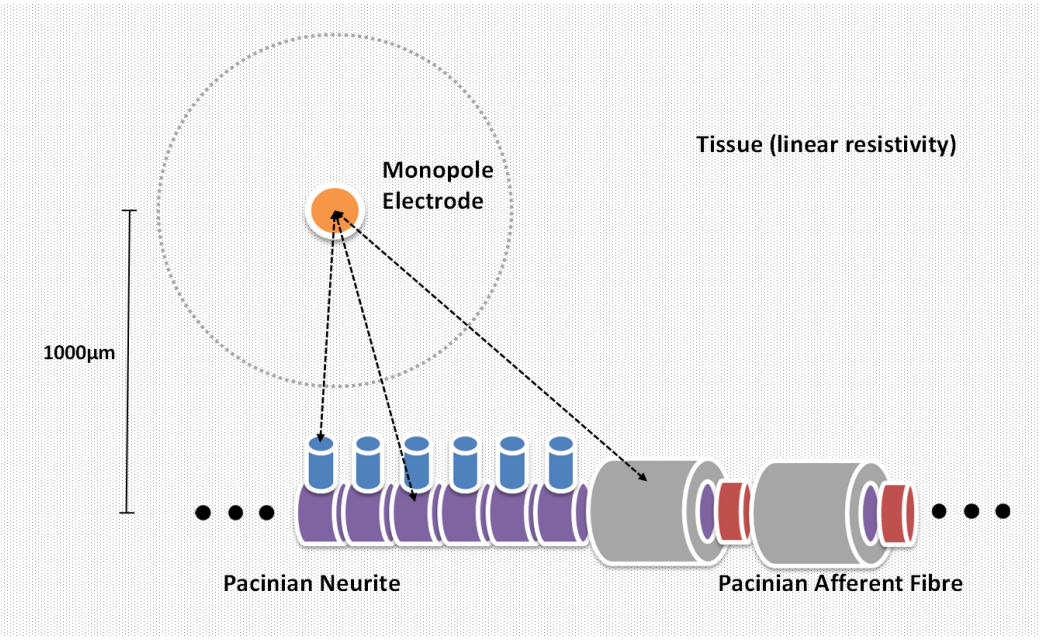

Figure 3.5: Diagram of electrode stimulation experiment. A simple monopole electrode is modeled as stimulating the Pacinian corpuscle neuron model. The electrode $1000\mu m$ away from the center of the Pacinian's neurite in a linearly resistive tissue.

Chapter 4

Results

This chapter describes the results of the simulation of the PC model. This includes the various simulation experiments performed that are compared against published physiological data along with simulation experiments performed that can be used to guide our understanding of how the Pacinian corpuscle functions and how we can use these simulations apply to haptic systems. Figure 4.1 shows an example of one simulated stimuli where a 300 Hz 0.35 amplitude deformation stimuli is applied to the PC. The resulting action potential generated at a single spine, along with the action potential generated at the 2nd myelin segment (before the first extracorpuscular node) is shown.

The majority of simulation experiments will use stimuli and response recordings of the form shown in Figure 4.1. Each transient simulation is run for 50 ms. The stimulus space consists of the stimuli frequency, amplitude, and temperature, which are swept across in each experiment. The frequency is swept across at intervals similar to the frequencies Bolanowski used in their experiments [9], which are intervals of approximately 50-200 Hz. The amplitude is swept with an interval of 0.01, and the temperature is swept with an interval of 5 $^{\circ}C$ with the exception of 37 $^{\circ}C$ which is approximately body temperature. Table 4.1 shows a summary of the time it takes to run through one simulation experiment set at a fixed temperature. The baseline parameters that experiments will deviate from are shown in Table 4.2 with the simulation results in Section 4.1.

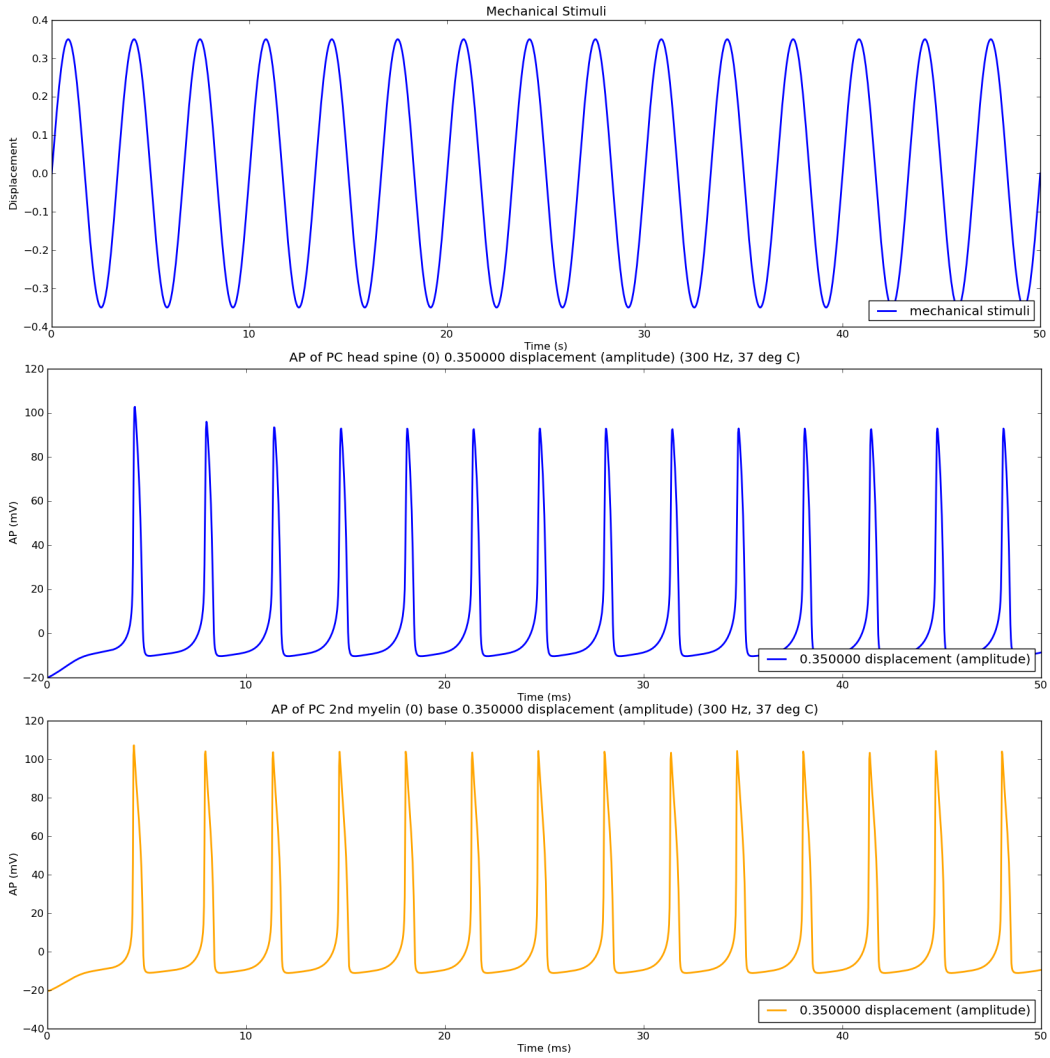

Figure 4.1: An example of the mechanical stimuli and the corresponding neural activity with stimuli of 300 Hz and amplitude of 0.35.

Simulation Time	50 ms
Avg. Real Time	20.1 s
Number of Runs	150
Total Time	30.15 hours

Table 4.1: Simulation times for a typical simulation experiment at a single temperature.

4.1 Baseline Simulation

The baseline values shown in Table 4.2 are used to simulate this experiment.

Parameter	**Value**
a_0	0.000792027
a_2	0.01
h subunit τ_h factor	5
$\bar{g}_{Na}$	0.18 S/cm^2
$\bar{g}_K$	0.018 S/cm^2
g_L	0.00005 S/cm^2
E_{Na}	115 V
E_K	-12 V
E_L	-3.8 V
Spine C_m	1.0 F/cm^2
Myelin g_m	0.000008 S/cm^2
Myelin C_m	0.02 F/cm^2

Parameter	**Value**
Spine length	1 μm
Spine diameter	1 μm
Neurite length	600 μm
Neurite diameter	3 μm
Myelin length	250 μm
Myelin diameter	5 μm
Node length	2 μm
Node diameter	5 μm

Table 4.2: Baseline parameters set. All experiments are deviations from this set of parameters.

The simulation results are presented in two types of plots that represent the intensity and sensitivity characteristics. The first set of plots (Figures 4.2 - 4.6) shows the neural spike frequency as a function of the stimuli displacement intensity with varying stimuli frequencies and temperature. The second plot (Figure 4.7) shows the minimum displacement required for the simulation to exhibit a 1:1 phase locking (i.e., ratio of neural frequency and stimuli frequency is 1:1) as a function of stimuli frequency where temperature is also varied. This second plot shows a measure of the Pacinian corpuscle's sensitivity that has been commonly used in physiological experiments since it has been hypothesized the phase-locking properties of the Pacinian corpuscle is a primary effect of its encoding

process [9].

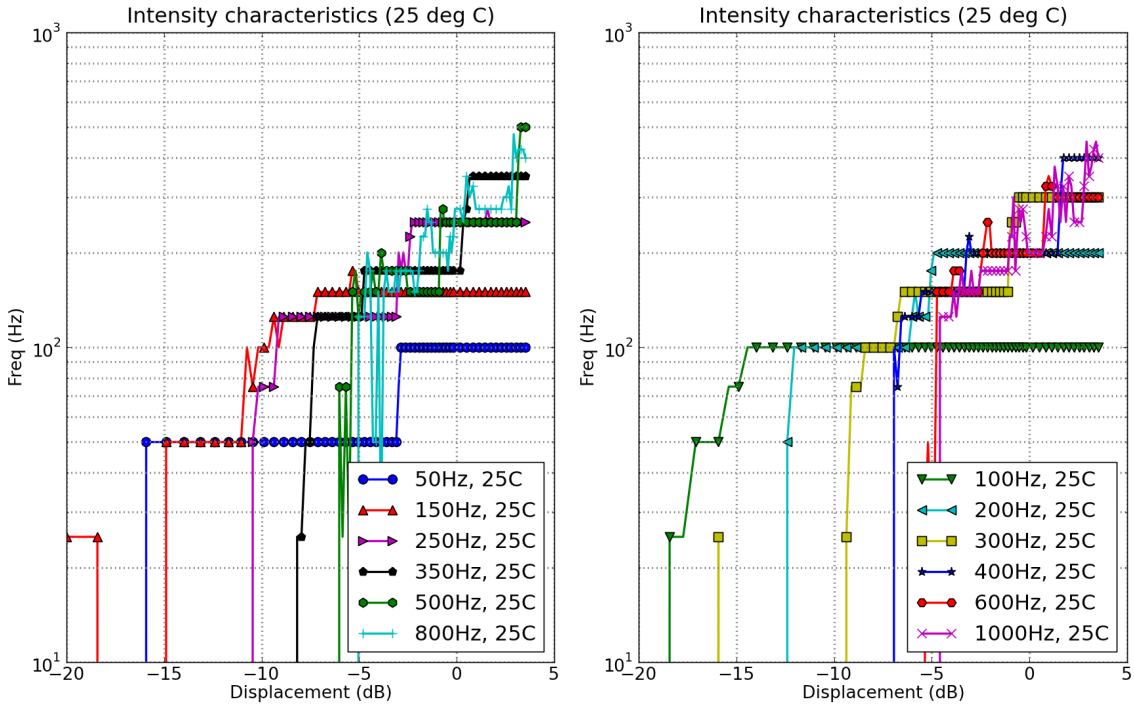

Figure 4.2: Intensity response of simulated PC at 25°C for baseline simulation.

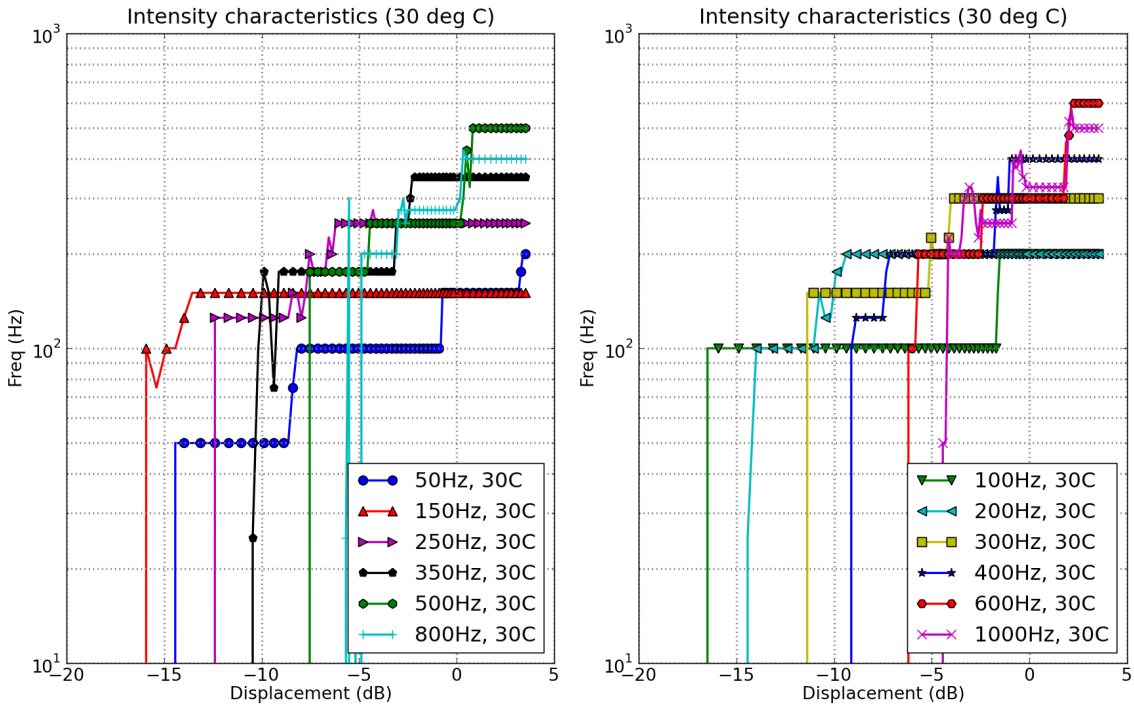

Figure 4.3: Intensity response of simulated PC at 30°C for baseline simulation.

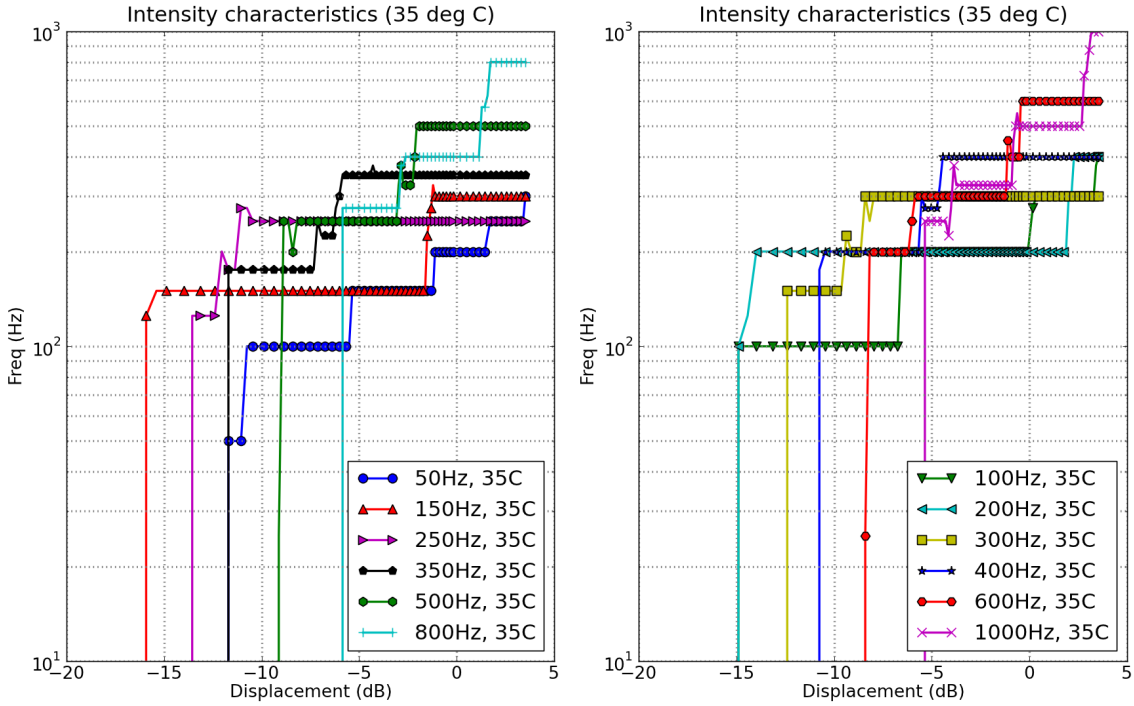

Figure 4.4: Intensity response of simulated PC at 35°C for baseline simulation.

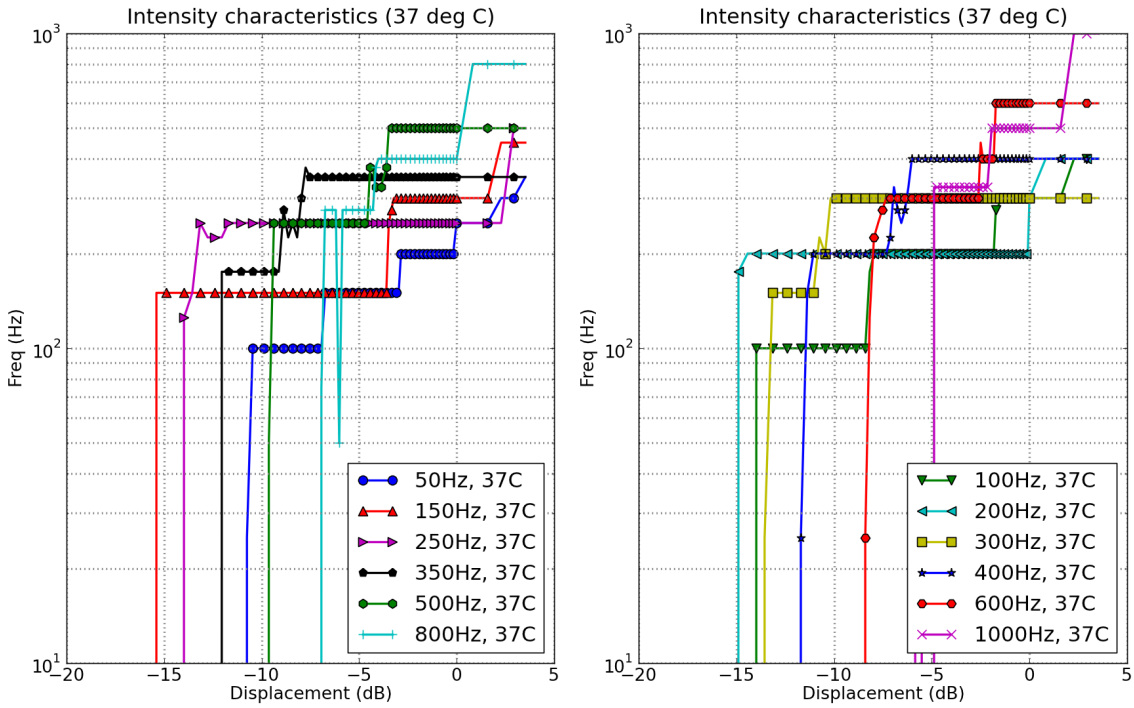

Figure 4.5: Intensity response of simulated PC at 37°C for baseline simulation.

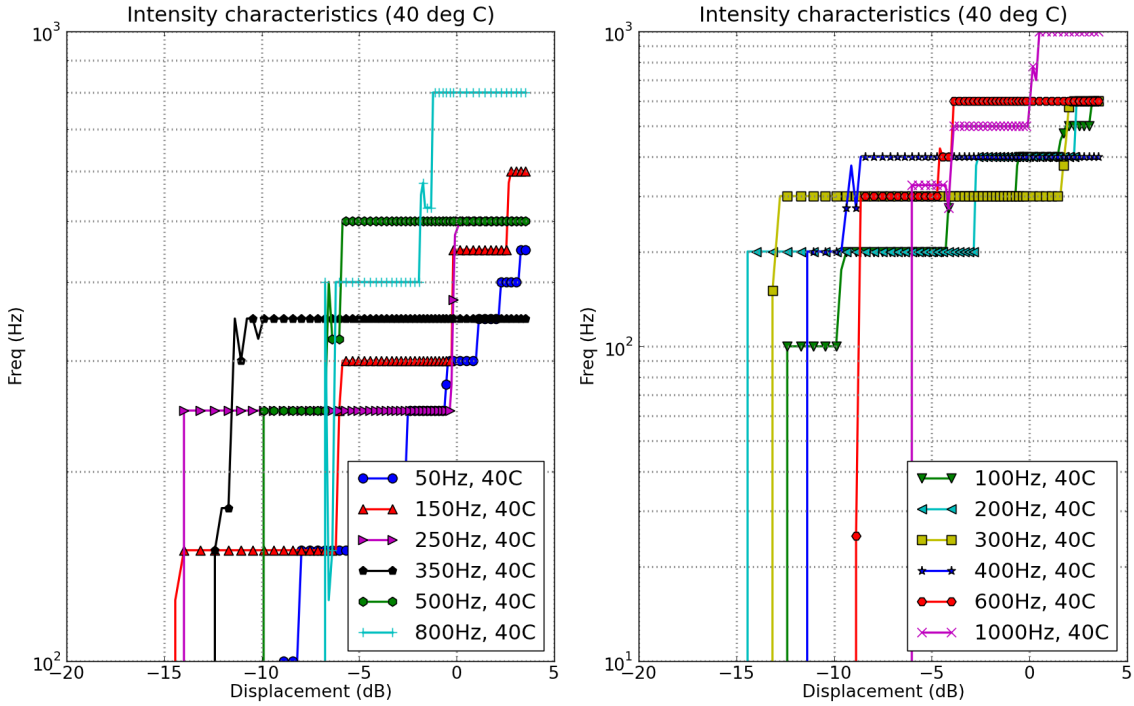

Figure 4.6: Intensity response of simulated PC at 40°C for baseline simulation.

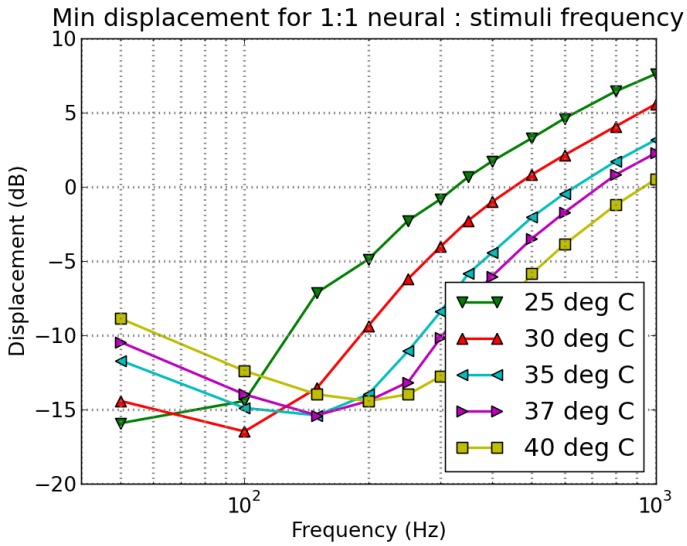

Figure 4.7: Minimum displacement required for 1 neural spike per 1 stimuli cycle for baseline simulation.

4.2 Geometry Simulation Experiments

The following are the neural frequency response to temperature, stimuli frequency, and stimuli amplitude given varying geometries. The baseline experiment in Section 4.1 is used as a baseline reference for variations in geometry. Table 4.2 shows the baseline parameters that all experiments are based on and Table 4.3 shows which parameters are being varied in each experiment.

Parameter	**Value**
Geometric Experiment 1	
Neurite diameter	1 μm
Geometric Experiment 2	
Number of Spines	1884
Geometric Experiment 3	
Number of Spines	1884
Neurite Diameter	1 μm

Table 4.3: Parameters being varied from the baseline parameters for the geometric simulation experiments.

These experiments show the effects of altering the the neurite diameter and the number

of spines. While these are only two of the nine geometric parameters shown in Table 3.5, these simple simulation tests begin to show how the geometric parameters influence the key characteristics of the Pacinian corpuscle response.

4.2.1 Geometry Experiment 1

In geometry experiment 1, the diameter of the Pacinian corpuscle's neurite was reduced to 1 μm. With the reduced neurite size, the minimum displacement for 1:1 phase locking is reduced by an average of 3dB. By reducing the diameter of the neurite, the overall are of the neurite decreases, which means the net membrane capacitance, membrane conductance and axial conductance decreases. This means the time constant of the neurite cable does not changing, but the length constant is decreasing. Given the decreased length constant, the overall sensitivity of the system increases, shown in Table 4.4. There is also an increase in the best frequency, although the amount of increase in not clear due to the low frequency resolution of frequency in current simulations conducted.

Temperature	**Average change in minimum displacement**	**Best frequency**	**Best frequency change**
30 $^{\circ}C$	-2.43 dB	100(+0) Hz	-2.69 dB
35 $^{\circ}C$	-2.57 dB	150(+0) Hz	-2.50 dB
40 $^{\circ}C$	-2.04 dB	250(+50) Hz	-2.50 dB

Table 4.4: Summary of differences between geometry experiment 1 and baseline experiment.

4.2.2 Geometry Experiment 2

In geometry experiment 2 the number of spines in the simulation was increased to 1884. The length of the neurite remained constant, which meant the concentration of spines increases. This effectually increases the surface area of the active mechanosensitive membrane, allowing a larger current density to be injected into the passive neurite body. This

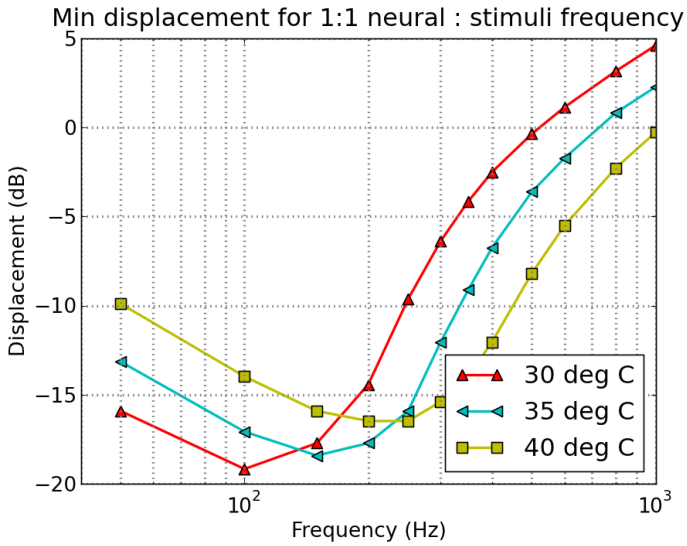

Figure 4.8: Minimum displacement required for 1 neural spike per 1 stimuli cycle for geometry experiment 1.

increases the sensitivity of the receptor's response to force when compared with the baseline experiments (See Table 4.5).

Temperature	**Average change in minimum displacement**	**Best frequency**	**Best frequency change**
30 $^{\circ}C$	-0.37 dB	100(+0) Hz	-0.60 dB
35 $^{\circ}C$	-0.27 dB	150(+0) Hz	0.00 dB
40 $^{\circ}C$	-0.34 dB	200(+0) Hz	-0.47 dB

Table 4.5: Summary of differences between geometry experiment 2 and baseline experiment.

4.2.3 Geometry Experiment 3

In geometry experiment 3 the number of spines in the simulation was increased to 1884 and the neurite diameter was decreased to 1 μm. This is a combination of geometry experiments 1 and 2, which decreases the length constant of the neurite and increases the surface area of the mechanosensitive membrane. The results found in Table 4.6 show the combination has an aggregate effect on the average sensitivity of the receptor. The combined response

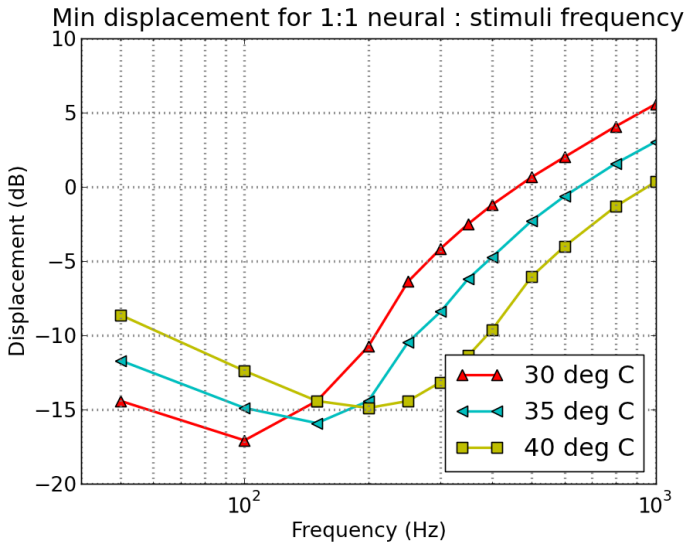

Figure 4.9: Minimum displacement required for 1 neural spike per 1 stimuli cycle for geometry experiment 2.

is more sensitive than either of the individual responses.

Temperature	**Average change in minimum displacement**	**Best frequency**	**Best frequency change**
30 $^{\circ}C$	-2.90 dB	100(+0) Hz	-2.69 dB
35 $^{\circ}C$	-2.75 dB	150(+0) Hz	-2.50 dB
40 $^{\circ}C$	-2.10 dB	200(+0) Hz	-2.65 dB

Table 4.6: Summary of differences between geometry experiment 3 and baseline experiment.

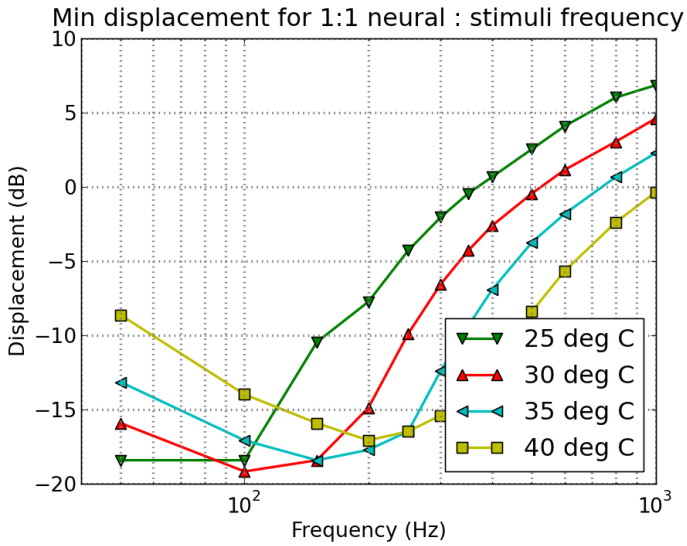

Figure 4.10: Minimum displacement required for 1 neural spike per 1 stimuli cycle for geometry experiment 3.

4.3 Functional Experiments

The following experiments are used to determine the functional significance of incorporating a model in the PC system, such as the difference between attaching the myelin afferent fibre or simulating without one of the thermal membrane dynamic models. All models are based on the the parameters in Table 4.2 and Section 4.1.

4.3.1 Functional Experiment 1

In functional experiment 1 the myelin afferent fibre is removed from the simulation. From Table 4.7 it can be seen at low temperatures the sensitivity of the receptor without the myelin increases but as the temperature increases, the sensitivity decreases.

4.3.2 Functional Experiment 2

In functional experiment 2 experiment the η factor proposed by FitzHugh (Section 2.4.4) is removed. The maximum conductance of each ion channel remains constant over temperature. The effect of removing η means at 37 $^{\circ}C$ there should be no effective change to the

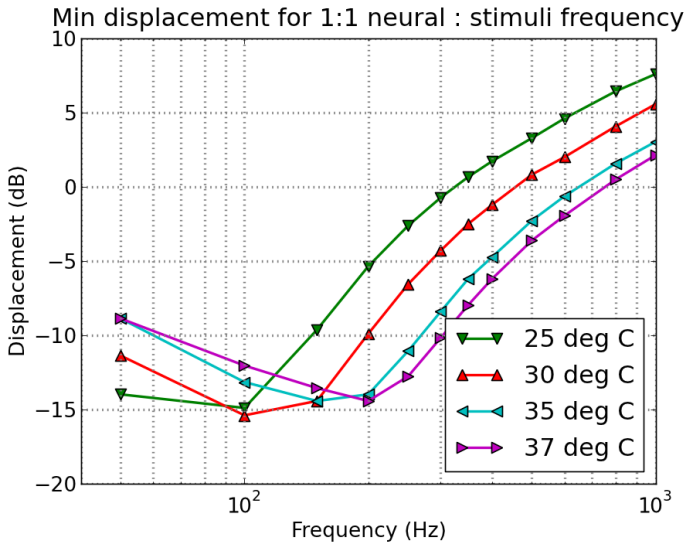

Figure 4.11: Minimum displacement required for 1 neural spike per 1 stimuli cycle for functional experiment 1.

Temperature	**Average change in minimum displacement**	**Best frequency**	**Best frequency change**
25 $^{\circ}C$	-1.22 dB	100(+0) Hz	-0.47 dB
30 $^{\circ}C$	-0.38 dB	100(+0) Hz	1.09 dB
35 $^{\circ}C$	0.17 dB	150(+0) Hz	1.49 dB

Table 4.7: Summary of differences between functional experiment 1 and baseline experiment.

baseline, while the difference in conductance increases as the temperature difference increases. This is seen in Table 4.8 where temperatures closer to 37 $^{\circ}C$ have smaller changes to their minimum displacement.

Temperature	**Average change in minimum displacement**	**Best frequency**	**Best frequency change**
25 $^{\circ}C$	-1.32 dB	100(+0) Hz	-2.05 dB
30 $^{\circ}C$	-0.91 dB	100(+0) Hz	-0.60 dB
35 $^{\circ}C$	-0.36 dB	150(+0) Hz	0.00 dB

Table 4.8: Summary of differences between functional experiment 2 and baseline experiment.

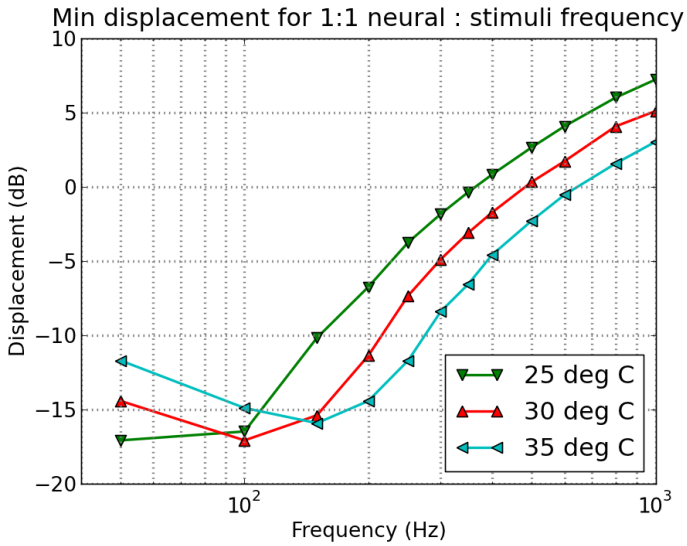

Figure 4.12: Minimum displacement required for 1 neural spike per 1 stimuli cycle for functional experiment 2.

4.3.3 Functional Experiment 3

In functional experiment 3, the Nernst potentials no longer varies based on temperature and they are assigned the original Nernst potentials used in the Hodgkin Huxley model. These Nernst potentials were derived from Hodgkin Huxley's experiments at 6.3 $^{\circ}C$. The results in Table 4.9 show that the sensitivity increases without this temperature consideration. This means when the Nernst potentials are scaled to the appropriate temperature (e.g., scaled by a positive factor greater than 1), the sensitivity of the system increases.

Temperature	**Average change in minimum displacement**	**Best frequency**	**Best frequency change**
25 $^{\circ}C$	-0.05 dB	100(+0) Hz	0.87 dB
30 $^{\circ}C$	0.07 dB	100(+0) Hz	1.09 dB
35 $^{\circ}C$	0.20 dB	150(+0) Hz	1.49 dB

Table 4.9: Summary of differences between functional experiment 3 and baseline experiment.

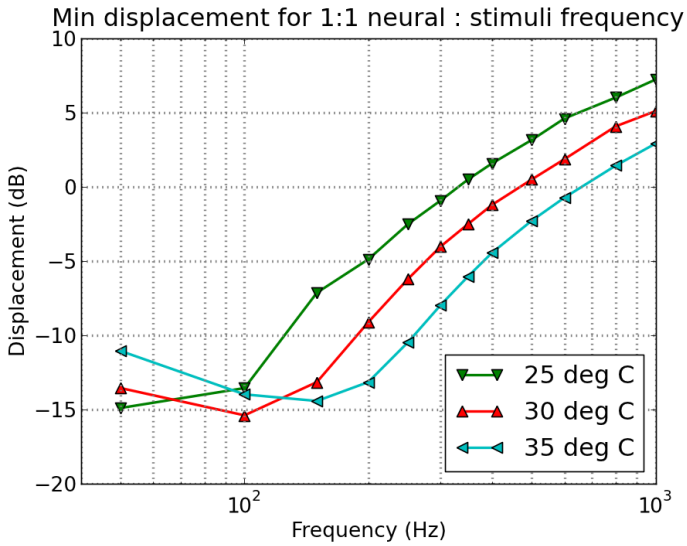

Figure 4.13: Minimum displacement required for 1 neural spike per 1 stimuli cycle for functional experiment 3.

4.4 Haptic Experiments

4.4.1 Haptic Experiment 1

In this experiment the PC model properties are identical to the baseline experiment in Section 4.1. The extracellular space is modeled as tissue with a resistivity of 70 Ωcm. The PC model's central axis coordinates are set between the points (-600,0,0) and (1006,0,0) where the the unmyelinated neurite lies between (-600,0,0) and (0,0,0). All of the spines are oriented in the positive y direction between (x_i,0,0) and (x_i,1,0) where x_i is the x coordinate of the i-th spine that is distributed uniformly across the length of the neurite. The electrode is placed at the coordinate (-300,1000,0), a distance of 1000 μm away from the center of the neurite portion of the model. The electrode is a simple monopole electrode and the electrode current is a sinusoidal current centered around 0 with varying frequency and amplitude.

The response of the system is shown in Figure 4.14. It is seen that given a sinusoidal current, it is possible to elicit a neural response of up to 600 Hz where the current frequency is the same as the neural spike frequency. However at higher frequencies this is not possible

and above 800 Hz, with sufficient current, the neural response of the PC is completely blocked.

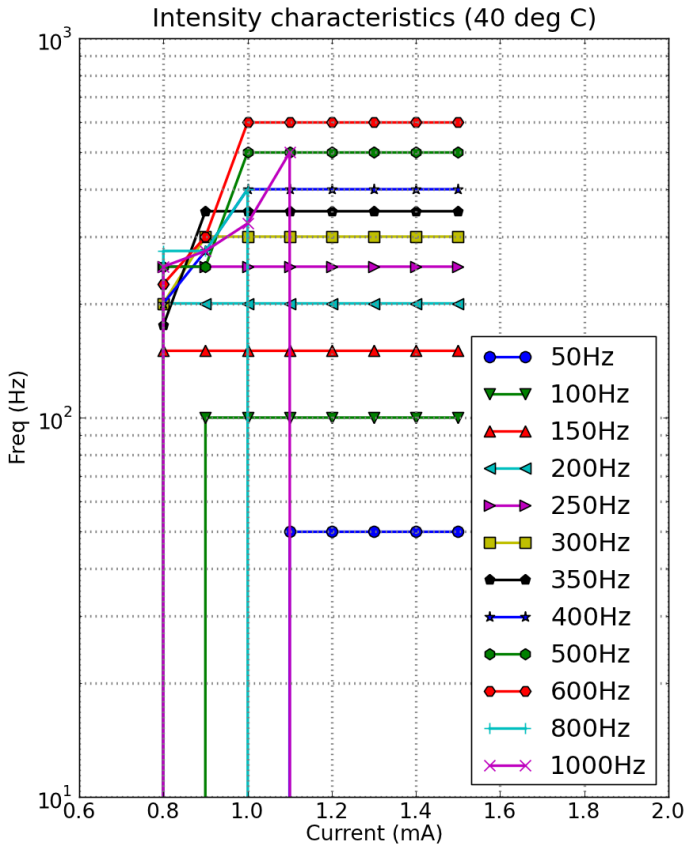

Figure 4.14: Intensity response of simulated PC at $40°C$ for haptic experiment 1.

Chapter 5

Discussion

From the intensity, frequency, and temperature response results of the simulations, a number of key characteristics are captured by the simulations.

- For frequencies above 100 Hz, 2:1, 1:1, and 1:2 phase locking is able to occur. The range between phase locking transitions is smaller than experiments in most of Bolanowski's experiments (e.g., Figure 4.5 at 200 Hz the 1:1 plateau has a 15 dB range before transition to 2:1, while Bolanowski's experiments [11] show 1:1 plateau from 20dB) although there is not a statistically significant sample to verify this.

- The minimum displacement required to match a 1:1 neural frequency to stimuli frequency is U-shaped.

- As temperature decreases, the most sensitive frequency also decreases, and this has been shown experimentally by Bolanowski [11].

From the simulation results, a number of discrepancies from experimental reports are noticed.

- At the nominal temperature (37 $^{\circ}C$) in Figure 4.5, at 60 Hz stimuli there is no 1:1 phase locking where the neural response is 60 Hz for the 60 Hz input stimuli. At lower temperatures the 1:1 phase locking effect does occur at 60 Hz (Figure 4.3 and Figure 4.4).

- The best frequency ranges from 200 Hz at 40°C to 100 Hz at 25°C. Experimental literature reports the best frequency range from 400 Hz at 41°C to 150 Hz at 21°C.

- At 60 Hz and low frequencies across all temperatures there exists phase locking at 4:1 (4 neural spikes per mechanical stimuli cycle) and higher phase locking ratios which have not been reported in the experimental literature. The average difference between 60 Hz minimum displacement and the best frequency is 20dB while in this simulation the different ranges from 4dB at 35°C to 12dB at 25°C (See Figure 4.7).

- The most sensitive temperature is 30 °C and not the anticipated 35-40 °C as reported by experimental literature [23] [11]. At higher frequencies the most sensitive temperatures are greater than 35 °C.

As noted above, it is seen that certain published properties of the Pacinian corpuscle's behavior are replicated by the model. There are other properties of the simulation model that do not match the published observations and data of the receptor's characteristics. It is currently unclear whether or not these discrepancies are a result of improper choice of parameter values that do not match the true biophysical properties or if there are flaws and significant missing processes that are not considered.

An intrinsic problem of this study is that some of the modeling theories applied make major assumptions that are difficult to defend and verify since this work is purely computational and no physical experiments are performed. These assumptions include the passive neurite body, the model of mechanosensitive ion channels, the 8 factor increase in ionic maximum conductance, and the parameters chosen to match standard Hodgkin Huxley values. There is little direct evidence these assumptions are valid, although each assumption is applied given indirect evidence or hypothesis of the PC's properties. Without the ability the design experiments to verify these theories or experiments to show the model predicts novel properties, the limited published data must be relied on.

Despite this flaw, the model does show promising results and given more extensive parametric sweeps, the flaws of the model can be pinpointed and a closer fit to experimental data

can be obtained. The example given is based on incorporating a simple monopole electrotactile system with the receptor model. A simple sinusoidal current is used as the stimulus which is shown to be limited to generating neural responses of up to 600 Hz. Additional experiments can be conducted to test different stimulus waveforms and patterns to generate different response ranges or properties. It is also possible to design additional experiments that couple theoretical haptic systems with this receptor to determine what signals a haptic system (e.g., electrotactile display) must use to create an accurate representation of a different environment (e.g., mechanical vibration). As our understanding of this receptor improves with more accurate models and as other receptor models are developed, it may be possible to simulate a wider range of sensory modalities and their interactions with haptic systems.

There is a concern of whether a model of this complexity is needed in the design of haptic systems, or if simplified representations of our somatosensory system is sufficient in understanding how haptic systems interface with our sensory system. There are benefits to studying these biophysical models of receptors. Not only can they reveal the mechanisms responsible for the transduction process (which is of scientific interest) it can be used to study novel phenomenons to suggest new strategies for the design and signals of haptic systems, such as using electrical stimulation. These models also capture the nonlinear dynamics of these systems, which may otherwise be difficult to model without using knowledge of the biophysical properties. While the exact biophysics and mechanisms of transduction is currently not of direct interest of haptic systems engineering, through understanding these details it may be possible to gain insight into designing devices that can reach the goals of sensory substitution.

Chapter 6

Future Work

There are a number of future research topics that should be pursued in the continued development of this physiological model and related haptic systems. First the results of the model needs to be compared against statistically significant experimental data. In this study, the available data is published qualitative descriptions of the Pacinian corpuscle's neural response characteristics and graphs of a limited number of samples of receptor sensitivity, intensity, and frequency responses. More detailed and larger samples of data need to be used in order to understand exactly what discrepancies exist between the simulation model and physiological receptor. Due to the many assumptions made by this model, including the details of the mechanosensitive Na^+ channel and neurite properties, additional experiments beyond the receptor's overall neural response need to be designed and conducted in order to verify or refute these assumptions. This includes patch clamp experiments on the unmyelinated neurite and continued biomolecular experiments to determine the chemical pathways involved in Pacinian corpuscle mechanotransduction.

In order to fully characterize the simulation model, the different ranges of parameters that have high variance or are uncertain (see Table 3.5) need to be explored. This means characterizing the parametric sweeps across the different parameters or employing optimization methods to tune the parameters to match physiological data. This requires significant computational power since to conduct a single simulation experiment for three different temperatures requires approximately 35 hours to complete.

In addition to running more simulations, additional models can be developed of haptic

systems. These haptic systems model can be coupled with models of the Pacinian corpuscle to understand how the haptic systems are generating mechanical stimuli and how it is being encoded by the receptor. Differences between various haptic systems, including the simple electrotactile system simulated in this study, can be compared to understand how these systems are able to emulate virtual or remote environments.

Chapter 7

Conclusions

The targeted receptor of this study, the Pacinian corpuscle, is of interest in the field of haptics because of its unique extreme sensitivity to high frequency vibrations and its hypothesized role in the control of tools. It is also the target of a wide range of vibrotactile haptic systems. Moving towards systematic analysis and engineering design of such haptic systems, this thesis developed a simulation model representing the biophysical properties of the Pacinian corpuscle. The model created is derived from the mechanical model developed by Loweneski and Skalak [46], the electrophysiological and mechanotransduction theories of Bell and Holmes [5][6], thermal effects of Hodgkin Huxley's neuron model [34][18], and other electrophysiological theories developed by different researchers [2][42][59]. This integration of different models and theories into a computer simulation model is the main contribution of this work, allowing researchers to take a systems approach to understanding the Pacinian corpuscle's mechanotransduction process.

With a simulation model of this receptor, we can begin exploring the contributions of the functional units of the transduction process, the complex dynamics of the system, and the large parametric space of the model. We can use this model to improve our understanding of the Pacinian corpuscle transduction theory and of mechanotransduction in general, along with characterizing the accuracy and flaws of the theoretical models. This integrated model can be further be used to complement experimentations on the receptor, to design new experiments to understand the purpose and mechanisms of the receptor.

Through the simulation results collected in this study, it is shown the simulation model

is able to represent a subset of published characteristics. Discrepancies in the simulation results, when compared with experimental studies, suggest there are gaps between our theoretical understanding of the system. It is possible that the model parameters selected are not accurate, assumptions made in the development of the model are incorrect, or critical transduction pathways are not represented in the model. To reconcile the deviations of the model from published characteristics, future simulation experiments should be performed, including testing new theories of the transduction pathway. In addition to simulations, statistically significant physiological experiments need to be conducted to test the assumptions made in model and the resulting simulations.

Even with the described limitations, the developed simulation model enables a systematic design and analysis of haptic systems. An example scenario is demonstrated with a theoretical electrotactile haptic system coupled to a model of a human receptor. This coupled model is simulated as a closed system, characterizing the combined response of the haptic device and receptor. The resulting characteristics predict effects that should be investigated further in device and physiological experiments. As the biophysical theories of the Pacinian corpuscle are improved, more realistic results may be achievable in the future. Additional models of haptic systems can also be coupled with the Pacinian model to quantitatively study and compare the effects of haptic stimuli in terms of neural encoding of the receptor. This new framework will provide a new tool and analysis method to aid in the development of modern haptic systems as the devices attempt to provide meaningful cues to users of human computer interfaces and as they approach mimicking realistic tactile sensations.

Bibliography

[1] "Immersion TouchSense," 2011. [Online]. Available: http://www.immersion.com/products/touchsense-tactile-feedback/

[2] S. M. Baer and J. Rinzel, "Propagation of dendritic spikes mediated by excitable spines: a continuum theory," *Journal of neurophysiology*, vol. 65, no. 4, pp. 874–90, Apr. 1991. [Online]. Available: http://www.ncbi.nlm.nih.gov/pubmed/2051208

[3] L. Beccai, S. Roccella, A. Arena, F. Valvo, P. Valdastri, A. Menciassi, M. Carrozza, and P. Dario, "Design and fabrication of a hybrid silicon three-axial force sensor for biomechanical applications," *Sensors and Actuators A: Physical*, vol. 120, no. 2, pp. 370–382, 2005. [Online]. Available: http://linkinghub.elsevier.com/retrieve/pii/S0924424705000063

[4] J. Bell, S. Bolanowski, and M. Holmes, "The structure and function of Pacinian corpuscles: a review." *Progress in neurobiology*, vol. 42, no. 1, p. 79, 1994. [Online]. Available: http://www.ncbi.nlm.nih.gov/pubmed/7480788/

[5] J. Bell and M. Holmes, "Model of the dynamics of receptor potential in a mechanoreceptor," *Mathematical biosciences*, vol. 110, no. 2, pp. 139–174, 1992. [Online]. Available: http://linkinghub.elsevier.com/retrieve/pii/002555649290034T

[6] J. Bell and M. H. Holmes, "A note on modeling mechano-chemical transduction with an application to skin receptor," *Journal of Mathematical Biology*, vol. 32, pp. 275–285, 1994.

[7] S. J. Bensmaïa, Y. Y. Leung, S. S. Hsiao, and K. O. Johnson, "Vibratory adaptation of cutaneous mechanoreceptive afferents." *Journal of neurophysiology*, vol. 94, no. 5, pp. 3023–36, Nov. 2005. [Online]. Available: http://www.ncbi.nlm.nih.gov/pubmed/16014802

[8] S. Bensmaïa, "A transduction model of the Meissner corpuscle." *Mathematical biosciences*, vol. 176, no. 2, pp. 203–17, Apr. 2002. [Online]. Available: http://www.ncbi.nlm.nih.gov/pubmed/11916509

[9] S. J. Bolanowski and J. J. Zwislocki, "Intensity and frequency characteristics of pacinian corpuscles. I. Action potentials." *Journal of neurophysiology*, vol. 51, no. 4, pp. 793–811, Apr. 1984. [Online]. Available: http://www.ncbi.nlm.nih.gov/pubmed/6716124

[10] S. Bolanowski, J. Schyuler, and N. Slepecky, "Semi-serial electron-micrographic reconstruction of putative transducer sites in Pacinian corpuscles," *Somatosensory & Motor Research*, vol. 11, no. 3, pp. 205–218, 1994. [Online]. Available: http://informahealthcare.com/doi/abs/10.3109/08990229409051389

[11] S. J. Bolanowski Jr and R. T. Verrillo, "Temperature and criterion effects in a somatosensory subsystem: a neurophysiological and psychophysical study," *Journal of Neurophysiology*, vol. 48, no. 3, pp. 836–55, 1982. [Online]. Available: http://jn.physiology.org/cgi/reprint/48/3/836.pdf

[12] N. T. Carnevale and M. L. Hines, *The NEURON Book*, 1st ed. Cambridge, UK: Cambridge University Press, 2006.

[13] C. Chorley, C. Melhuish, T. Pipe, and J. Rossiter, "Development of a Tactile Sensor Based on Biologically Inspired Edge Encoding," in *International Conference on Advanced Robotics*, 2009, pp. 1–6. [Online]. Available: http://www.brl.ac.uk/projects/InspiredEdgeEncoding.pdf

[14] M. O. Culjat, C.-h. King, M. L. Franco, C. E. Lewis, J. W. Bisley, E. P. Dutson, and W. S. Grundfest, "A tactile feedback system for robotic surgery." in *Annual International IEEE Engineering in Medicine and Biology Society Conference*, vol. 2008, Jan. 2008, pp. 1930–4. [Online]. Available: http://www.ncbi.nlm.nih.gov/pubmed/19377124

[15] G. Di Pino, E. Guglielmelli, and P. M. Rossini, "Neuroplasticity in amputees: main implications on bidirectional interfacing of cybernetic hand prostheses." *Progress in neurobiology*, vol. 88, no. 2, pp. 114–26, Jun. 2009. [Online]. Available: http://www.ncbi.nlm.nih.gov/pubmed/19482228

[16] M. Eltaib and J. Hewit, "Tactile sensing technology for minimal access surgerya review," *Mechatronics*, vol. 13, no. 10, pp. 1163–1177, 2003. [Online]. Available: http://linkinghub.elsevier.com/retrieve/pii/S0957415803000485

[17] H. Fischer, R. Trapp, L. Schüle, and B. Hoffmann, "Actuator Array for Use in Minimally Invasive Surgery," *Le Journal de Physique IV*, vol. 07, no. C5, pp. C5–609–C5–614, Nov. 1997. [Online]. Available: http://www.edpsciences.org/10.1051/jp4:1997596

[18] R. Fitzhugh, "Theoretical effect of temperature on threshold in the Hodgkin-Huxley nerve model." *The Journal of general physiology*, vol. 49, no. 5, pp. 989–1005, May 1966. [Online]. Available: http://www.pubmedcentral.nih.gov/articlerender.fcgi?artid=2195517\&tool=pmcentrez\&rendertype=abstract

[19] R. Fitzhugh and K. S. Cole, "Theoretical Potassium Loss from Squid Axons as a Function of Temperature," *Biophysical Journal*, vol. 4, no. 4, pp. 257–265, Jul. 1964. [Online]. Available: http://linkinghub.elsevier.com/retrieve/pii/S0006349564867813

[20] P. G. Gillespie and R. G. Walker, "Molecular basis of mechanosensory transduction." *Nature*, vol. 413, no. 6852, pp. 194–202, Sep. 2001. [Online]. Available: http://www.ncbi.nlm.nih.gov/pubmed/11557988

[21] F. Grandori and A. Pedotti, "A mathematical model of the Pacinian corpuscle," *Cybernetics*, vol. 18, no. 5, pp. 670–679, 1983.

[22] F. Grandori and A. Pedotti, "Theoretical analysis of mechano-to-neural transduction in Pacinian corpuscle," *IEEE transactions on bio-medical engineering*, vol. 27, no. 10, pp. 559–65, Oct. 1980. [Online]. Available: http://www.ncbi.nlm.nih.gov/pubmed/7439915

[23] B. Green, S. Lederman, and J. Stevens, "The effect of skin temperature on the perception of roughness," *Sensory processes*, vol. 3, pp. 327–333, 1979. [Online]. Available: http://psycserver.psyc.queensu.ca/lederman/013.pdf

[24] B. Güçlü and S. J. Bolanowski, "Tristate markov model for the firing statistics of rapidly-adapting mechanoreceptive fibers." *Journal of computational neuroscience*, vol. 17, no. 2, pp. 107–26, 2004. [Online]. Available: http://www.ncbi.nlm.nih.gov/pubmed/15306734

[25] F. Guharay and F. Sachs, "Stretch-activated single ion channel currents in tissue-cultured embryonic chick skeletal muscle." *The Journal of physiology*, vol. 352, no. 1, p. 685, 1984. [Online]. Available: http://jp.physoc.org/content/352/1/685.short

[26] K. S. Hale and K. M. Stanney, "Deriving Haptic Design Guidelines from Human Physiological, Psychophysical, and Neurological Foundations," *Ieee Computer Graphics And Applications*, vol. 24, no. 2, pp. 33–39, 2004.

[27] O. P. Hamill, *Mechanosensitive Ion Channels, Part A*, O. P. Hamill, Ed. San Diego, CA: Elsevier, 2007.

[28] O. P. Hamill, *Mechanosensitive Ion Channels, Part B*, O. P. Hamill, Ed. San Diego, CA: Elsevier, 2007.

[29] M. L. Hines and N. T. Carnevale, "NEURON: a tool for neuroscientists." *The Neuroscientist : a review journal bringing neurobiology, neurology and psychiatry*, vol. 7, no. 2, pp. 123–35, Apr. 2001. [Online]. Available: http://www.ncbi.nlm.nih.gov/pubmed/11496923

[30] M. L. Hines, A. P. Davison, and E. Muller, "NEURON and Python." *Frontiers in neuroinformatics*, vol. 3, no. January, p. 1, Jan. 2009. [Online]. Available: http://www.ncbi.nlm.nih.gov/pubmed/19198661

[31] M. Hines and N. Carnevale, "Expanding NEURON's repertoire of mechanisms with NMODL," *Neural Computation*, vol. 12, no. 5, pp. 995–1007, May 2000. [Online]. Available: http://www.mitpressjournals.org/doi/pdf/10.1162/089976600300015475

[32] H.-N. Ho and L. A. Jones, "Development and evaluation of a thermal display for material identification and discrimination," *ACM Transactions on Applied Perception*, vol. 4, no. 2, pp. 13–es, 2007. [Online]. Available: http://portal.acm.org/citation.cfm?doid=1265957.1265962

[33] H.-N. Ho and L. A. Jones, "Modeling the thermal responses of the skin surface during hand-object interactions," *Journal of biomechanical engineering*, vol. 130, no. 2, Apr. 2008. [Online]. Available: http://www.ncbi.nlm.nih.gov/pubmed/18412492

[34] A. Hodgkin and A. Huxley, "A quantitative description of membrane current and its application to conduction and excitation in nerve," *The Journal of Physiology*, vol.

117, no. 4, p. 500, 1952. [Online]. Available:
http://jp.physoc.org/content/117/4/500.full.pdf

[35] S. J. Hubbard, "A study of rapid mechanical events in a mechanoreceptor," *Journal of Physiology*, vol. 141, pp. 198–219, 1958.

[36] K. O. Johnson, "The roles and functions of cutaneous mechanoreceptors." *Current opinion in neurobiology*, vol. 11, no. 4, pp. 455–61, Aug. 2001. [Online]. Available:
http://www.ncbi.nlm.nih.gov/pubmed/11502392

[37] K. O. Johnson, T. Yoshioka, and F. Vega-Bermudez, "Tactile functions of mechanoreceptive afferents innervating the hand," *Journal of clinical neurophysiology*, vol. 17, no. 6, pp. 539–58, Nov. 2000. [Online]. Available:
http://www.ncbi.nlm.nih.gov/pubmed/11151974

[38] L. Jones and H.-N. Ho, "Warm or Cool, Large or Small? The Challenge of Thermal Displays," *IEEE Transactions on Haptics*, vol. 1, no. 1, pp. 53–70, 2008. [Online]. Available: http://ieeexplore.ieee.org/lpdocs/epic03/wrapper.htm?arnumber=4543167

[39] H. Kajimoto, N. Kawakami, T. Maeda, and S. Tachi, "Electro-Tactile Display with Tactile Primary Color Approach," in *Proceedings of International Conference. on Intelligent Robots and Systems (IROS)*, 2004. [Online]. Available:
http://libach.inrf.uci.edu/groups/bats/uploads/Xsense/Kajimoto_IROS_2004.pdf

[40] H. Kajimoto, N. Kawakami, T. Maeda, and S. Tachi, "Tactile Feeling Display using Functional Electrical," *International Conference on Artificial Reality and Telexistence*, vol. 9, pp. 107–114, 1999.

[41] H. Kajimoto, N. Kawakami, S. Tachi, and M. Inami, "SmartTouch: Electric skin to touch the untouchable," *IEEE Computer Graphics and Applications*, vol. 24, no. 1, pp. 36–43, 2004. [Online]. Available:
http://scholar.google.com/scholar?hl=en\&btnG=Search\&q=intitle:SmartTouch+:+Electric+Skin+to+Touch+the+Untouchable\#0

[42] E. R. Kandel, J. H. Schwartz, and T. M. Jessell, *Principles of neural science*, 4th ed. New York, NY: McGraw-Hill, 2000. [Online]. Available:
http://ftp.kermit-project.org/itc/gsas/g9600/2003/HenReadings/KandellCh3.pdf

[43] S. Kim, A. Sripati, and S. Bensmaia, "Predicting the timing of spikes evoked by tactile stimulation of the hand," *Journal of neurophysiology*, vol. 104, no. 3, p. 1484, 2010. [Online]. Available: http://jn.physiology.org/content/104/3/1484.short

[44] A. Kron and G. Schmidt, "Multi-fingered tactile feedback from virtual and remote environments," in *11th Symposium on Haptic Interfaces for Virtual Environment and Teleoperator Systems*. IEEE Comput. Soc, 2003, pp. 16–23. [Online]. Available: http://ieeexplore.ieee.org/lpdocs/epic03/wrapper.htm?arnumber=1191219

[45] T. a. Kuiken, P. D. Marasco, B. a. Lock, R. N. Harden, and J. P. a. Dewald, "Redirection of cutaneous sensation from the hand to the chest skin of human amputees with targeted reinnervation." *Proceedings of the National Academy of Sciences of the United States of America*, vol. 104, no. 50, pp. 20 061–6, Dec. 2007. [Online]. Available: http://www.pubmedcentral.nih.gov/articlerender.fcgi?artid=2148422\&tool=pmcentrez\&rendertype=abstract

[46] W. R. Loewenstein and R. Skalak, "Mechanical transmission in a Pacinian corpuscle, an analysis and a theory," *Journal of Physiology*, vol. 182, no. 2, pp. 346–378, 1966.

[47] W. R. Loewenstein, "Generator processes of repetitive activity in a pacinian corpuscle," *Journal of General Physiology*, vol. 41, no. 4, pp. 825–845, 1958.

[48] W. Loewenstein and R. Rathkamp, "The sites for mechano-electric conversion in a Pacinian corpuscle," *The Journal of General Physiology*, vol. 41, no. 6, p. 1245, 1958. [Online]. Available: http://jgp.rupress.org/content/41/6/1245.abstract

[49] E. a. Lumpkin and M. J. Caterina, "Mechanisms of sensory transduction in the skin." *Nature*, vol. 445, no. 7130, pp. 858–65, Feb. 2007. [Online]. Available: http://www.ncbi.nlm.nih.gov/pubmed/17314972

[50] P. D. Marasco, A. E. Schultz, and T. a. Kuiken, "Sensory capacity of reinnervated skin after redirection of amputated upper limb nerves to the chest." *Brain: A Journal of Neurology*, vol. 132, no. 6, pp. 1441–8, Jun. 2009. [Online]. Available: http://www.ncbi.nlm.nih.gov/pubmed/19369486

[51] Y. Mukaibo, H. Shirado, M. Konyo, and T. Maeno, "Development of a texture sensor emulating the tissue structure and perceptual mechanism of human fingers," *IEEE International Conference on Robotics and Automation*, pp. 2576–81, Apr. 2005. [Online]. Available:

http://scholar.google.com/scholar?hl=en\&btnG=Search\&q=intitle:
Development+of+a+Texture+Sensor+Emulating+the+Tissue+Structure+and+
Perceptual+Mechanism+of+Human+Fingers\#0

[52] A. M. Okamura, "Haptic feedback in robot-assisted minimally invasive surgery." *Current opinion in urology*, vol. 19, no. 1, pp. 102–7, Jan. 2009. [Online]. Available: http://www.ncbi.nlm.nih.gov/pubmed/19057225

[53] M. A. Otaduy, N. Jain, A. Sud, and M. C. Lin, "Haptic display of interaction between textured models," in *IEEE Visualization*. IEEE Comput. Soc, 2004, pp. 297–304. [Online]. Available: http://ieeexplore.ieee.org/lpdocs/epic03/wrapper.htm?arnumber=1372210

[54] M. V. Ottermo, "Virtual Palpation Gripper," PhD Thesis, Norwegian University of Science and Technology, 2006.

[55] L. Pawson, "Immunocytochemical identification of proteins within the Pacinian corpuscle," *Somatosensory & Motor Research*, vol. 17, no. 2, pp. 159–170, 2000. [Online]. Available: http://informahealthcare.com/doi/abs/10.1080/08990220050020571

[56] L. Pawson and S. J. Bolanowski, "Voltage-gated sodium channels are present on both the neural and capsular structures of Pacinian corpuscles," *Somatosensory & motor*, 2002. [Online]. Available: http://informahealthcare.com/doi/abs/10.1080/0899022021000009152

[57] L. Pawson, L. T. Prestia, G. K. Mahoney, B. Güçlü, P. J. Cox, and A. K. Pack, "GABAergic/glutamatergic-glial/neuronal interaction contributes to rapid adaptation in pacinian corpuscles." *The Journal of neuroscience : the official journal of the Society for Neuroscience*, vol. 29, no. 9, pp. 2695–705, Mar. 2009. [Online]. Available: http://www.pubmedcentral.nih.gov/articlerender.fcgi?artid=2727419\ &tool=pmcentrez\&rendertype=abstract

[58] D. Pease and T. Quilliam, "Electron microscopy of the Pacinian corpuscle," *The Journal of Biophysical and Biochemical Cytology*, vol. 3, no. 3, p. 331, 1957. [Online]. Available: http://jcb.rupress.org/content/3/3/331.abstract

[59] R. Plonsey and R. C. Barr, *Bioelectricity: A Quantitative Approach*, 3rd ed. New York, NY: Springer Science and Business Media, LLC, 2007.

[60] M. A. Qasaimeh, S. Sokhanvar, J. Dargahi, and M. Kahrizi, "PVDF-Based Microfabricated Tactile Sensor for Minimally Invasive Surgery," *Journal of Microelectromechanical Systems*, vol. 18, no. 1, pp. 195–207, 2009.

[61] T. a. Quilliam and M. Sato, "The distribution of myelin on nerve fibres from Pacinian corpuscles." *The Journal of physiology*, vol. 129, no. 1, pp. 167–76, Jul. 1955. [Online]. Available: http://www.pubmedcentral.nih.gov/articlerender.fcgi?artid=1365924\&tool=pmcentrez\&rendertype=abstract

[62] F. Sachs and H. Lecar, "Stochastic models for mechanical transduction," *Biophysical journal*, vol. 59, no. 5, p. 1143, 1991. [Online]. Available: http://www.ncbi.nlm.nih.gov/pmc/articles/PMC1281349/

[63] M. Sato, "Response of Pacinian corpuscles to sinusoidal vibration," *Journal of Physiology*, vol. 159, pp. 391–409, 1961.

[64] M. A. Srinivasan, O. Lahav, D. W. Schloerb, J. Hu, S. Kumar, and M. Srikanth, "Human and Machine Haptics," *Research Laboratory of Electronics Progress Report*, vol. 151, 2009.

[65] A. P. Sripati, S. J. Bensmaia, and K. O. Johnson, "A continuum mechanical model of mechanoreceptive afferent responses to indented spatial patterns." *Journal of neurophysiology*, vol. 95, no. 6, pp. 3852–64, Jun. 2006. [Online]. Available: http://www.ncbi.nlm.nih.gov/pubmed/16481453

[66] C. Taveggia, M. L. Feltri, and L. Wrabetz, "Signals to promote myelin formation and repair," *Nature Reviews Neurology*, vol. 6, pp. 276–287, 2010.

[67] M. Tsunozaki and D. M. Bautista, "Mammalian somatosensory mechanotransduction," *Current opinion in neurobiology*, vol. 19, no. 4, pp. 362–9, Aug. 2009. [Online]. Available: http://www.ncbi.nlm.nih.gov/pubmed/19683913

[68] J. A. Vega, O. García-Suárez, J. A. Montaño, B. Pardo, and J. M. Cobo, "The Meissner and Pacinian sensory corpuscles revisited new data from the last decade." *Microscopy research and technique*, vol. 72, no. 4, pp. 299–309, Apr. 2009. [Online]. Available: http://www.ncbi.nlm.nih.gov/pubmed/19012318

[69] S. A. Wall and S. Brewster, "Sensory substitution using tactile pin arrays: Human factors, technology and applications," *Signal Processing*, vol. 86, no. 12, pp.

3674–3695, 2006. [Online]. Available:
http://linkinghub.elsevier.com/retrieve/pii/S0165168406001411

[70] Y. Zhang, Y. Mukaibo, and T. Maeno, “A multi-purpose tactile sensor inspired by human finger for texture and tissue stiffness detection,” in *IEEE International Conference on Robotics and Biomimetics*, 2006, pp. 159–164. [Online]. Available:
http://scholar.google.com/scholar?hl=en\&btnG=Search\&q=intitle:
A+multi-purpose+tactile+sensor+inspired+by+human+finger+for+texture+and+
tissue+stiffness+detection\#0

Appendix A

Simulation Experiment Data

A.1 Geometry Experiment 1

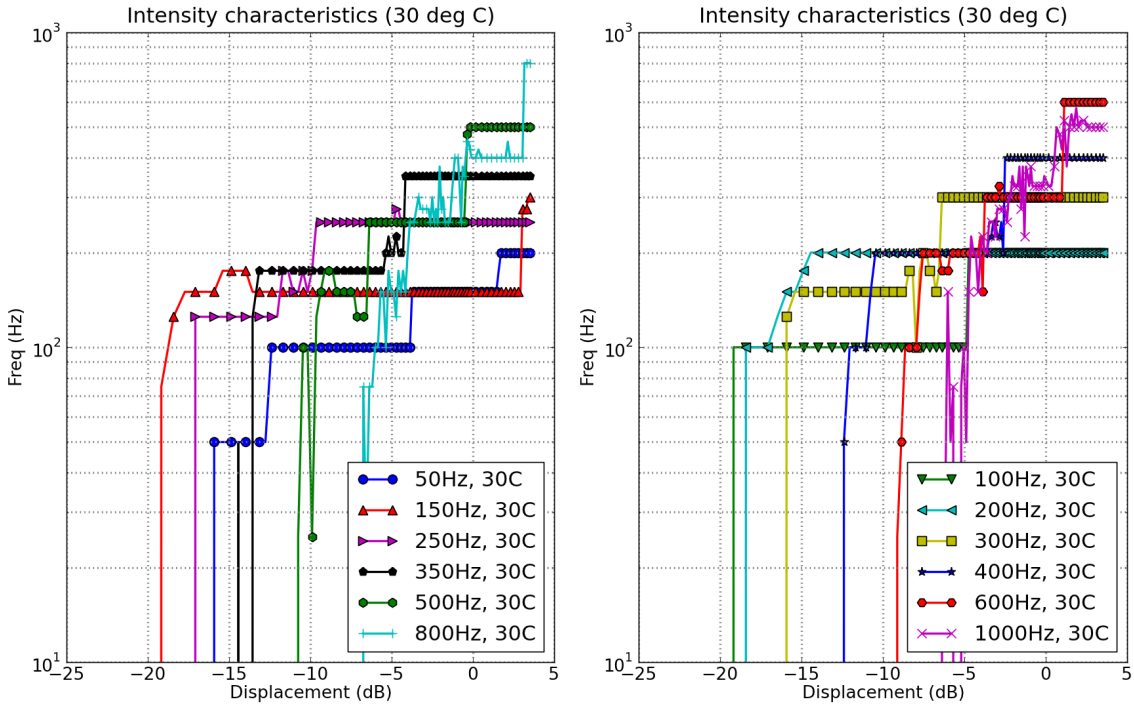

Figure A.1: Intensity response of simulated PC at 30°C for geometry experiment 1.

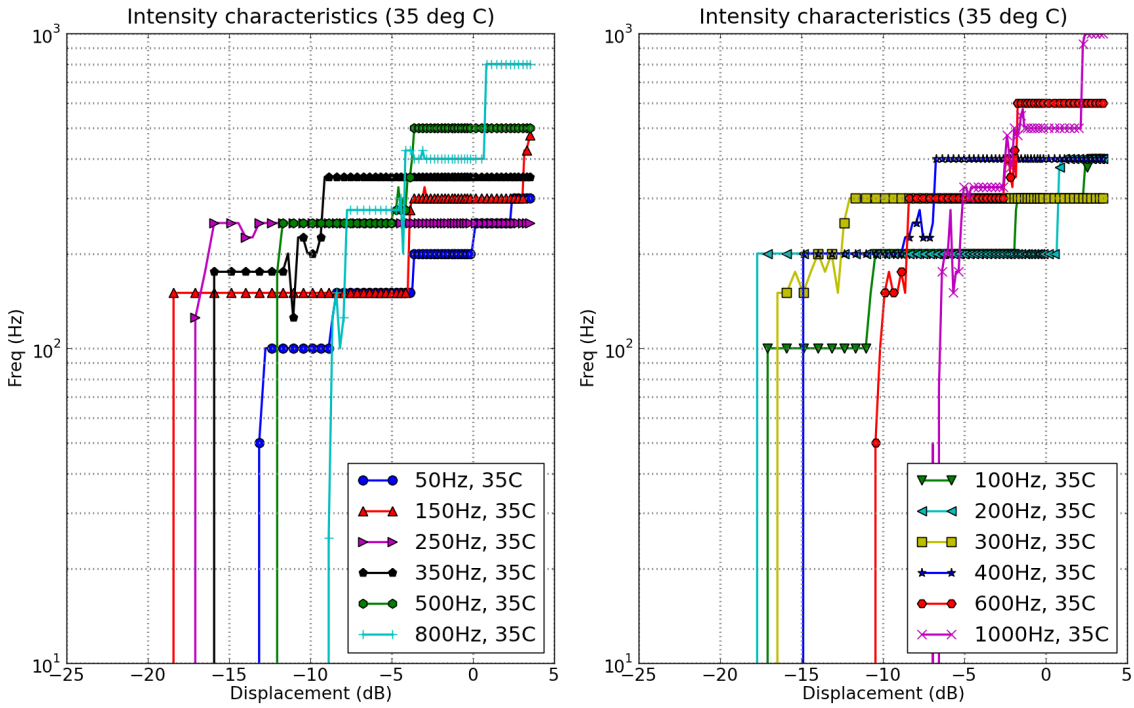

Figure A.2: Intensity response of simulated PC at 35°C for geometry experiment 1.

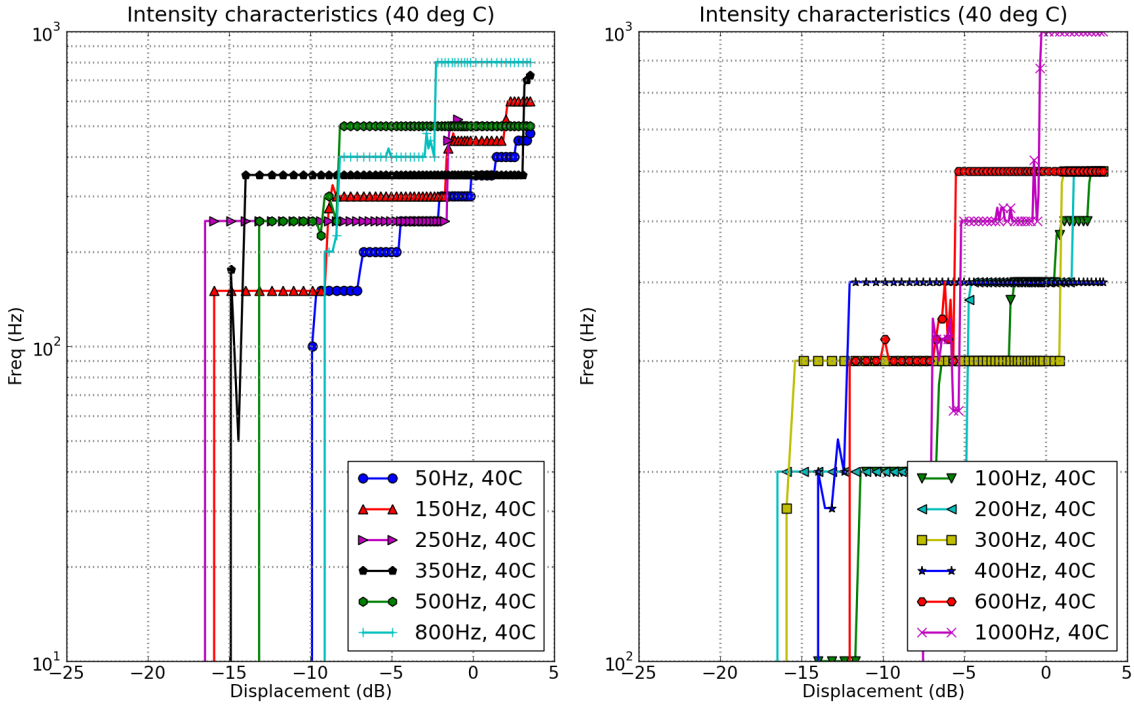

Figure A.3: Intensity response of simulated PC at 40°C for geometry experiment 1.

A.2 Geometry Experiment 2

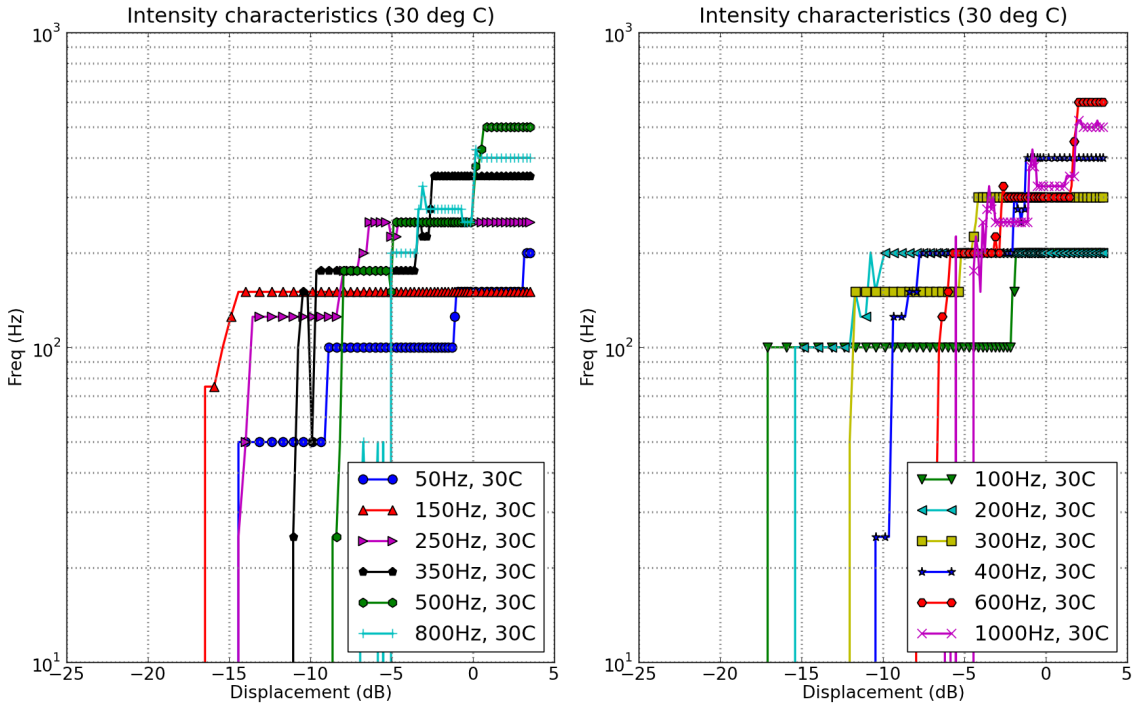

Figure A.4: Intensity response of simulated PC at 30°C for geometry experiment 2.

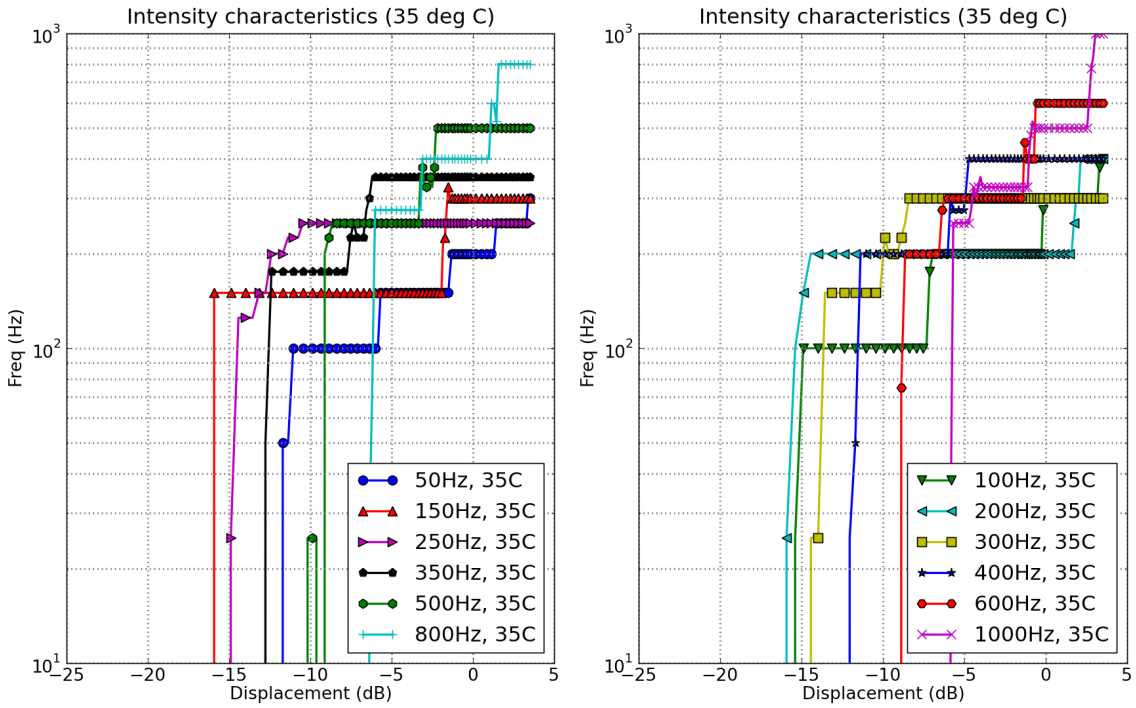

Figure A.5: Intensity response of simulated PC at 35°C for geometry experiment 2.

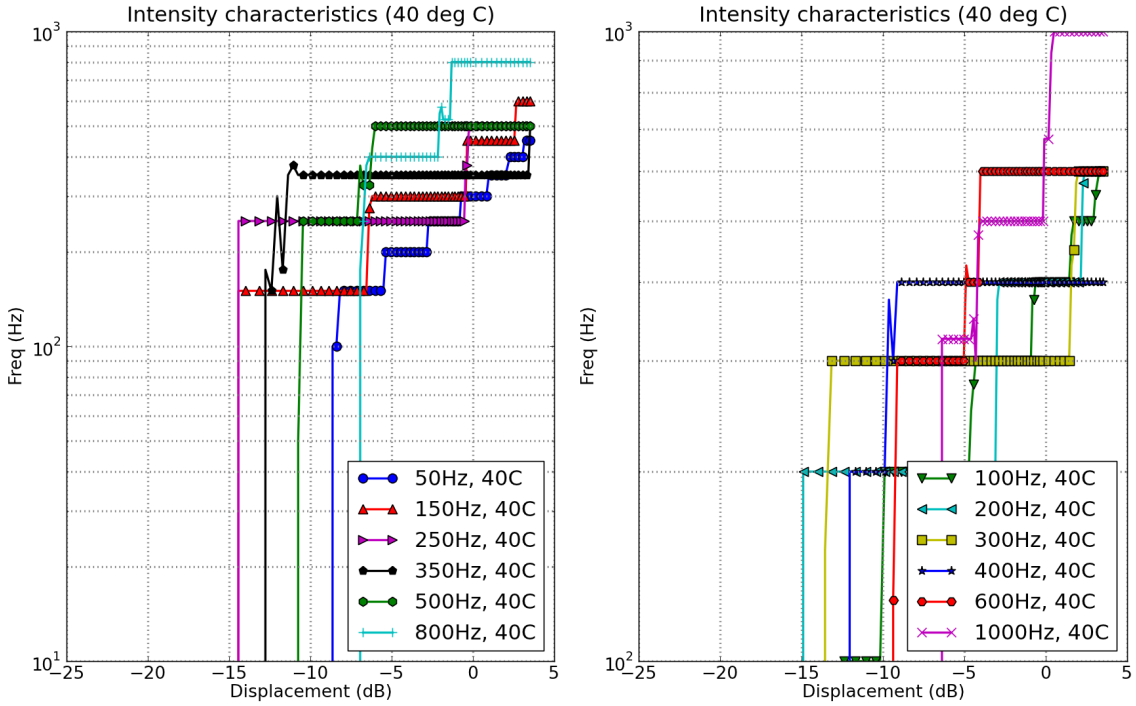

Figure A.6: Intensity response of simulated PC at 40°C for geometry experiment 2.

A.3 Geometry Experiment 3

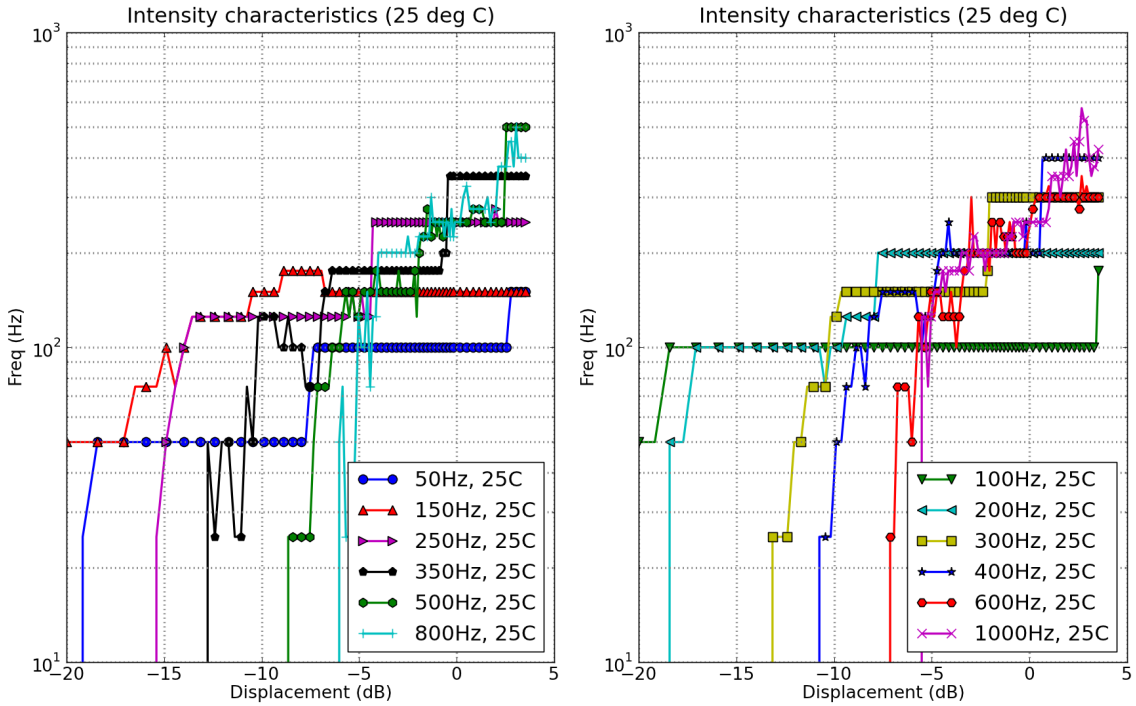

Figure A.7: Intensity response of simulated PC at 25°C for geometry experiment 3.

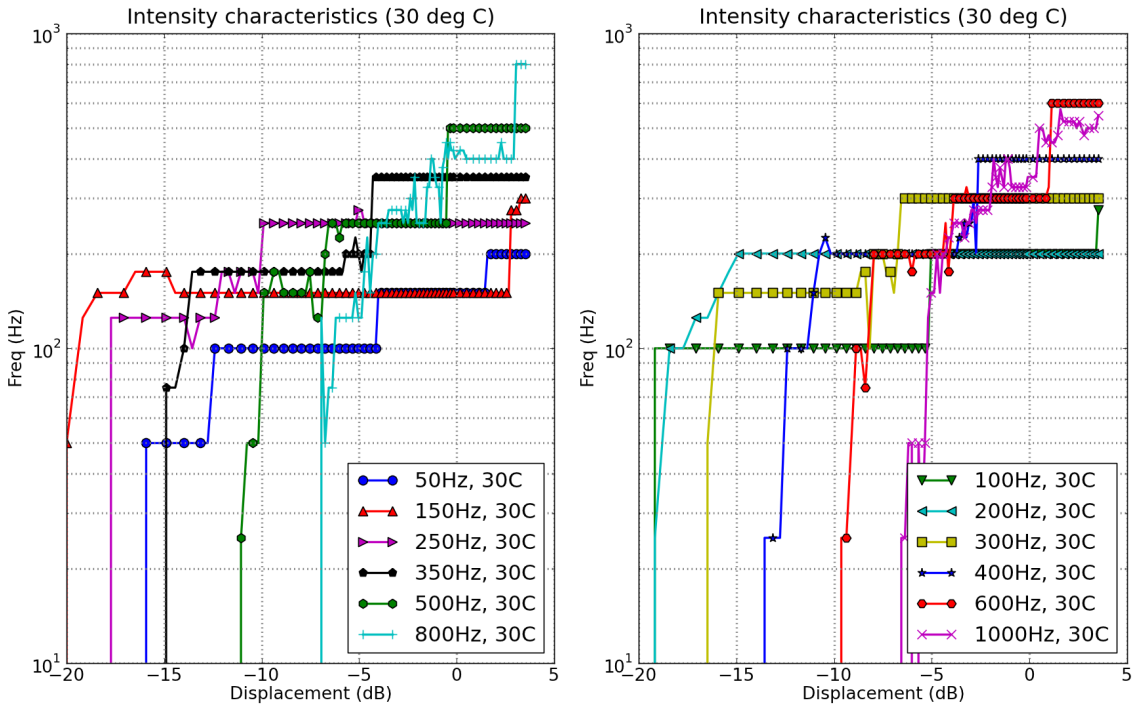

Figure A.8: Intensity response of simulated PC at 30°C for geometry experiment 3.

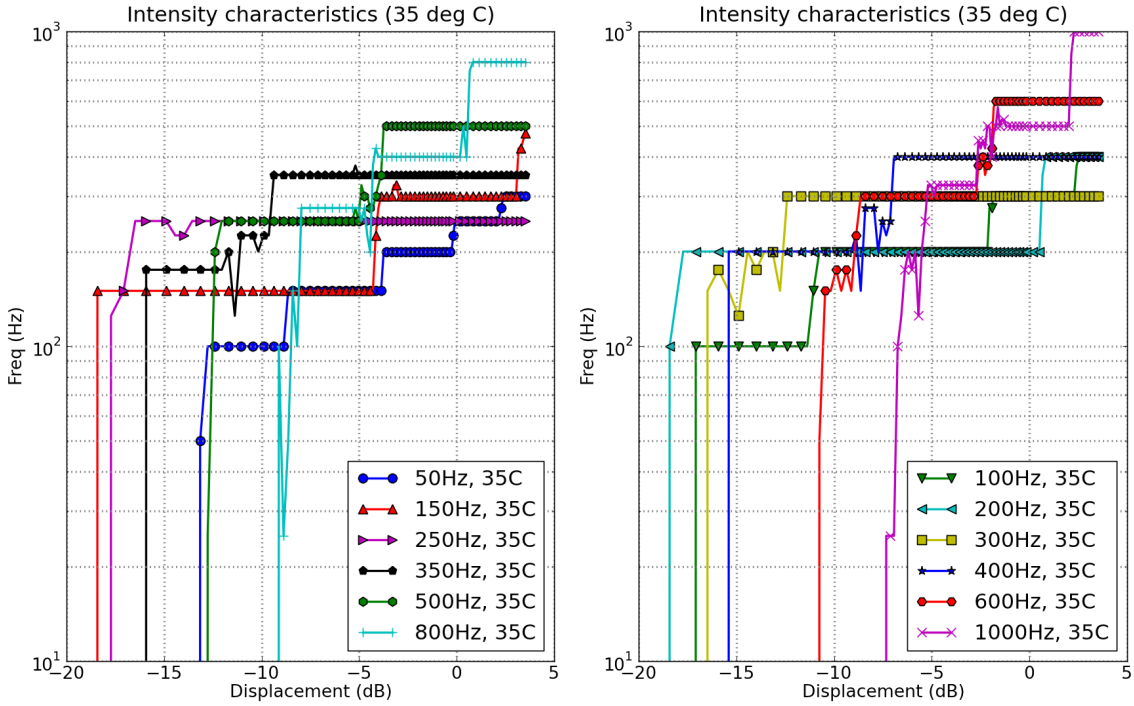

Figure A.9: Intensity response of simulated PC at 35°C for geometry experiment 3.

A.4 Functional Experiment 1

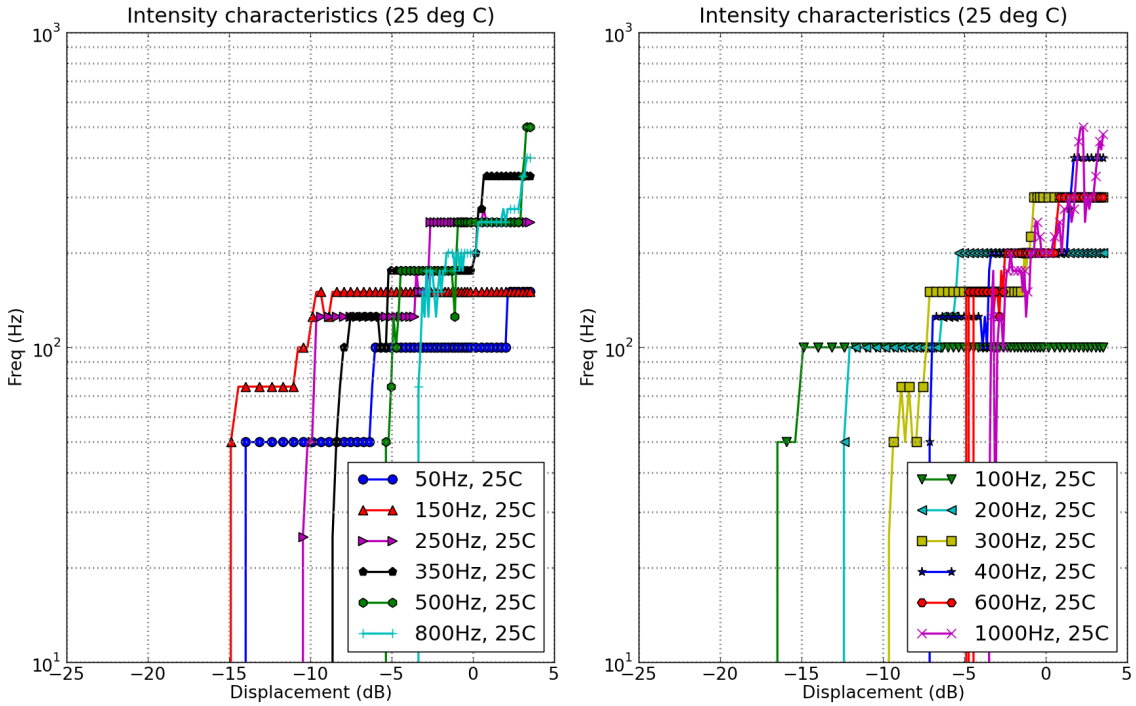

Figure A.10: Intensity response of simulated PC at 25°C for function experiment 1.

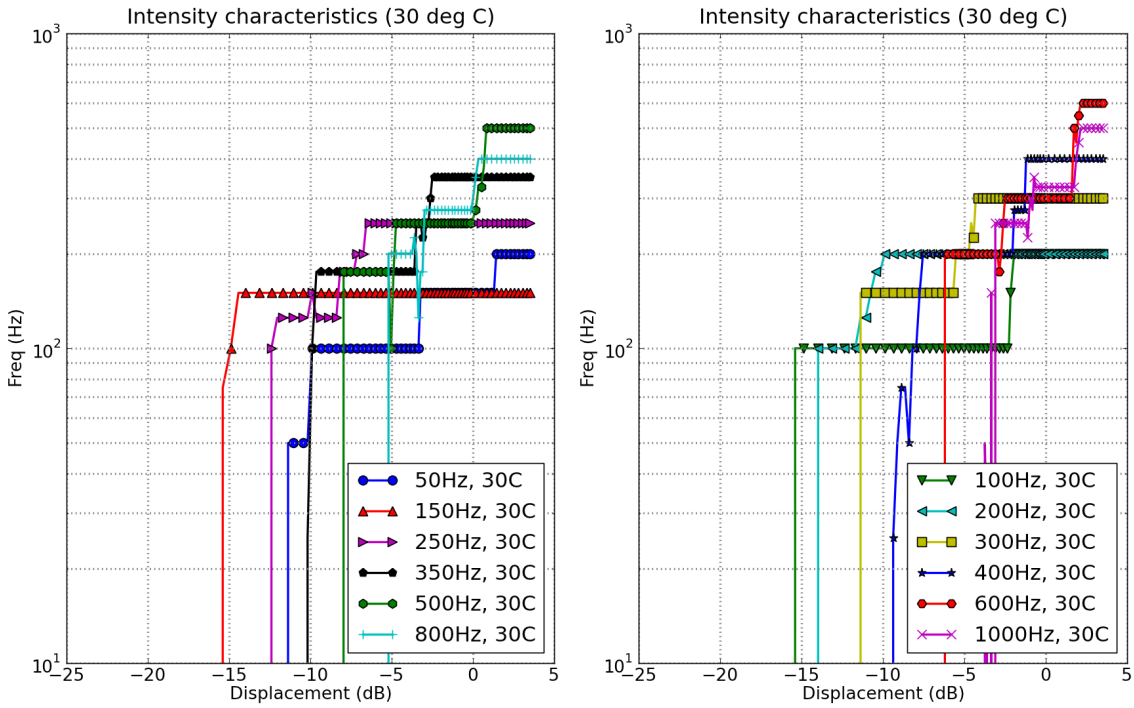

Figure A.11: Intensity response of simulated PC at 30°C for function experiment 1.

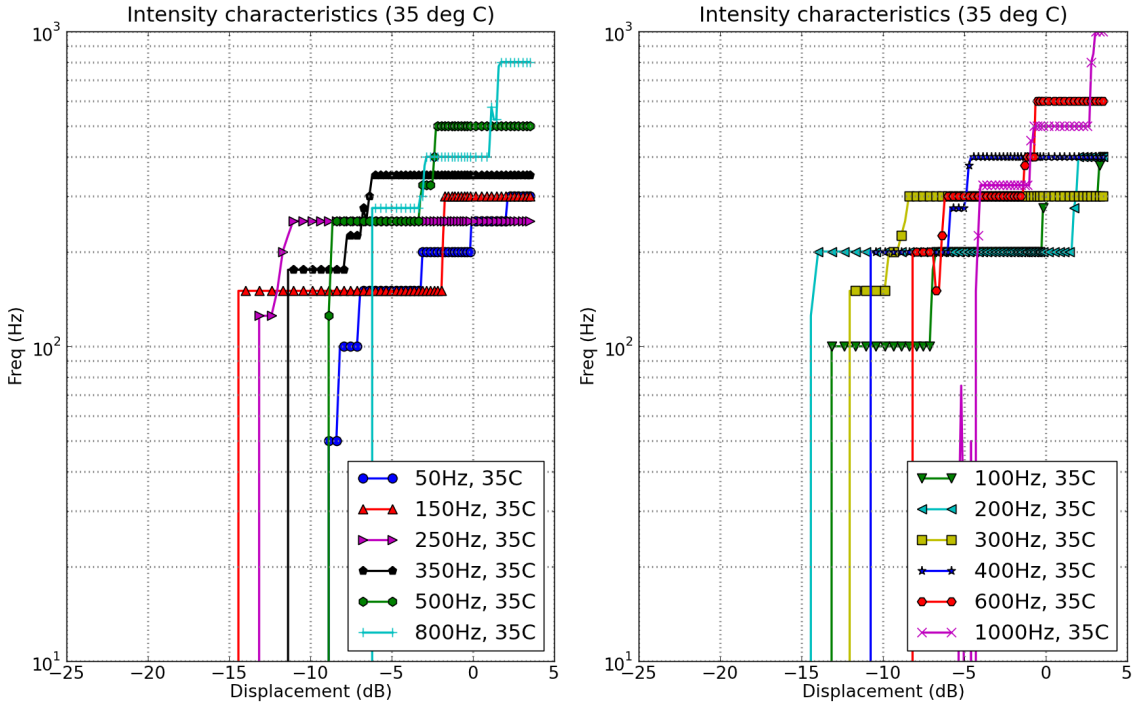

Figure A.12: Intensity response of simulated PC at 35°C for function experiment 1.

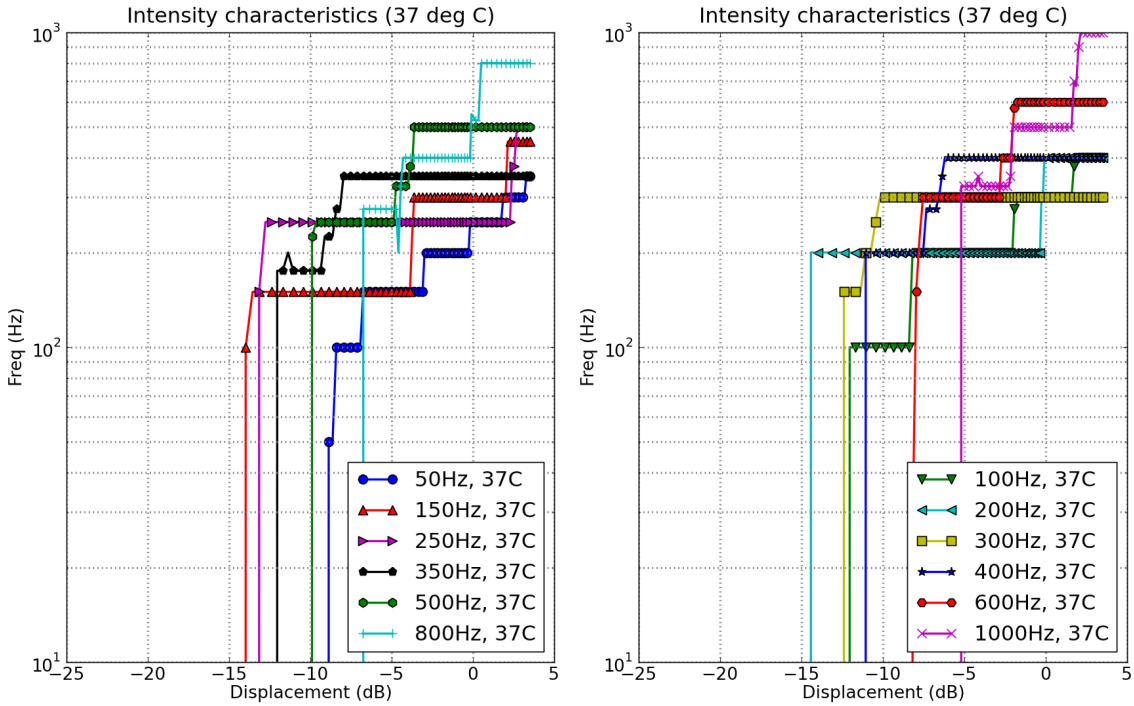

Figure A.13: Intensity response of simulated PC at 37°C for function experiment 1.

A.5 Functional Experiment 2

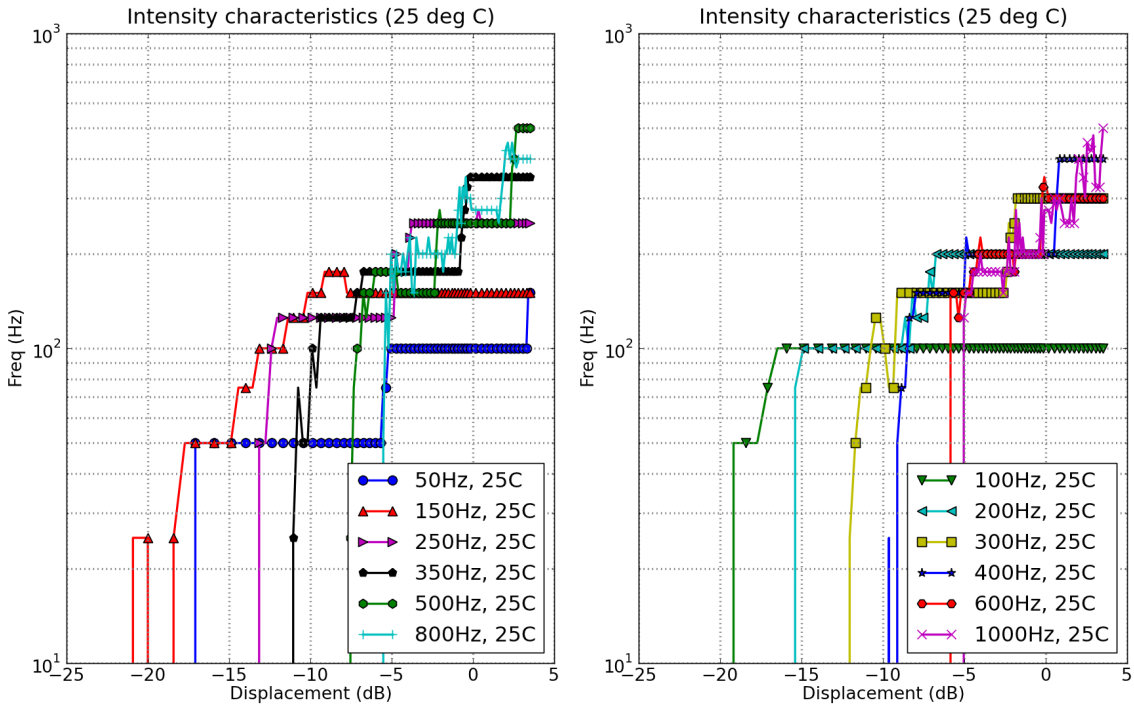

Figure A.14: Intensity response of simulated PC at 25°C for function experiment 2.

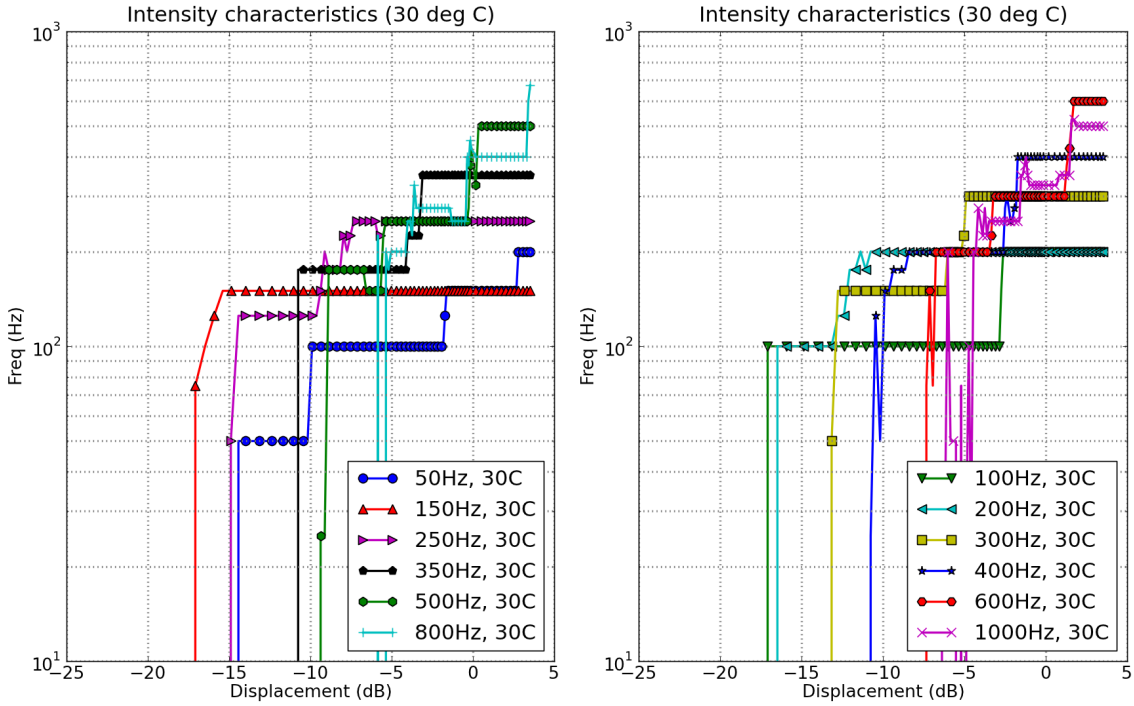

Figure A.15: Intensity response of simulated PC at 30°C for function experiment 2.

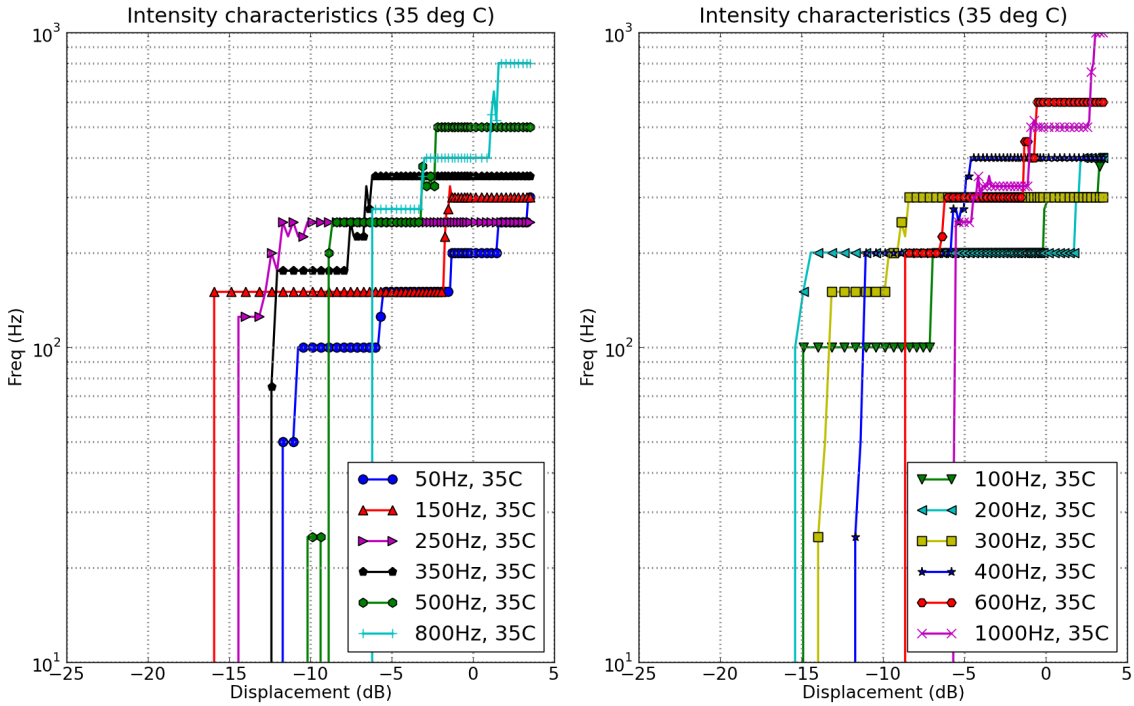

Figure A.16: Intensity response of simulated PC at 35°C for function experiment 2.

A.6 Functional Experiment 3

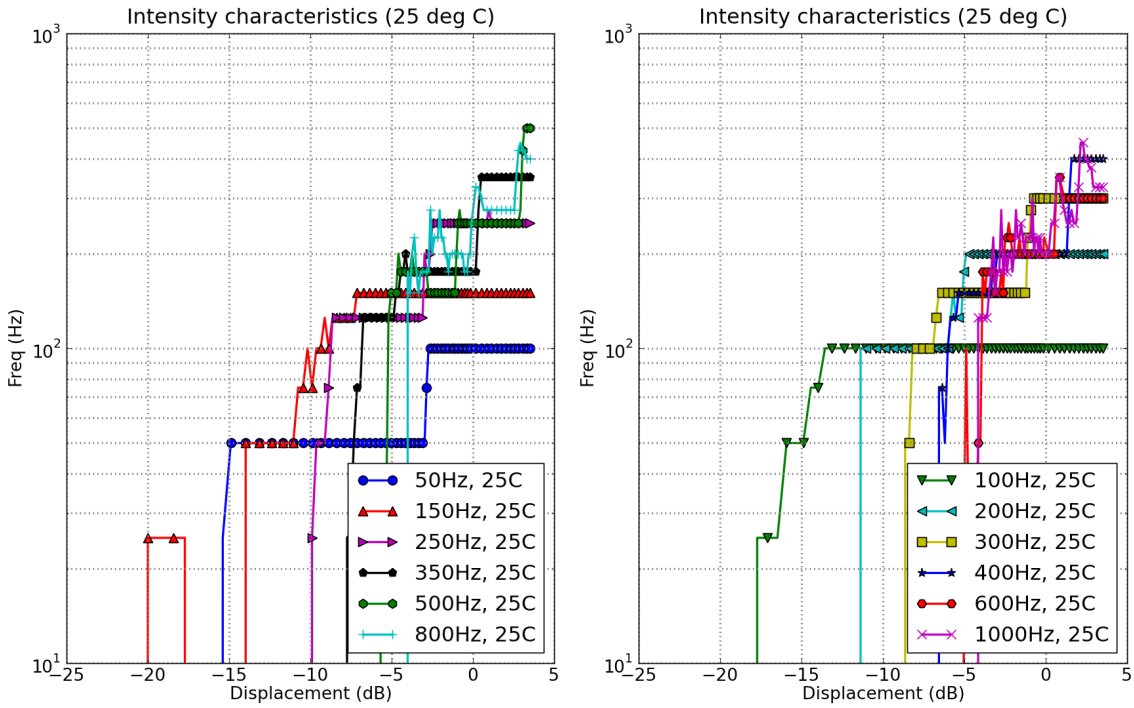

Figure A.17: Intensity response of simulated PC at 25°C for function experiment 3.

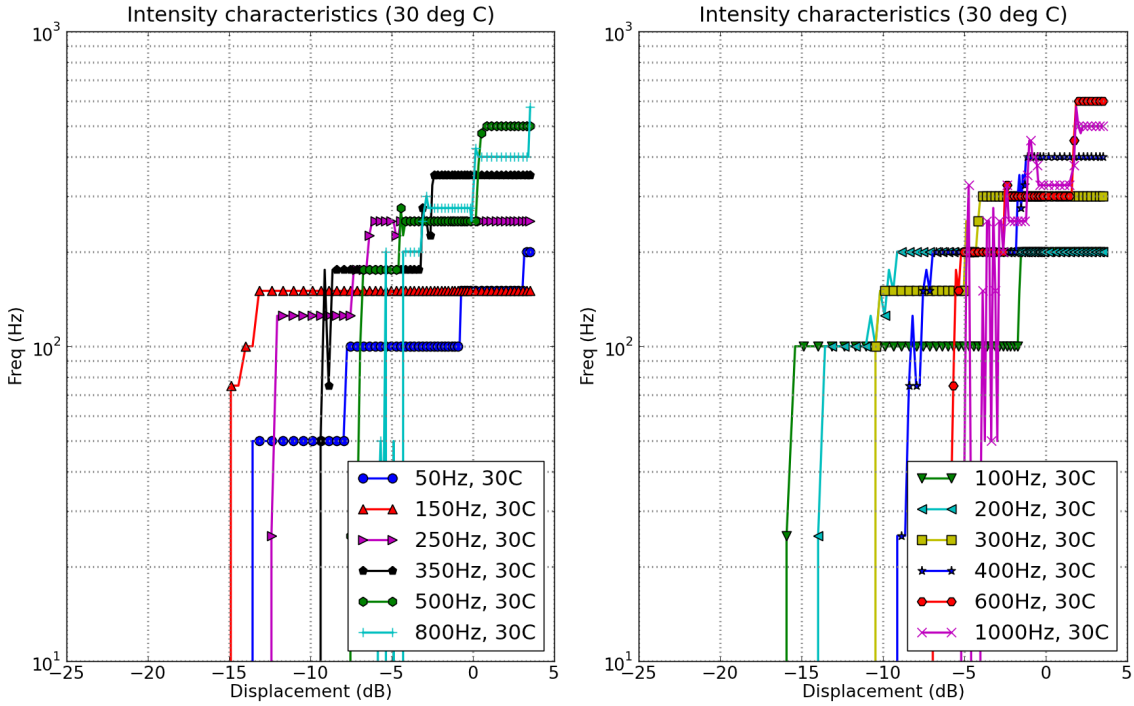

Figure A.18: Intensity response of simulated PC at 30°C for function experiment 3.

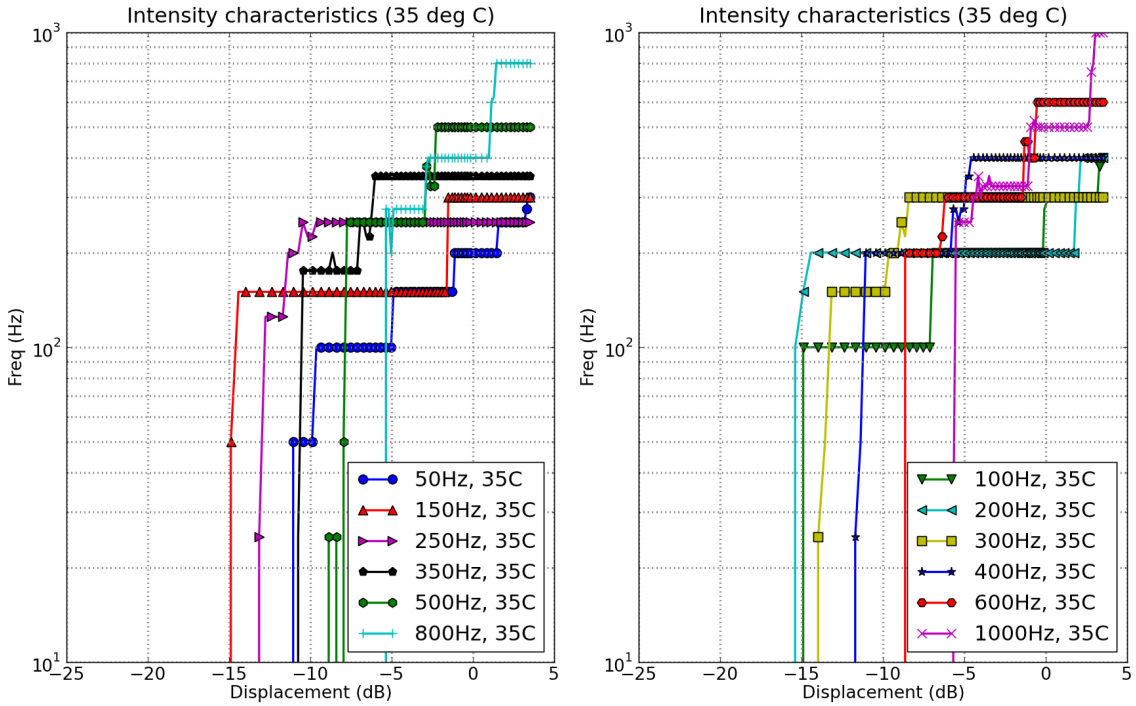

Figure A.19: Intensity response of simulated PC at 35°C for function experiment 3.